UNCLASSIFIED

SECURITY CLASSIFICATION OF THIS PAGE *(When Data Entered)*

REPORT DOCUMENTATION PAGE	READ INSTRUCTIONS BEFORE COMPLETING FORM
1. REPORT NUMBER: AFOSR-TR- 83-1297	2. GOVT ACCESSION NO. / 3. RECIPIENT'S CATALOG NUMBER
4. TITLE *(and Subtitle)*: Body and Surface Wave Modeling of Observed Seismic Events	5. TYPE OF REPORT & PERIOD COVERED: Final
	6. PERFORMING ORG. REPORT NUMBER
7. AUTHOR(s): David G. Harkrider, Donald V. Helmberger	8. CONTRACT OR GRANT NUMBER(s): F49620-81-C-0008
9. PERFORMING ORGANIZATION NAME AND ADDRESS: California Institute of Technology, Seismological Laboratory, 252-21, Pasadena, California 91125	10. PROGRAM ELEMENT, PROJECT, TASK AREA & WORK UNIT NUMBERS: ARPA Order No. 3291.40, 61102F, 2309/A1
11. CONTROLLING OFFICE NAME AND ADDRESS: AFOSR/NP, Building 410, Bolling AFB, D.C. 20332	12. REPORT DATE: 1 May 1982 - 31 October 1982
	13. NUMBER OF PAGES: 110
14. MONITORING AGENCY NAME & ADDRESS *(if different from Controlling Office)*	15. SECURITY CLASS. *(of this report)*: Unclassified
	15a. DECLASSIFICATION/DOWNGRADING SCHEDULE

16. DISTRIBUTION STATEMENT *(of this Report)*

Approved for public release; distribution unlimited

17. DISTRIBUTION STATEMENT *(of the abstract entered in Block 20, if different from Report)*

18. SUPPLEMENTARY NOTES

ELECTE JAN 20 1984 D A

19. KEY WORDS *(Continue on reverse side if necessary and identify by block number)*

Near-field synthetics, tectonic release below NTS, body wave travel time and amplitude anomalies across North America

20. ABSTRACT *(Continue on reverse side if necessary and identify by block number)*

The research performed under the contract during the period 1 May through 31 October 1982 can be divided into three main topics, efficient generation of near field synthetics, body wave amplitude and travel time correlations across North America, and long period P-wave evidence for tectonic-release at depth below NTS events.

In Section II, expressions for the displacements on the surface of a layered half-space due to a point source in terms of the generalized

DD FORM 1 JAN 73 1473

UNCLASSIFIED

SECURITY CLASSIFICATION OF THIS PAGE *(When Data Entered)*

AD A137083

DTIC FILE COPY

reflection and transmission coefficient matrices of Kennett are numerically evaluated by the discrete wave number summation method of Bouchon. This Kennett-Bouchon (KB) technique is an efficient algorithm for calculating near field synthetics. Numerical examples are given comparing this method with synthetics generated with the Cagniard-de Hoop technique, P-SV modes, and a discrete wavenumber finite element (DWFE) code.

In Section III, relationships between travel time and amplitude station anomalies are examined for short and long period SH waves and short period P-waves recorded at North American WWSN and CSN stations. Data for two azimuths of approach are analyzed. Short period P and S wave amplitudes have similar regional variations, being relatively low in the western tectonic region and enhanced in the shield and mid-continental regions. The east coast has intermediate amplitude anomalies and systematic large azimuthal travel time variations. There is a general correlation between diminished short period amplitudes and late S wave arrival times and enhanced amplitudes and early arrivals. However, this correlation is not obvious within eastern and western provinces separately, and the data are consistent with a step like shift in amplitude level across the Rocky Mountain front. Long period S waves show no overall correlation between amplitude and travel time anomalies.

In Section IV, long period body waves are studied at regional and upper mantle distances from large underground explosions at Pahute Mesa, Nevada Test Site. A comparison of the seismic records from neighboring explosions show that t-e more recent events have much simpler waveforms. In fact, many of the early events produce waveforms which are similar to those produced by shallow moderate size, strike slip earthquakes. A phase which can be identified as sP is particularly obvious. In particular, the event GREELEY (1966) can be matched by simply adding synthetic waveforms appropriate for a shallow strike slip earthquake to the observations of the KASSERI (1975) event. The identification of the sP phase at upper mantle distances indicates that the double couple source depth is 4 km or less.

A-1

AFOSR-TR- 83-1297

Final

TECHNICAL REPORT

- 31 October 1982

1 Nov 80 -

ARPA Order No.:	3291-40
Program Code:	1A10
Name of Contractor:	California Institute of Technology
Effective Date of Contract:	1 November 1980
Contract Expiration Date:	31 October 1982
Amount of Contract:	$369,939
Contract Number:	F49620-81-C-0008
Principal Investigators:	David G. Harkrider (213) 356-6910 Donald V. Helmberger (213) 356-6911
Program Manager and Telephone Number:	William J. Best (202) 767-4908
Short Title of Work:	Body and Surface Wave Modeling of Observed Seismic Events

The views and conclusions contained in this document are those of the authors and should not be interpreted as necessarily representing the official policies, either expressed or implied, of the Defense Advanced Research Projects Agency of the U.S. Government

Sponsored by
Advanced Research Projects Agency (DOD)
ARPA Order No. 3291-40
Monitored by AFOSR Under Contract No. F49620-i1-C-0008

Seismological Laboratory
Division of Geological and Planetary Sciences
California Institute of Technology
Pasadena, California 91125

84 01 19 11 $

Approved for public release;
distribution unlimited.

TABLE OF CONTENTS

AIR FORCE OFFICE OF SCIENTIFIC RESEARCH (AFSC)
NOTICE OF TRANSMITTAL TO DTIC
This technical report has been reviewed and is
approved for public release IAW AFR 190-12.
Distribution is unlimited.
MATTHEW J. KERPER
Chief, Technical Information Division

I. SUMMARY

The research performed under the contract during the period 1 May through 31 October 1982 can be divided into three main topics, efficient generation of near field synthetics, body wave amplitude and travel time correlations across North America, and long period P-wave evidence for tectonic-release at depth below NTS events.

In Section II, expressions for the displacements on the surface of a layered half-space due to a point source in terms of the generalized reflection and transmission coefficient matrices of Kennett are numerically evaluated by the discrete wave number summation method of Bouchon. This Kennett-Bouchon (KB) technique is an efficient algorithm for calculating near field synthetics. Numerical examples are given comparing this method with synthetics generated with the Cagniard-de Hoop technique, P-SV modes, and a discrete wavenumber finite element (DWFE) code.

In Section III, relationships between travel time and amplitude station anomalies are examined for short and long period SH waves and short period P-waves recorded at North American WWSN and CSN stations. Data for two azimuths of approach are analyzed. Short period P and S wave amplitudes have similar regional variations, being relatively low in the western tectonic region and enhanced in the shield and mid-continental regions. The east coast has intermediate amplitude anomalies and systematic large azimuthal travel time variations. There is a general correlation between diminished short period amplitudes and late S wave arrival times and enhanced amplitudes and early arrivals.

However, this correlation is not obvious within eastern and western provinces separately, and the data are consistent with a step like shift in amplitude level across the Rocky Mountain front. Long period S waves show no overall correlation between amplitude and travel time anomalies.

In Section IV, long period body waves are studied at regional and upper mantle distances from large underground explosions at Pahute Mesa, Nevada Test Site. A comparison of the seismic records from neighboring explosions show that the more recent events have much simpler waveforms. In fact, many of the early events produce waveforms which are similar to those produced by shallow moderate size, strike slip earthquakes. A phase which can be identified as sP is particularly obvious. In particular, the event GREELEY (1966) can be matched by simply adding synthetic waveforms appropriate for a shallow strike slip earthquake to the observations of the KASSERI (1975) event. The identificaton of the sP phase at upper mantle distances indicates that the double couple source depth is 4 km or less.

II

A GENERALIZED REFLECTION - TRANSMISSION COEFFICIENT MATRIX AND DISCRETE WAVENUMBER METHOD FOR SYNTHETIC SEISMOGRAMS

BY Z. X. YAO AND D. G. HARKRIDER

ABSTRACT

Expressions for displacements on the surface of a layered half-space due to point force are given in terms of generalized reflection and transmission coefficient matrices (Kennett 1980) and the discrete wavenumber summation method (Bouchon 1981). The Bouchon method with complex frequencies yields accurate near field dynamic and static solutions.

The algorithm is extended to include simultaneous evaluation of multiple sources at different depths. This feature is the same as in Olson's finite element discrete fourier bessel code (DWFE) (Olson 1982).

As numerical examples, we calculate some layered half-space problems. The results agree with synthetics generated with the Cagniard de-Hoop technique, P-SV modes, and DWFE codes. For a ten layered crust upper mantle model with a bandwidth of 0-10 Hz, this technique requires one tenth the time of the DWFE calculation. In the presence of velocity gradients, where finer layering is required, the DWFE code is more efficient.

INTRODUCTION

Economic near field solutions of a point source in a layered half-space are important in the fields of seismology and earthquake engineering. Recently many approaches have been proposed to evaluate the layered half-space response. For example, there are generalized ray theory (Helmberger, 1968; Helmberger and Harkrider, 1978), reflectivity method (Fuchs and Muller, 1971), reflection and transmission coefficients matrix method (Kennett,

1974, 1980; Kennett and Kerry, 1980; Apsel, 1979), discrete wavenumber method (Bouchon, 1981), discrete wavenumbers - finite element method (DWFE)(Olson, 1982), among others.

In this paper a generalized reflection-transmission matrix and discrete wavenumber method for near field synthetic seismograms is proposed. This approach is based on Kennett's reflection and transmisson matrix method for the wavenumber integrands (1974, 1981) and the discrete wavenumber summation method (Bouchon, 1981) for the wavenumber integration. The reflection-transmission matrix is an effective procedure to evaluate the wavenumber integrand. Phase-delayed reflection and transmission coefficients are used which are slightly different than Kennett's expressions (1980). The algorithm includes simultaneous evaluation of the Green's functions of multiple sources at different depths.

As a numerical example, we calculate some layered half-space problems. The results agree with synthetics generated by the Cagniard-de Hoop technique and Olson's (1982) DWFE codes. For a ten layered crust upper mantle model with a bandwidth of 0-10Hz, this technique requires one tenth the time of the DWFE calculaton.

INTEGRAND EXPRESSIONS

The displacement integrands on the free surface for buried source problems given by Kennett and Kerry (1979) eqn. (5.22) are

$$W(0^+) = (M_U + M_D \tilde{R})[I - R_D^{RS} \tilde{R}]^{-1} T_U^{RS} [I - R_D^{SL} R_U^{FS}]^{-1} (R_D^{SL} \delta\Phi_D - \delta\Phi_U) \qquad (1)$$

The notation used is that of Kennett and Kerry (1979). Slightly different relations are used for the reflection and transmission coefficients, which except for differences in normalization, are given by their eqn. (4.26). The relations and additional definitions are found in the Appendix.

$\tilde{R}$ is the reflection coefficient matrix on the free surface, $(M_U+M_D\tilde{R})$ is the receiver function matrix (Helmberger, 1974).

$$\tilde{R} = \frac{1}{\Delta}\begin{bmatrix} \Omega_1^2+a_1b_1 & 2kb_1\Omega_1 \\ 2ka_1\Omega_1 & \Omega_1^2+a_1b_1 \end{bmatrix} \tag{2}$$

$$(M_U+M_D\tilde{R}) = \frac{1}{\Delta}\begin{bmatrix} k_{\beta_1}^2 ka_1b_1 & k_{\beta_1}^2 b_1\Omega_1 \\ k_{\beta_1}^2 a_1\Omega_1 & k_{\beta_1}^2 ka_1b_1 \end{bmatrix} \tag{3}$$

where

$$\Delta = k^2a_1b_1 - \Omega_1^2 \tag{4}$$

with

k = wave number,

α = P wave velocity,

β = S wave velocity,

μ = rigidity,

$k_\alpha = \omega/\alpha$,

$k_\beta = \omega/\beta$,

$a = \sqrt{k^2-k_\alpha^2}$, Re $a \geq 0$,

$b = \sqrt{k^2-k_\beta^2}$, Re $b \geq 0$,

and

$\Omega = k^2 - k_\beta^2$.

R_U^{SL} is the generalized relection coefficient matrix for the P-SV waves between $z = z_s^+$ and $z = z_L^+$ (Figure 1). Using the relations for reflection and transmission coefficients given by Kennett (1974, 1980), and Kennett and Kerry (1979), we can calculate R_D^{SL} from

$$Q(z_s^+, z_L^+) = Q(z_s^+, z_{s+1}^+) \ldots Q(z_{L+1}^+, z_L^+) \tag{6}$$

with

$$Q(z_{K-1}^+, z_K^+) = \begin{bmatrix} \tilde{T}_U - \tilde{R}_D \tilde{T}_D^{-1} \tilde{R}_U & \tilde{R}_D \tilde{T}_D^{-1} \\ -\tilde{T}_D^{-1} \tilde{R}_U & \tilde{T}_D^{-1} \end{bmatrix} \tag{7}$$

where the submatrices correspond to the normalized reflection and transmission coefficients matrices given in the Appendix. R_D^{RS} and T_U^{RS} are the generalized reflection and transmission coefficient between $z = 0^+$ and $z = z_s^-$. R_U^{FS} is the generalized reflection coefficient between $z = 0$ and $z = z_s^+$ and is calculated by the relation

$$R_U^{FS} = R_U^{RS} + R_D^{RS} \tilde{R} [I - R_D^{RS} \tilde{R}]^{-1} T_U^{RS} \tag{8}$$

For SH waves, the displacement integrand on the free surface is as follows

$$V(o^+) = 2k(1 - R_{D,SH}^{RS})^{-1} T_{U,SH}^{RS} (1 - R_{D,SH}^{SL} R_{U,SH}^{FS})^{-1} (R_{D,SH}^{SL} \delta\chi_D - \delta\chi_U) \tag{9}$$

with the subscript denoting reflection and transmission coefficients appropriate for SH waves.

$\delta\Phi$ and $\delta\chi$ represents the source's terms which have been given by Langston and Helmberger (1975).

For many problems, a fault is treated as a summation of subfaults which can be considered point sources. Thus there is need for rapid construction of Green's functions for several different source depths. Since the terms necessary for a given source depth calculations are obtained by the iterative relations of Kennett, we in effect calculate similar source depth terms for every interface above and below the source plane. The only additional effort

for obtaining as many source depth Green's function as there are interfaces is in saving the intermediate values. This feature is similar to codes based on reciprocity, i.e. surface source and receiver at depth, such as DWFE (Olson, 1982) and PROSE (Apsel, 1979).

INTEGRAL SOLUTIONS

For a buried double couple, the free surface displacements are

$$w(t) = \frac{M_o}{4\pi\rho}\frac{d}{dt}[\dot{D}(t)^* \sum_{m=0}^{2} A_m(\lambda,\delta,\varphi) w_m(t)]$$

$$q(t) = \frac{M_o}{4\pi\rho}\frac{d}{dt}[\dot{D}(t)^* \sum_{m=0}^{2} A_m(\lambda,\delta,\varphi) q_m(t)] \qquad (10)$$

$$v(t) = \frac{M_o}{4\pi\rho}\frac{d}{dt}[\dot{D}(t)^* \sum_{m=1}^{2} A_{m+3}(\lambda,\delta,\varphi) v_m(t)]$$

where

$$A_0(\lambda,\delta,\varphi) = \frac{1}{2}\sin\lambda \sin 2\delta$$

$$A_1(\lambda,\delta,\varphi) = \cos\varphi \cos\lambda \cos\delta - \sin\varphi \sin\lambda \cos 2\delta$$

$$A_2(\lambda,\delta,\varphi) = \sin 2\varphi \cos\lambda \sin\delta + \frac{1}{2}\cos 2\varphi \sin\lambda \sin 2\delta$$

$$A_3(\lambda,\delta,\varphi) = 0 \qquad (11)$$

$$A_4(\lambda,\delta,\varphi) = -\cos\varphi \sin\lambda \cos 2\delta - \sin\varphi \cos\lambda \cos\delta$$

$$A_5(\lambda,\delta,\varphi) = \cos 2\varphi \cos\lambda \sin\delta - \frac{1}{2}\sin 2\varphi \sin\lambda \sin 2\delta$$

φ = azimuth from the fault strike,

λ = rake angle,

δ = dip angle,

M_o = seismic moment,

$\dot{D}$ = far-field time history,

ρ = density, and $w_m(t)$,$u_m(t)$ and $v_m(t)$ are step responses which correspond to the vertical, radical and tangential displacements of three fundamental shear dislocations (m = 2, strike-slip fault; m = 1, dip-slip fault; m = 0, isotropic component of the 45° dip-slip fault). In the frequency domain they are as follows

$$w_m(\omega) = \int_0^\infty W_m J_m(kr)\, k\, dk$$

$$q_m(\omega) = \int_0^\infty [U_m J_m'(kr) - V_m \frac{m}{kr} J_m(kr)]\, k\, dk \qquad (12)$$

$$v_m(\omega) = \int_0^\infty [U_m \frac{m}{kr} J_m(kr) - V_m J_m'(kr)]\, k\, dk$$

where

$$J_m'(x) = \frac{dJ_m}{dx}$$

$$\begin{bmatrix} U_m \\ W_m \end{bmatrix} = \frac{1}{\omega^4}(M_U + M_D\tilde{R})\,(I - R_U^{RS}\tilde{R})^{-1} T_U^{RS} (I - R_D^{SL} R_U^{FS})^{-1} \left[R_D^{SL} \begin{bmatrix} P_m^+ \\ SV_m^+ \end{bmatrix} + \begin{bmatrix} P_m^- \\ SV_m^- \end{bmatrix} \right] \qquad (13)$$

from (1)

$$V_m = \frac{2k}{\omega^4}(1 - R_{D,SH}^{RS})^{-1} T_{U,SH}^{RS}\,(1 - R_{D,SH}^{SL} R_{U,SH}^{FS})\,(R_{D,SH}^{SL}\, SH_m^+ + SH_m^-) \qquad (14)$$

from (9), with

$$
\begin{array}{lll}
P_0 = (2k_\alpha^2 - 3k^2)/a & SV_0 = -\varepsilon 3k & SH_0 = 0 \\
P_1 = \varepsilon 2k & SV_1 = (2k^2 - k_\beta^2)/b & SH_1 = -\varepsilon k_\beta^2/k \\
P_2 = -k^2/a & SV_2 = -\varepsilon k & SH_2 = k_\beta^2/b
\end{array} \qquad (15)
$$

and

$$
\varepsilon = \begin{cases} -1 & \text{for } - \text{ superscript} \\ 1 & \text{for } + \text{ superscript} \end{cases}
$$

For an explosion type source,

$$
w(t) = \frac{d}{dt}\left[\ \dot{\Psi}(t) * w_0(t)\right] \qquad (16)
$$

$$
g(t) = \frac{d}{dt}\left[\ \dot{\Psi}(t) * g_0(t)\right]
$$

where w_0 and g_0 are given as before from (12) and all the source coefficients are zero except

$$
P_0 = \omega^2/a
$$

and $\dot{\Psi}(t)$ is the reduced velocity potential of the explosion.

WAVENUMBER INTEGRATION

The Hankel transform-type integral representation of the displacements in the frequency domain involves quantities of the form

$$
I_m = \int_0^\infty F(k,\omega)\, J_m(kr)\, k\, dk \qquad m=0,1,2 \qquad (17)
$$

The kernel $F(k,\omega)$ depends upon wavenumber, frequency source depth and layer properties which we evaluate with generalized reflection and transmission coefficient matrices. Now it is important to look for an efficient numerical

integration scheme to handle the wave number integration.

Bouchon (1981) has demonstrated that the wavenumber integration (17) can be evaluated by a discrete wavenumber summation

$$I_m = \frac{\pi}{L} \sum_{j=0}^{\infty} \varepsilon_j \, k_j \, F(k_j,\omega) \, J_m(k_j r) \qquad (17)$$

$$\varepsilon_j = \begin{cases} 2 & \text{for } j \neq 0 \\ 1 & \text{for } j = 0 \end{cases}$$

$$k_j = 2\pi j / L$$

if relations $r < L/2$ and $[(L-r)^2 + z^2]^{1/2} > \alpha t$ are satisfied. To avoid the influence of the singularities of the integrand $F(k,\omega)$, and the discretization, he gave to the frequency an imaginary part, the effect of which is later removed from the time domain solution.

This discretization scheme is simpler than that used by the DWFE method (Olson, 1982). In the DWFE method the discrete wavenumbers are determined by the roots of $J_0(kL)$ and $J_1(kL)$. An advantage of the Bouchon method over Kennett's wavenumber integration is that it is straightforward to obtain the near field static solutions. The static contribution comes from zero frequency and is treated the same in Bouchon's technique as any other complex frequency. On the other hand the slowness method requires special handling at zero frequency. The combinaton of Kennett's integrand algorithm with Bouchon's discrete wavenumber evaluation will be referred to as the Kennett-Bouchon (KB) algorithm.

The k loop is controlled by a previously specified precision e. If the ratio of the terms

$$|k_j F(k_j,\omega)J_m(k_j r)| \;/\; |\sum_{i=1}^{j} k_i F(k_i,\omega)J_m(k_i r)|$$

is less than e, the k loop stops. This condition must be met for every calculation in the loop. Since at least one of the calculations will involve a Bessel function of order one different than than the others, the loop will not be terminated by a zero of the Bessel functions. As one might expect the higher the frequency the larger the number of k terms required for convergence.

NUMERICAL EXAMPLES

As a first numerical example, we calculate the vertical and radial velocity field at the free surface due to an explosion source in a homogeneous half-space (Table 1). Taking r = 10km, h = 1.2 km, Δ t = 0.05 sec, and L =10 km, we obtain the velocities shown at the bottom of each pair in Figure 2. The calculation used the reflection and transmission coefficients generated by a three layer model of the homogeneous half-space. The upper trace for each velocity component of Figure 2 is calculated from the explicit discrete wavenumber expressions of Bouchon (1981). The differences of amplitude are only in the third decimal place.

TABLE 1

LAYER PARAMETERS FOR THE HALF-SPACE MODEL.

h km	α km/sec	β km/sec	ρ gm/cm^3
∞	3.000	1.900	1.900

In the second example we calculate the displacements of a dislocation source in another half-space model (Table 2) and compare with ray theory using the Cagniard-de Hoop technique. These are shown in Figures 3 and 4, the top traces of each pair is the displacement obtained with rays. The far-field source time function is a triangle with one second width, focal depth 8

km, the epicenter ranges are 16 km (Figure 3) and 32 km (Figure 4) respectively. The bottom traces are from the KB algorithm. The differences are very small and come mostly from the difference in time increments used in the two methods. In the generalized ray theory we use $\Delta t = 0.03$ sec, in the other $\Delta t = 0.1$ sec.

TABLE 2

LAYER PARAMETERS FOR THE CRUST HALF-SPACE MODEL.

h km	α km/sec	β km/sec	ρ gm/cm^3
∞	6.200	3.500	2.700

For the layered half-space problem we use solutions obtained by the DWFE method to check the KB result. Dislocation source displacements for a one layer half-space, with the source in the layer, h = 2.5 km, r = 10 km are shown in Figure 5. In Figure 6 the source is in the underlaying medium, h = 7.0 km, r = 10 km. The layer model parameters are given in Table 3. The results of the two methods again show good agreement.

TABLE 3

LAYER PARAMETERS FOR THE ONE LAYER MODEL.

h km	α km/sec	β km/sec	ρ gm/cm^3
6.0	3.500	2.000	2.400
∞	5.500	3.300	2.700

In Figure 7, we show a comparison between the KB and DWFE algorithms for an explosion at a depth of 1.2 km in an 8 layer model (Table 4) of the Amchitka crust over a mantle half-space. This structure was used to model the near field records from the nuclear test event Milrow (Burdick,1983). The synthetics are the free surface vertical particle velocities at ranges of 9.8 and 11.5 kms. The nominal maximum frequency in each synthetic is 5 Hz

although the DWFE record is Butterworth filtered down to 5 Hz and the KB spectral calculation is truncated or terminated at 5 Hz. Because of this the frequency content is slightly greater in the KB calculation. This difference can be seen in the relative excitation between the body waves and the Rayleigh wave pulse at the end of each synthetic. Considering their differences at high frequency, the time domain agreement is excellent.

TABLE 4

LAYER PARAMETERS FOR THE MILROW MODEL.

h km	α km/sec	β km/sec	ρ gm/cm^3
0.2	3.400	1.700	2.300
0.6	3.700	1.900	2.400
0.5	4.200	2.100	2.400
0.5	4.600	2.300	2.500
0.7	4.900	2.800	2.600
0.5	5.100	2.900	2.700
6.0	5.900	3.300	2.700
28.0	6.900	4.000	2.800
∞	8.200	4.700	3.200

For this model, 5 Hz is not sufficient to resolve pP from the direct P arrivals. Increasing the maximum frequency to 10 Hz, the pP arrival is seen in the double peaked overswing following the direct P arrival at distances of 10 and 12 kms on the vertical velocity KB record (Figure 8) and the radial velocity KB record (Figure 9). This identification was verifyed with the spliced generalized ray and modal synthetics appearing above the KB synthetics (Burdick, 1983) in Figures 8 and 9. The generalized ray (Helmbeger, 1968) sum was restricted to direct and first multiple compressional waves . The only mode (Harkrider, 1964 and 1970) used was the fundamental Rayleigh mode. With this structure, the 10 Hz DWFE calculation takes 10 times longer than the KB calculation.

CONCLUSIONS

We have presented a generalized reflection-transmission coefficient matrix and discrete wavenumber method for synthetic seismograms. For a dislocation source, the displacements on the free surface are represented as a linear combination of three fundamental shear dislocation. The wavenumber integrands are calculated by reflection and transission coefficients, and the wavenumbers integration by discrete wavenumber summation method with complex frequencies which can yield accurate near field static solutions.

Vertical integration schemes used in the near field have been either spectral (Apsel,1979,Bouchon,1981) as in the regional techniques or finite-element (Olson,1982) and finite-difference (Alexseev and Mikhailenko, 1980) in the time domain. The finite element schemes have the disadvantage in that the vertical step size is determined by the desired maximum frequency content, which in turn determines the time step required for stability. This time step is usually many times smaller than the time increment associated with the maximum frequency.

If portions of the vertical velocity and density profile are homogeneous, spectral techniques propagate across the region in one vertical step while the finite element-difference methods reqire many. On the other hand, in the vicinity of moderate vertical gradients the step size or layer thickness of the spectral techniques will be at least as small as the finite element-difference scheme and the number of numerical operations are considerably more. In this situation spectral techniques, in particular the KB method ,are not as efficient as the time domain techniques. Convergence as the number of wave numbers is increased is more straightforward using the spectral schemes and, as one would expect, the number of wave numbers for a given convergence depends on the frequency being evaluated with fewer wave numbers at the lower

frequencies.

For the layered half-space problems presented, our results agree very well with synthetics generated by the Cagniard-de Hoop technique, P-SV modes, and the DWFE codes. For the ten layered crust upper mantle model with a bandwidth of 0-10 Hz, this technique required only one tenth the time of the DWFE calculation.

ACKNOWLEDGMENTS

This research was supported by the Advanced Projects Agency of the Department of Defense and was monitored by the Air Force Office of Scientific Research under Contract F49620-81-C-0008.

REFERENCES

Alekseev, A. S., and B. G. Mikhailenо (1980). Solution of dynamic problems of elastic wave propagation in inhomogeneous media by a combination of partial separation of variables and finite diference methods, *J. Geophys. 48.*, 161-172.

Apsel, R. J. (1979). *Dynamic Green's functions for layered media and applications to boundary-value problems*, Ph.D. Thesis , University of California, San Diego.

Bouchon, M. (1981). A simple method to calculate Green's functions for elastic layered media, *Bull. Seism. Soc. Am.* , 71, 959 - 971.

Burdick, L. J. (1983). Simultaneous modeling of body waves and surface waves in near field records of nuclear explosions, WCCP-R-83-02, Woodward-Clyde Consultants, Pasadena, California.

Fuchs, K. and G. Muller (1971). Computation of synthetic seismograms with the reflectivity method and comparison with observations, *Geophys. J. R. astr. Soc.* , 23 , 417 - 433.

Harkrider, D. G. (1964). Surface waves in multilayered media. I. Rayleigh and Love waves from buried sources in a multilayered half-space, *Bull. Seism. Soc.*

Am. , 54 , 627 - 679.

Harkrider, D. G. (1970). Surface waves in multilayerd elastic media. Part II. Higher mode spectra and spectral ratios from point sources in plane layered earth models, *Bull. Seism. Soc. Am.* , 60 , 1937 - 1987.

Helmberger, D. V. (1968). The crust-mantle transition in the Bering Sea, *Bull. Seism. Soc. Am.* , 58 , 179 - 214.

Helmberger, D. V. (1974). Generalized ray theory for shear dislocations, I. Bull. Seism. Soc. Am. , 64, 45 - 64.

Helmberger, D. V., and D. G. Harkrider (1978). Modeling earthquakes with generalized ray theory, in *Modern Problems in Elastic Wave Propagation* , ed Miklowitz, J., and J. Achenbach, John Wiley and Sons, New York, 499 - 518.

Kennett, B. L. N. (1974). Reflections, rays, and reverberations, *Bull. Seis. Soc. Am.* , 64 , 1685 - 1696.

Kennett, B. L. N. (1980). Seismic waves in a stratified half-space - II. Theoretical seisograms, *Geophys. J. R. astr. Soc.* , 61 , 1 - 10.

Kennett, B. L. N., and N. J. Kerry (1979). Seismic waves in a stratified half-space, *Geophys. J. R. astr. Soc.* , 57 , 557 - 583.

Langston, C. A., and D. V. Helmberger (1975). A procedure for modelling shallow dislocation sources, *Geophys. J. R. astr. Soc.* , 42 , 117 - 130.

Olsen, A. H. (1982), *Forward simulation and linear inversion of earthquake ground motions*, Ph.D. Thesis , University of California, San Diego.

INSTITUTE OF GEOPHYSICS
ACADEMIA SINICA
BEIJING
PEOPLE'S REPUBLIC OF CHINA

SEISMOLOGICAL LABORATORY
CALIFORNIA INSTITUTE OF TECHNOLOGY
PASADENA, CALIFORNIA 91125
USA
CONTRIBUTION NO. 3889

APPENDIX

The relations for phase normalized reflection and transmission coefficients are as follows:

$$\tilde{r}^D_{PP} = e^{-2ad}\, r^D_{PP} \qquad \tilde{t}^D_{PP} = e^{-ad}\, t^D_{PP}$$

$$\tilde{r}^D_{SP} = e^{-(a+b)d}\, r^D_{SP} \qquad \tilde{t}^D_{SP} = e^{-bd}\, t^D_{SP}$$

$$\tilde{r}^D_{PS} = e^{-(a+b)d}\, r^D_{PS} \qquad \tilde{t}^D_{PS} = e^{-ad}\, t^D_{PS}$$

$$\tilde{r}^D_{SS} = e^{-2bd}\, r^D_{SS} \qquad \tilde{t}^D_{SS} = e^{-bd}\, t^D_{SS}$$

$$\tilde{r}^U_{PP} = r^U_{PP} \qquad \tilde{t}^U_{PP} = e^{-ad}\, t^U_{PP}$$

$$\tilde{r}^U_{SP} = r^U_{SP} \qquad \tilde{t}^U_{SP} = e^{-ad}\, t^U_{SP}$$

$$\tilde{r}^U_{PS} = r^U_{PS} \qquad \tilde{t}^U_{PS} = e^{-bd}\, t^U_{PS}$$

$$\tilde{r}^U_{SS} = r^U_{SS} \qquad \tilde{t}^U_{SS} = e^{-bd}\, t^U_{SS}$$

where

$$\tilde{R}_D = \begin{bmatrix} \tilde{r}^D_{PP} & \tilde{r}^D_{PS} \\ \tilde{r}^D_{SP} & \tilde{r}^D_{SS} \end{bmatrix}$$

with similar matrix indexing for $\tilde{R}_U$, $\tilde{T}_D$, and $\tilde{T}_D$.

For the interface reflection and transmission coefficients, say from layer 1 to layer 2, we have

$$r^D_{PP} = [\, k^2 a_1 b_1 a_2 b_2 (\mu_2 - \mu_1)^2 - k^2 (\mu_1 \Omega_1 - \mu_2 \Omega_2)^2 - a_1 b_1 (\mu_2 \Omega_2 - k^2 \mu_1)^2$$

$$+ a_2 b_2 (\mu_1 \Omega_1 - k^2 \mu_2)^2 - \frac{1}{4} \mu_1 \mu_2 \, k^2_{\beta_1} \, k^2_{\beta_2} (a_1 b_2 - b_1 a_2) \,] / \Delta_1$$

$$r^D_{SP} = -2k b_1 [(\mu_2 \Omega_2 - k^2 \mu_1)(\mu_1 \Omega_1 - \mu_2 \Omega_2) - a_2 b_2 (\mu_2 - \mu_1)(\mu_1 \Omega_1 - k^2 \mu_2)] / \Delta_1$$

$$r^D_{PS} = \frac{a_1}{b_1} r^D_{SP}$$

$$r_{SS}^{D} = [\, k^2 a_1 b_1 a_2 b_2 (\mu_2 - \mu_1)^2 - k^2 (\mu_1 \Omega_1 - \mu_2 \Omega_2)^2 - a_1 b_1 (\mu_2 \Omega_2 - k^2 \mu_1)^2$$

$$+ a_2 b_2 (\mu_1 \Omega_1 - k^2 \mu_2)^2 + \frac{1}{4} \mu_1 \mu_2 \, k_{\beta_1}^2 \, k_{\beta_2}^2 (a_1 b_2 - b_1 a_2)] / \Delta_1$$

$$t_{PP}^{D} = \mu_1 k_{\beta_1}^2 a_1 [(\mu_2 \Omega_2 - k 2 \mu_1) b_1 + (\mu_1 \Omega_1 - k^2 \mu_2) b_2] / \Delta_1$$

$$t_{SP}^{D} = \mu_1 k_{\beta_1}^2 b_1 [(\mu_2 - \mu_1) a_1 b_2 + (\mu_1 \Omega_1 - \mu_2 \Omega_2)] / \Delta_1$$

$$t_{PS}^{D} = \mu_1 k_{\beta_1}^2 a_1 [(\mu_2 - \mu_1) b_1 a_2 + (\mu_1 \Omega_1 - \mu_2 \Omega_2)] / \Delta_1$$

$$t_{SS}^{D} = \mu_1 k_{\beta_1}^2 b_1 [(\mu_2 \Omega_2 - k^2 \mu_1) a_1 + (\mu_1 \Omega_1 - k^2 \mu_2) a_2] / \Delta_1$$

and

$$\Delta_1 = [\, k^2 a_1 b_1 a_2 b_2 (\mu_2 - \mu_1)^2 + k^2 (\mu_1 \Omega_1 - \mu_2 \Omega_2)^2 - a_1 b_1 (\mu_2 \Omega_2 - k^2 \mu_1)^2$$

$$- a_2 b_2 (\mu_1 \Omega_1 - k^2 \mu_2)^2 - \frac{1}{4} \mu_1 \mu_2 k_{\beta_1}^2 \, k_{\beta_2}^2 (a_1 b_2 + b_1 a_2)]$$

where Δ_i is the Stoneley wave equation for the interface between layers i and $i+1$.

For R_{ij}, and T_{ij}, we have

$$r_{PP}^{U} = [\, k^2 a_1 b_1 a_2 b_2 (\mu_2 - \mu_1)^2 - k^2 (\mu_1 \Omega_1 - \mu_2 \Omega_2)^2 + a_1 b_1 (\mu_2 \Omega_2 - k^2 \mu_1)^2$$

$$- a_2 b_2 (\mu_1 \Omega_1 - k^2 \mu_2)^2 + \frac{1}{4} \mu_1 \mu_2 \, k_{\beta_1}^2 \, k_{\beta_2}^2 (a_1 b_2 - b_1 a_2)\,] / \Delta_1$$

$$r_{SP}^{U} = 2k b_2 [(\mu_1 \Omega_1 - k^2 \mu_2)(\mu_2 \Omega_2 - \mu_1 \Omega_1) - a_1 b_1 (\mu_1 - \mu_2)(\mu_2 \Omega_2 - k^2 \mu_1)] / \Delta_1$$

$$r_{PS}^{U} = \frac{a_2}{b_2} r_{SP}^{U}$$

$$r_{SS}^{U} = [\, k^2 a_1 b_1 a_2 b_2 (\mu_2 - \mu_1)^2 - k^2 (\mu_1 \Omega_1 - \mu_2 \Omega_2)^2 + a_1 b_1 (\mu_2 \Omega_2 - k^2 \mu_1)^2$$

$$- a_2 b_2 (\mu_1 \Omega_1 - k^2 \mu_2)^2 - \frac{1}{4} \mu_1 \mu_2 \, k_{\beta_1}^2 \, k_{\beta_2}^2 (a_1 b_2 - b_1 a_2)] / \Delta_1$$

$$t_{PP}^{U} = \frac{\rho_2 a_2}{\rho_1 a_1} \, t_{PP}^{D}$$

$$t_{PS}^{U} = \frac{\rho_2 a_2}{\rho_1 b_1} \, t_{PS}^{D}$$

$$t_{SP}^{U} = \frac{\rho_2 b_2}{\rho_1 a_1} \, t_{SP}^{D}$$

$$t_{SS}^{U} = \frac{\rho_2 b_2}{\rho_1 b_1} \, t_{SS}^{D}$$

For SH waves

$$r_{SH}^{D} = \frac{\mu_1 b_1 - \mu_2 b_2}{\mu_1 b_1 + \mu_2 b_2}$$

$$t_{SH}^{D} = \frac{2 \mu_1 b_1}{\mu_1 b_1 + \mu_2 b_2}$$

$$r_{SH}^{U} = \frac{\mu_2 b_2 - \mu_1 b_1}{\mu_1 b_1 + \mu_2 b_2}$$

$$t_{SH}^{U} = \frac{2 \mu_2 b_2}{\mu_1 b_1 + \mu_2 b_2}$$

FIGURE CAPTIONS

FIG. 1. Source and structure geometry.

FIG. 2. Vertical and radial velocity record comparisons between an analytic and a three layer reflection-transmission coefficient calculation of an explosion in an homogeneous half-space.

FIG. 3. Vertical, radial, and tangential displacement comparisons between Cagniard-de Hoop and the KB techniques for a dislocation in an homogeneous half-space. The records are for the 3 fundamental fault orientations at a range of 16 km.

FIG. 4. As Figure 3, except the range is 32 km.

FIG. 5. Vertical, radial, and tangential displacement comparisons between the DWFE and KB techniques for a dislocation in a one layer over a half-space model. The records are for the 3 fundamental fault orientations at a range of 10 km. The source is in the upper layer at a depth of 2.5 km.

FIG. 6. AS Figure 5, except the source is below the layer at a depth of 7 km.

FIG. 7. Vertical velocity record comparisons between the DWFE and KB techniques for an explosion in the layered Milrow model. The Nyquist frequency is 5 Hz.

FIG. 8. Vertical velocity record comparisons between spliced ray-mode synthetics and the KB technique for an explosion in the layered Milrow model. The Nyquist frequency is 10 Hz.

FIG. 9. As Figure 8, except the velocity records are radial.

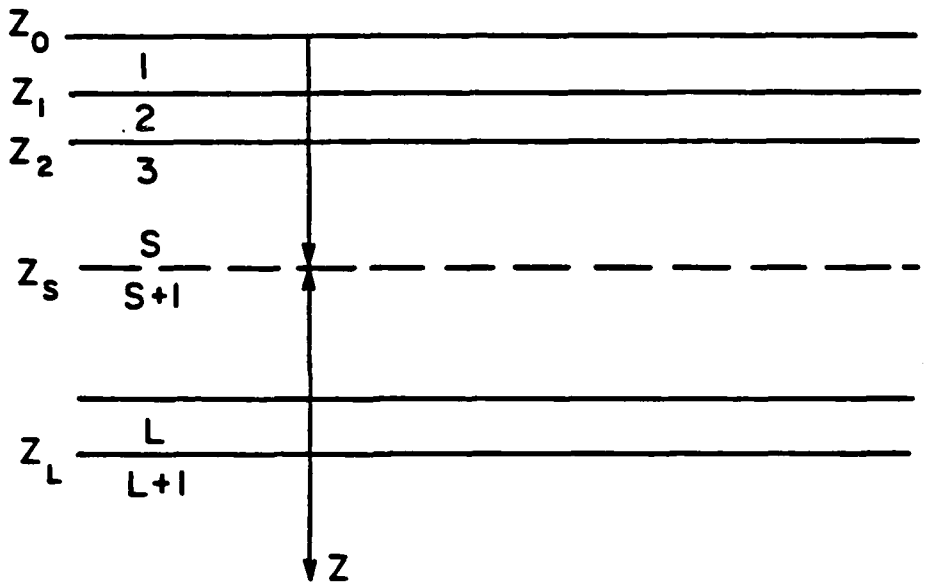

Fig. 1

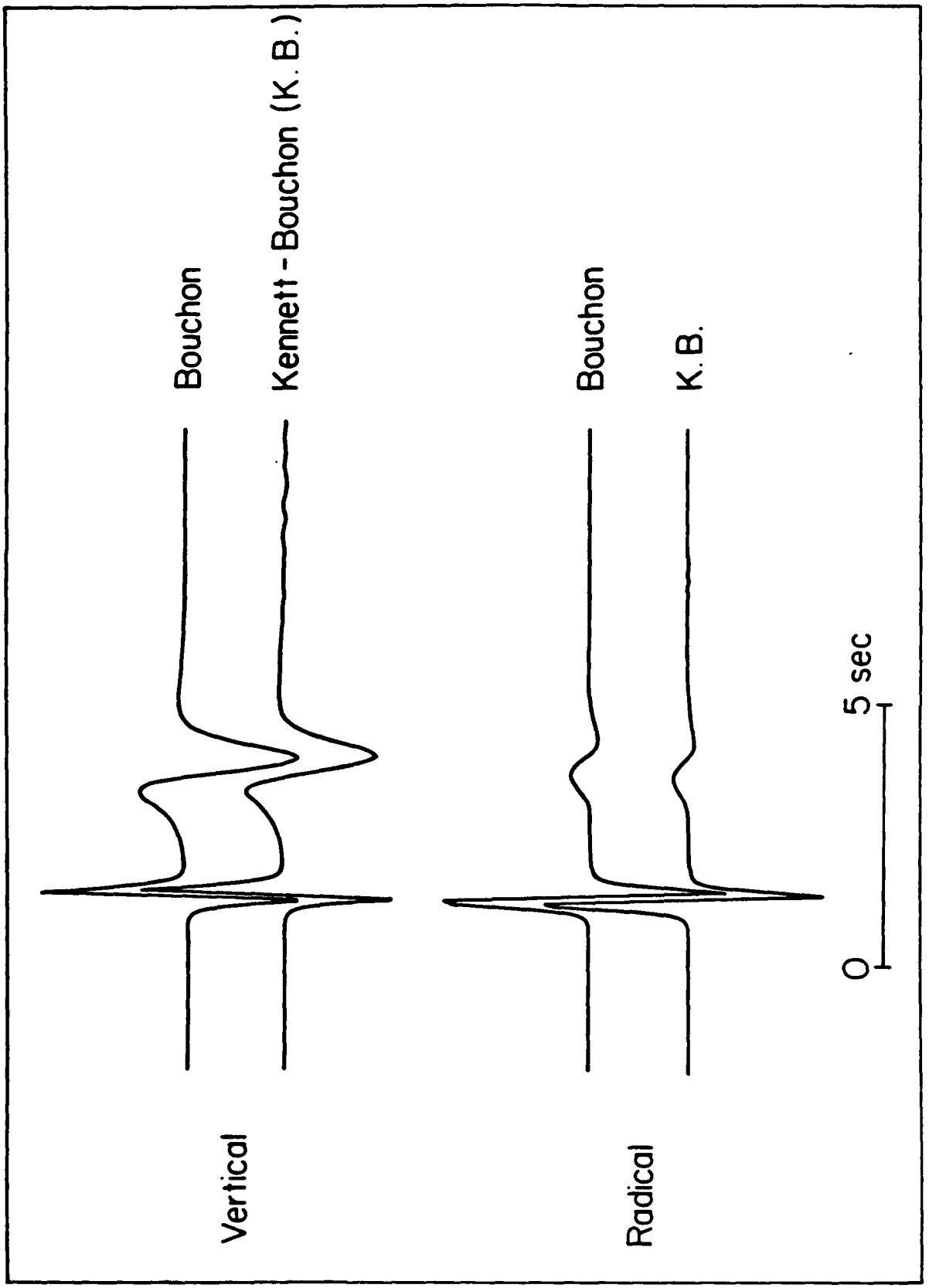
Vertical
Bouchon
Kennett - Bouchon (K. B.)
Radical
Bouchon
K.B.
0
5 sec

Fig. 2

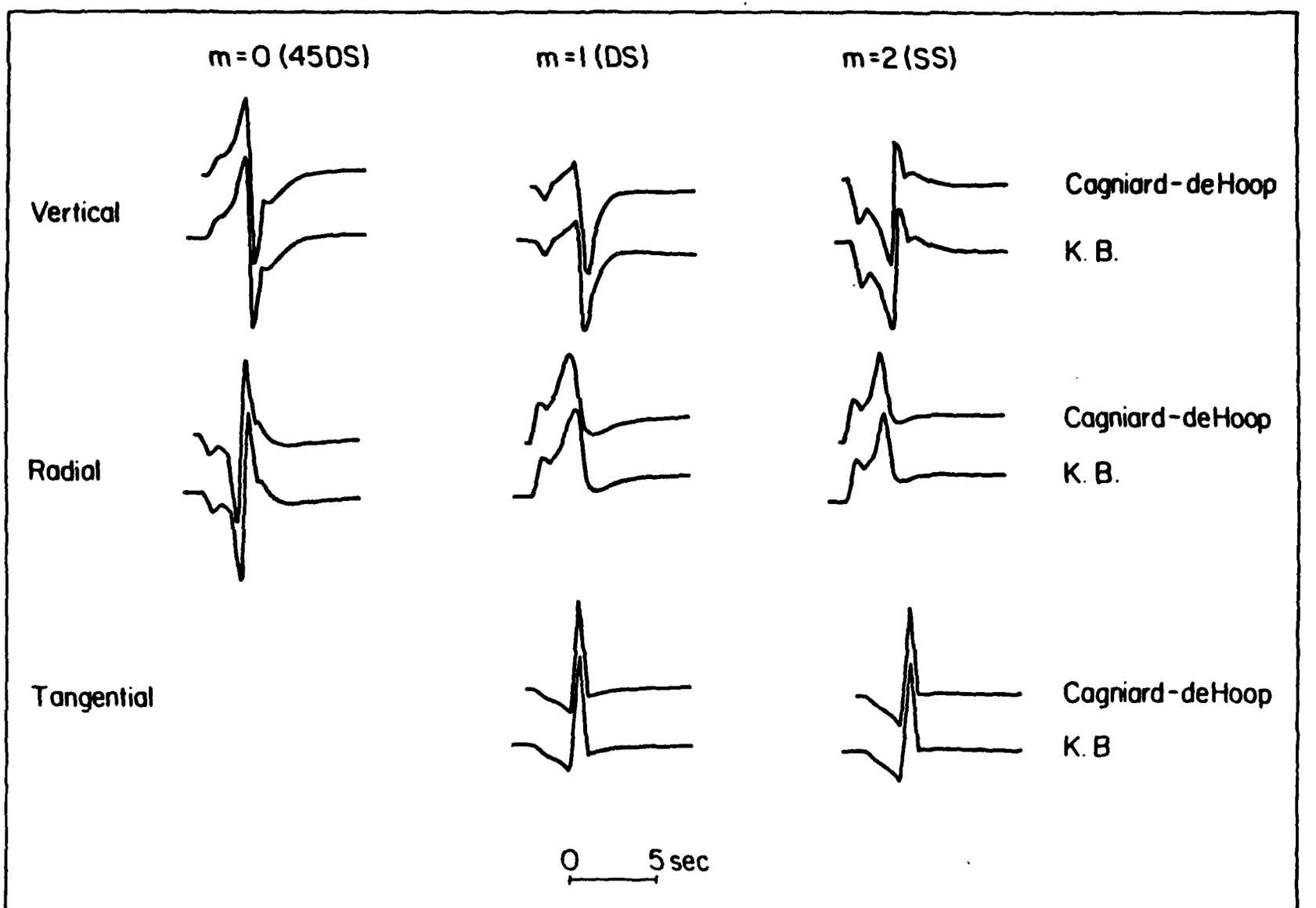
m=0 (45DS)
m=1 (DS)
m=2 (SS)
Vertical
Radial
Tangential
Cagniard-deHoop
K. B.
Cagniard-deHoop
K. B.
Cagniard-deHoop
K. B
0
5 sec

Fig. 3

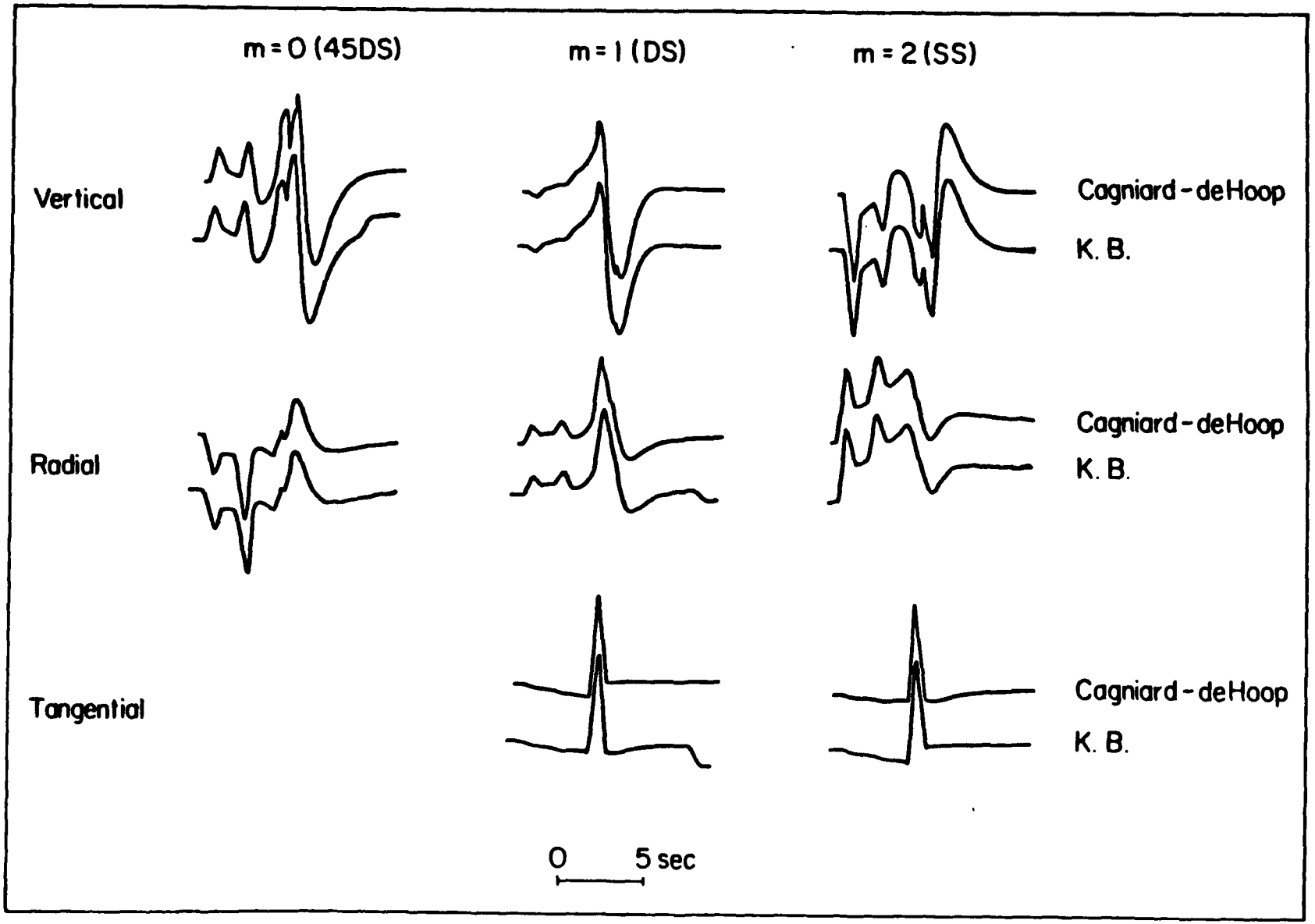
m = 0 (45DS)
m = 1 (DS)
m = 2 (SS)
Vertical
Radial
Tangential
Cagniard - deHoop
K. B.
Cagniard - deHoop
K. B.
Cagniard - deHoop
K. B.
0
5 sec

Fig. 4

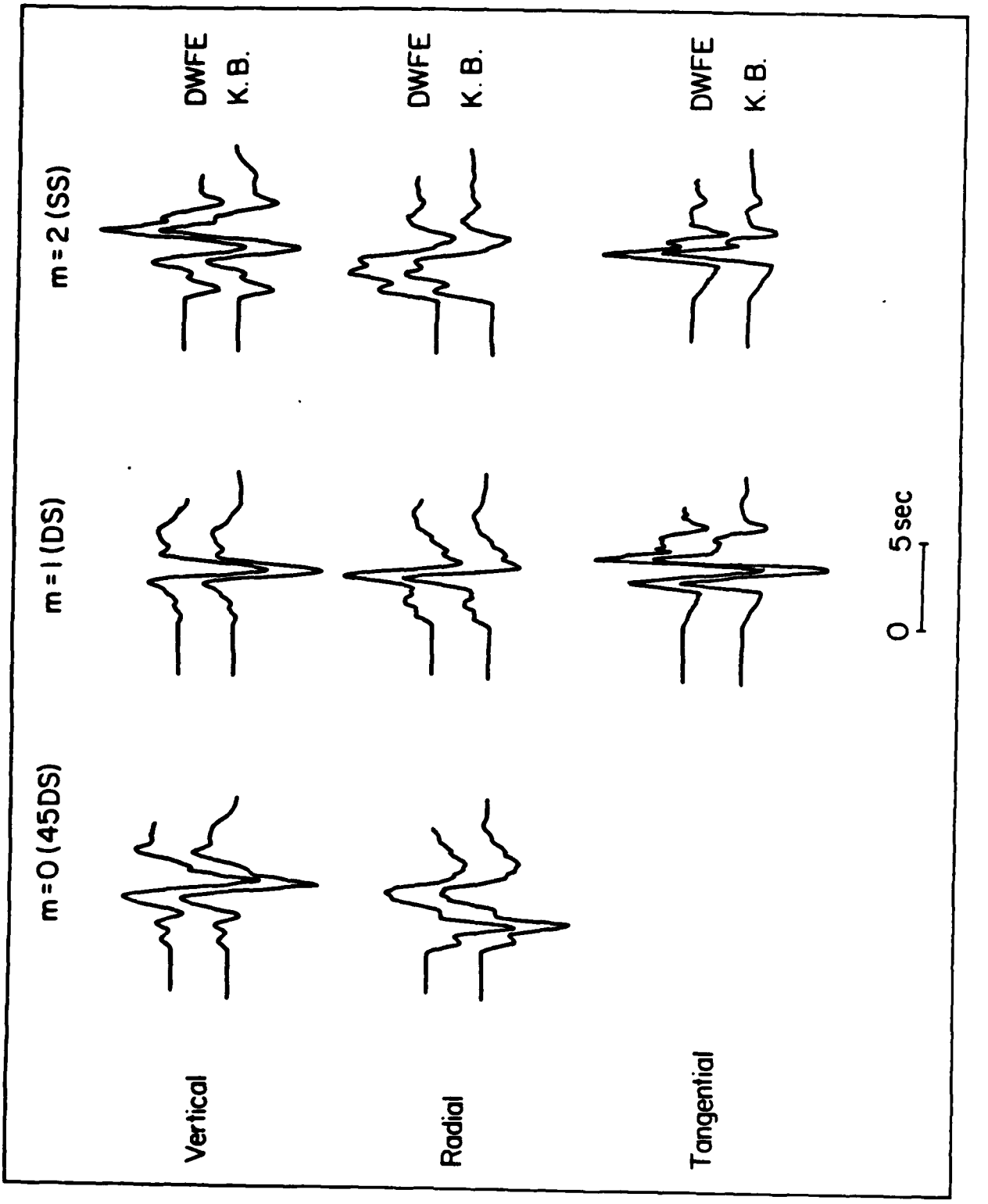
m=0 (45DS)
m=1 (DS)
m=2 (SS)
DWFE
K.B.
DWFE
K.B.
DWFE
K.B.
Vertical
Radial
Tangential
0
5 sec

Fig. 5

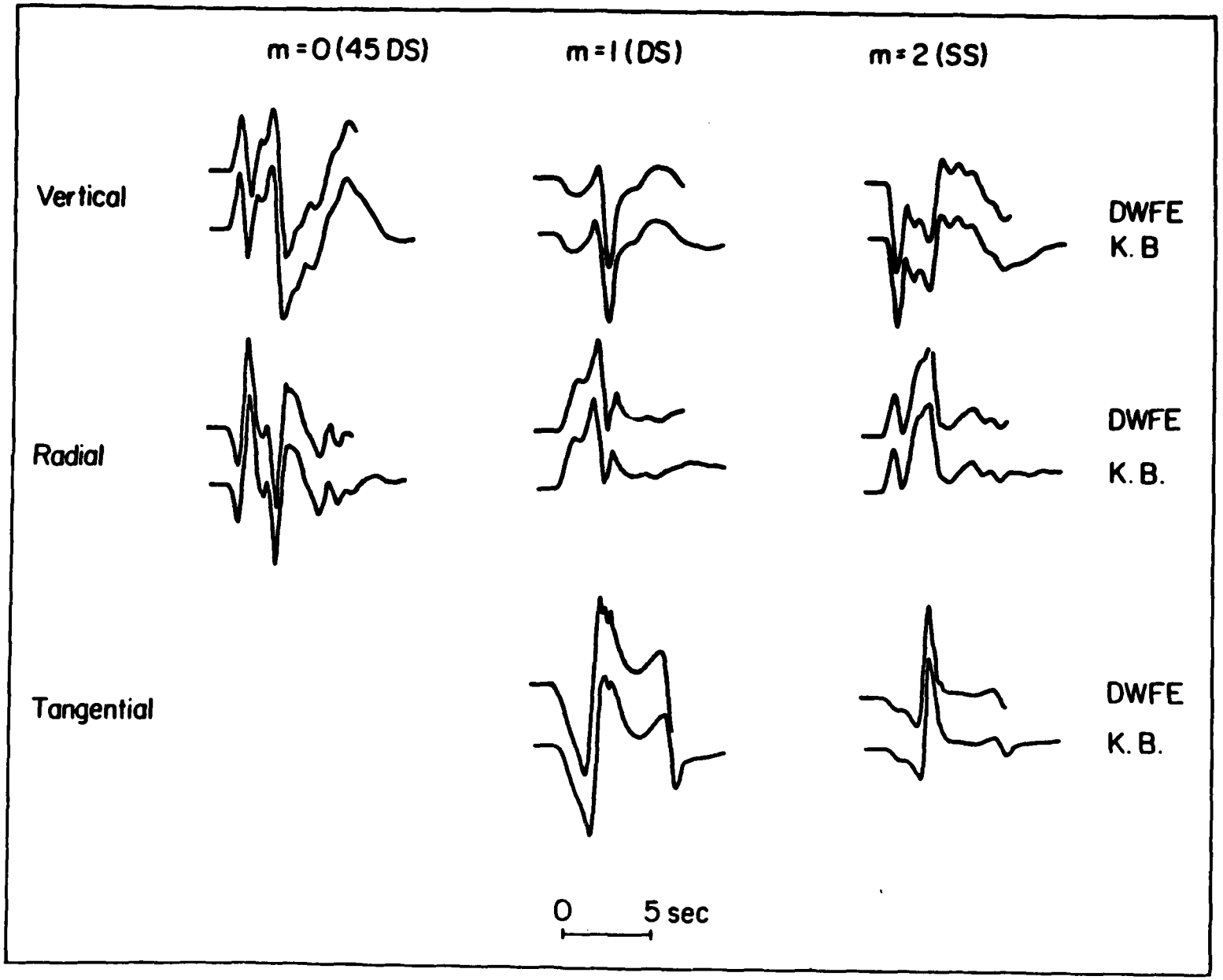
m = 0 (45 DS)
m = 1 (DS)
m = 2 (SS)
Vertical
Radial
Tangential
DWFE
K. B
DWFE
K. B.
DWFE
K. B.
0
5 sec

Fig. 6

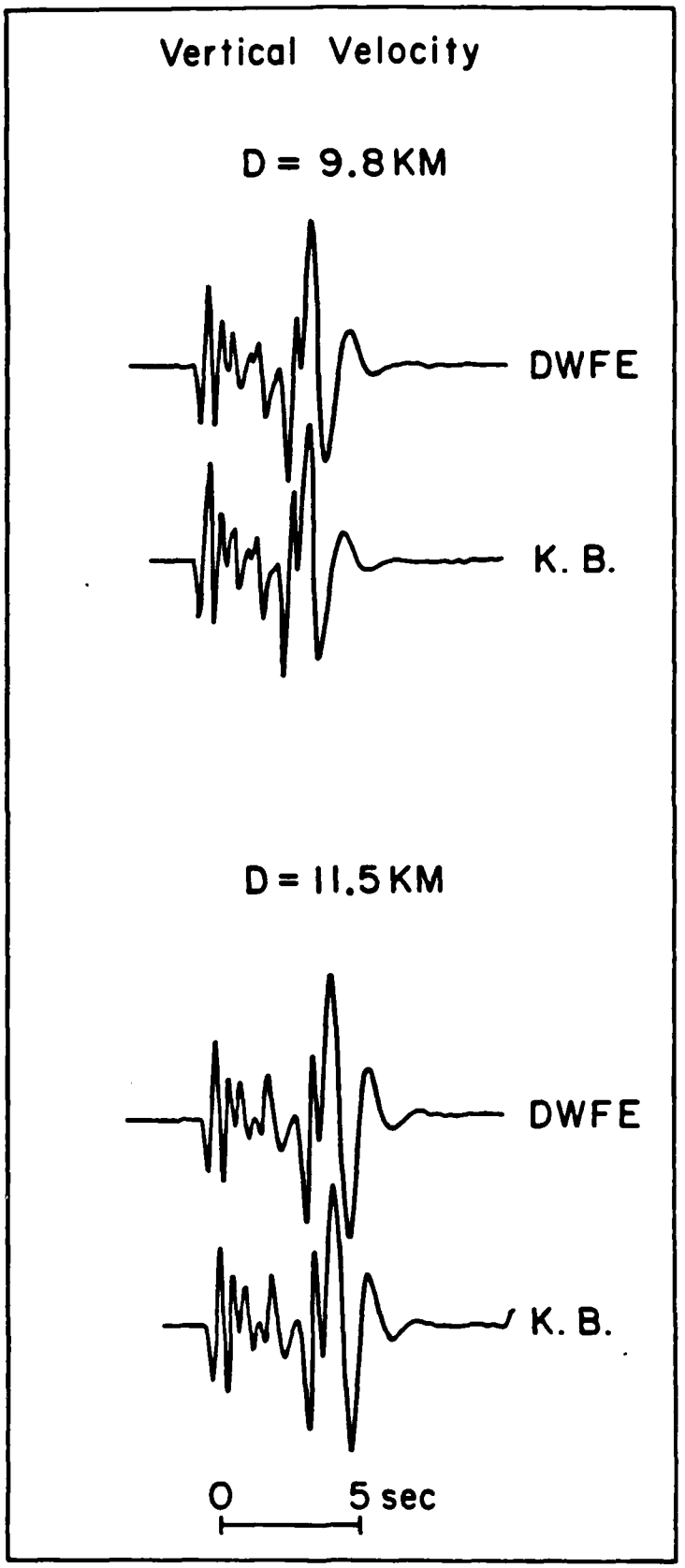

Fig. 7

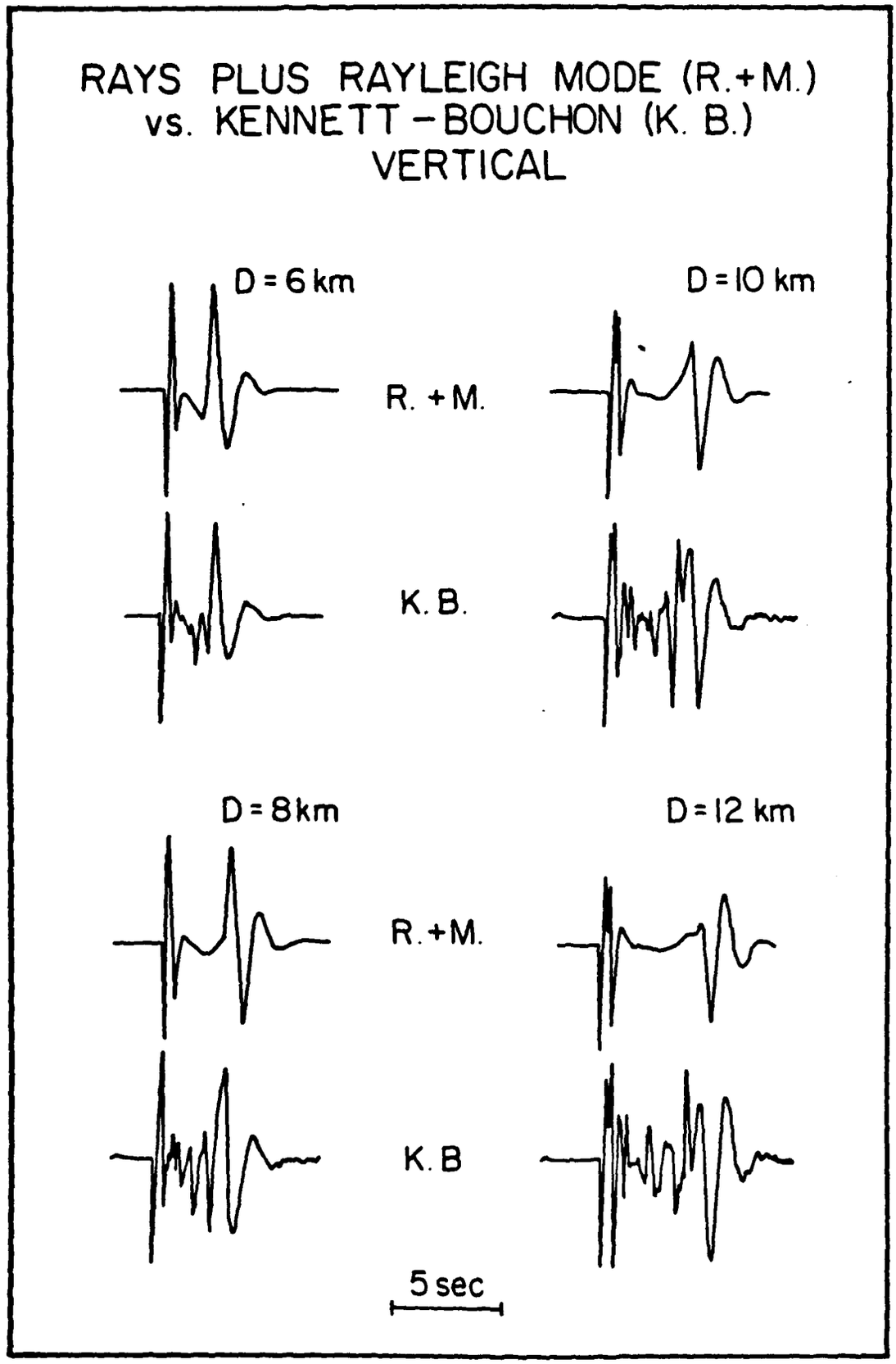
RAYS PLUS RAYLEIGH MODE (R.+M.)
vs. KENNETT-BOUCHON (K. B.)
VERTICAL
D = 6 km
D = 10 km
R. + M.
K. B.
D = 8 km
D = 12 km
R. + M.
K. B
5 sec

Fig. 8

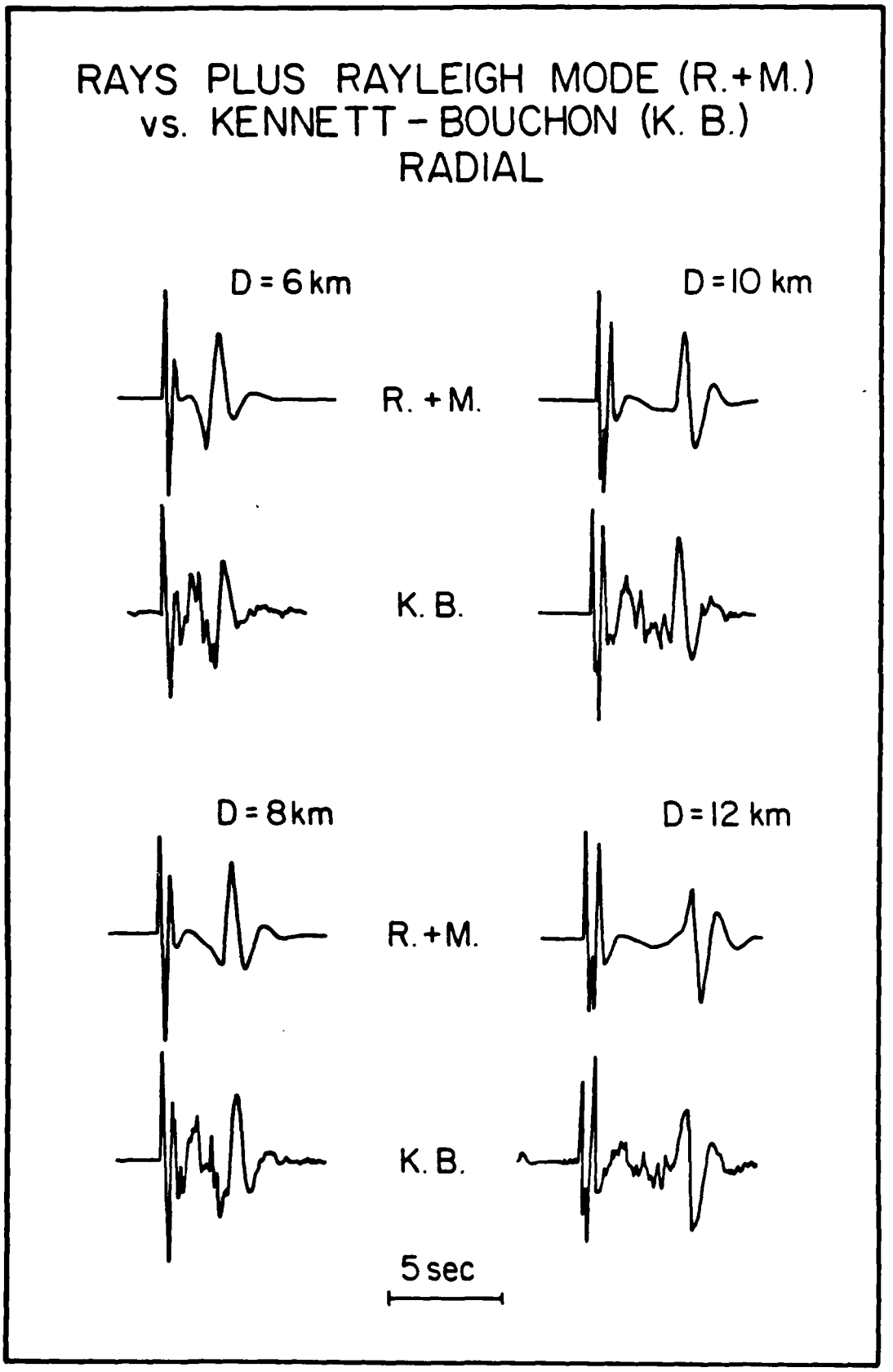
RAYS PLUS RAYLEIGH MODE (R.+M.)
vs. KENNETT - BOUCHON (K. B.)
RADIAL
D = 6 km
D = 10 km
R. + M.
K. B.
D = 8 km
D = 12 km
R. + M.
K. B.
5 sec

Fig. 9

III

Body Wave Amplitude and Travel Time Correlations Across North America

Thorne Lay and Donald V. Helmberger

Seismological Laboratory
California Institute of Technology
Pasadena, California 91125

Revised
February 15, 1983

Submitted to Bulletin of the Seismological Society of America

Abstract

Relationships between travel time and amplitude station anomalies are examined for short- and long-period SH-waves and short-period P-waves recorded at North American WWSSN and CSN stations. Data for two azimuths of approach to North America are analyzed. To facilitate intercomparison of the data, the S-wave travel times and amplitudes are measured from the same records, and the amplitude data processing is similar for both P- and S-waves. Short-period P- and S-wave amplitudes have similar regional variations, being relatively low in the western tectonic region and enhanced in the shield and mid-continental regions. The east coast has intermediate amplitude anomalies and systematic, large azimuthal travel time variations. There is a general correlation between diminished short-period amplitudes and late S-wave arrival times and enhanced amplitudes and early arrivals. However, this correlation is not obvious within the eastern and western provinces separately, and the data are consistent with a step-like shift in amplitude level across the Rocky Mountain front. Long-period S-waves show no overall correlation between amplitude and travel time anomalies.

Introduction

It has long been indicated that there is a general association between P-wave amplitude and travel time anomalies across North America [Herrin and Taggard, 1962; Romney et al., 1962]. P- and S-wave amplitude and travel time station anomalies show similar regional variations with diminished amplitudes and late arrival times in the Basin and Range and Rocky Mountain provinces, and enhanced amplitudes and early arrivals in the Great Plains and shield areas [e.g. Cleary,

1967; Evernden and Clark, 1970; Sengupta, 1975; North, 1977]. However, this correlation is not a simple one, even for the few studies which measure the amplitudes and travel times from the same data [Cleary, 1967; Sengupta, 1975], and does not appear to exist on a global basis [Shore, 1982].

The North American observations are usually attributed to coupled lateral variations in the upper mantle low velocity and low Q zones between western and eastern North America, [e.g. Hales et al., 1968; Hales and Herrin, 1972], though it is only relatively recently that actual measurements of lateral variations in attenuation have been shown to correlate with amplitude anomalies [Der and McElfresh, 1977; Der et al., 1979, 1982; Lay and Helmberger, 1981]. These studies have shown that there is a regional variation in attenuation associated with a baseline shift in amplitude levels between the two major provinces, but a large amount of amplitude variation within each region is not correlated with attenuation differences.

In this paper we attempt to quantify the degree of correlation between body wave amplitude and travel time variations across North America for short- and long-period SH and short-period P phases. Where possible, the amplitude and travel time measurements are made from the same records, and the method of amplitude analysis is the same for all observations, which allows us to more confidently compare the station anomalies than previous work. Data from two azimuths are processed and compared separately to avoid averaging out subtle trends.

Amplitude and Travel Time Data

The S-wave travel time and amplitude observations presented here

were recorded at North American WWSSN and Canadian Seismic Network (CSN) stations. Seventeen moderate size (m_b = 5.5-6.0) intermediate and deep focus earthquakes in Argentina and the Sea of Okhotsk were selected for analysis on the basis of their simple, impulsive waveforms and stable SH radiation patterns to North America. The station and event epicenter locations are shown in Figure 1. The short- and long-period horizontal components in the distance range 40^{o} to 80^{o} were digitized and rotated into transverse and radial polarizations, and amplitude and travel time measurements were made for the SH components. The first peak-to-first trough and first peak amplitudes were measured for the short- and long-period signals respectively. Figure 2 shows representative SH waveforms for one of the Argentine events. The travel times and amplitudes of these simple phases can be reliably measured. Radiation pattern corrections were determined from focal mechanisms constrained by P-wave first motions, S-wave polarizations, and long-period SV/SH amplitude ratios, and these corrections were applied to the amplitude data along with instrument gain and geometric spreading corrections. Station anomalies were then determined by removing relative event size factors (for amplitudes) and baseline shifts in the JB residuals (for travel times) using the procedures described in Lay and Helmberger [1981] and Lay [1982]. The data for the two source regions were processed separately.

A similar set of short-period P-wave amplitudes has been presented by Butler and Ruff [1980] and extended by Butler et al. [1979]. Earthquakes in South America and in source regions to the northwest of North America, as well as Russian nuclear explosions at five test sites

were used to determine relative P-wave amplitude patterns for three azimuths to North American WWSSN stations. The data were selected, measured, and processed in a manner similar to that used in the S-wave analysis, though radiation pattern corrections were not applied to the earthquake data. The stability of the relative amplitude behavior between events and the coherence of the waveforms for each event indicate that the source radiation corrections are small for the narrow azimuth range spanned by the receivers, as was found for the S-waves. The corresponding P-wave travel times were not measured, but a recent study by Dziewonski and Anderson [1982] provides the most reliable azimuthally dependent P-wave travel time station anomalies for North America presently available. The processing and quantity of data in that study were significantly different than for the other data sets, but it is of interest to compare the azimuthally dependent S- and P-wave station travel time anomalies.

Comparison of North American Station Anomalies

The Argentine and Sea of Okhotsk S-wave travel time and short-period amplitude anomalies are shown in Figure 3 and tabulated in Table 1. The travel time residuals were determined using the short- and long-period data combined (see Lay [1982] for procedure), because the relative residuals are not frequency dependent. S-wave station travel time anomalies for the Bolivian and Peruvian source regions are also shown in Figure 3. The amplitudes for these events were not measured because the signals are complicated and dominated by SV radiation. In the top figure the travel time anomaly patterns for each source region have been baseline shifted to minimize the scatter at the first 11

stations from the left, which are western and Texas stations. These small shifts were applied in order to simplify comparison of the relatve patterns across North America observed for each source region. The asterisked stations are located in western North America, as shown in Figure 1. The stations are ordered in azimuth from the Argentine source region, and only those stations at which anomalies could be determined from both azimuths are shown.

Figure 3 demonstrates that the SH travel times are relatively late (positive) and the amplitudes are relatively low at western stations for both azimuths. The central United States stations record arrivals 4 to 5 sec earlier than the western stations, and the amplitudes are 4 to 5 times larger as well. The east coast stations record intermediate amplitudes and show the clearest evidence for azimuthal variations in travel time anomalies. Relative to the central and western stations, the east coast stations record early arrivals from the Sea of Okhotsk and late arrivals from Argentina. Other South American source regions show relatively earlier arrivals in the east coast than observed for Argentina. This indicates that significant near-source or deep mantle velocity structure affects the relative travel time pattern from Argentina. This is discussed in greater detail below and by Lay [1982], who concludes that the Argentine signals recorded in the east coast are anomalously late because they encounter a localized low-velocity region in the lower mantle. Some of the azimuthal variation observed at east coast stations may also be due to strong lateral gradients in upper mantle shear velocity structure, with the velocity increasing toward the Canadian shield. The short period SH amplitudes do not show similar

azimuthal variations.

In Figure 4 the S-wave amplitude and travel time anomalies for both source regions are compared. All of the available determinations are included, with the solid symbols indicating Argentine observations. The general features are similar for both azimuths, though the long-period amplitudes from Argentina have more scatter than observed for the Sea of Okhotsk data. The short-period amplitude anomalies clearly have a much greater range in variation than the long-periods, as has been observed for P-waves [Booth et al., 1974; Sengupta, 1975]. The short-periods also show a tendency for late arrivals (positive residuals) to be low amplitude, which is not apparent in the long-periods. Booth et al. [1974] found little correlation between short- and long-period P-wave amplitude variations, and argued that this supports the interpretation that the short-period amplitude variations are due to Q variations.

Using the major axis regression described by York [1966], relations between the logarithms of the short-period S-wave amplitudes (A_{SPS}) and long-period S-wave amplitudes (A_{LPS}) and the S-wave travel time anomalies (T_S) have been determined. The relations found for equal weighting of each data point and using all of the data are indicated in Figure 4 and given by:

$$\log A_{SPS} = -0.340(\pm 0.035) - 0.047(\pm 0.015)T_S$$

$$\log A_{LPS} = -0.256(\pm 0.016) + 0.004(\pm 0.007)T_S$$

The intercept values are not significant due to the arbitrary baselines in both parameters. There is a weak, resolvable correlation between the log of the short-period amplitudes and the travel time anomalies, with a linear correlation coefficient, r, of -0.341, but the long-period

amplitudes do not show similar behavior, as the correlation coefficient is 0.077. More sophisticated weighting schemes can be employed, but the errors involved in amplitude and travel time measurements are quite different in nature, and rigorous statistics may not be useful. The regressions presented here are intended only to indicate the relative degree of correlation between parameters.

In a detailed investigation of S and ScS-S travel time anomalies for deep South American and Sea of Okhotsk events recorded in North America, Lay [1982] concluded that the Argentine S-wave data is contaminated by lower mantle anomalies. Large, localized velocity anomalies are observed at East Coast and Mississippi Valley stations. As seen in Figure 3, these stations show strong azimuthal variations in S-residuals as well as distance dependence of S-residuals between source regions in Peru, Bolivia and Argentina. The travel time anomalies are as much as 5 sec, and are not apparent in the ScS arrivals from the same events, which suggests a lower mantle origin. The greater range in long-period amplitude anomalies for the Argentine data appears to be associated with these travel time anomalies as well. To ensure that these strong anomalies do not dominate the patterns in Figure 4, we have omitted the Argentine observations identified as anomalous by Lay [1982] (see Table 1) in Figure 5. Different symbols have been used for stations to the east (circles) and to the west (triangles) of the Rocky Mountains. The stations placed in each category are indicated in Table 1 and Figure 1. Because the station distribution is rather sparse, we do not attempt to define more subregions, though there is ample evidence for distinct behavior for the Pacific Coast stations and central U.S.

stations. Figure 5 clearly indicates the tendency for western stations, which are slow, to record diminished short-period S-wave amplitudes, but the long-periods show no regional pattern. The regression curves shown in Figure 5 are given by:

$$\log A_{SPS} = -0.344(\pm 0.040) - 0.042(\pm 0.017)T_S$$

$$\log A_{LPS} = -0.250(\pm 0.016) - 0.001(\pm 0.006)T_S$$

The results are not significantly changed if all East Coast observations from the Sea of Okhotsk are omitted as well. The short periods have a correlation coefficient of r=-0.316 and the long periods yield r=-0.013.

The short-period S-wave amplitudes in Figure 5 appear to have more of a baseline shift between the eastern and western provinces than a smoothly varying distribution of amplitudes. The filled squares in Figure 5a indicate the average amplitude and travel time anomalies for each region. There is an amplitude factor of 2.4 and a 4.0 sec travel time shift between the means. Romanowicz and Cara [1980] have shown that if more than one physical parameter varies in the upper mantle (e.g. both velocity and thickness of the low velocity zone), it is possible to have baseline shifts in relative travel time variations. A similar line of argument applies to Δt^* variations and, thus, possibly to amplitude variations. To test this, we performed regressions for the short-period S-wave amplitudes and station travel time residuals for the eastern and western provinces separately. The following relations were found;

$$\log A_{SPS} = -0.130(\pm 0.053) + 0.038(\pm 0.022)T_S \text{ (East)}$$

$$\log A_{SPS} = -0.861(\pm 0.142) + 0.118(\pm 0.057)T_S \text{ (West)}$$

While the absolute levels of these lines are resolvably different, it is

interesting to note that the slopes have reversed in sign from that for the overall trend, as have the corresponding correlation coefficients, $r = 0.272$ (East) and $r = 0.428$ (West). This may be an artifact of the reduced population sizes and large intrinsic amplitude scatter, however it may also be taken as a breakdown of the correlation between amplitudes and attenuation if one adopts the assumption that attenuation variations are coupled to velocity variations. There are clearly many scattering and focusing effects that would produce anomalous amplitude behavior with no travel time signature, or with a correlation opposite to that expected for attenuation variations.

Lay [1982] suggests that the most pronounced long-period amplitude anomalies for the Argentine data are associated with the anomalous travel times produced by lower mantle anomalies, with enhanced amplitudes accompanying large travel time delays and diminished amplitudes accompanying large travel time advances. This indicates a geometric effect rather than attenuation-controlled behavior. If the eastern and western long-period data in Figure 5b are considered separately, the following regressions are found:

$$\log A_{LPS} = -0.190(\pm 0.026) + 0.021(\pm 0.011)T_S \text{ (East)}$$

$$\log A_{LPS} = -0.374(\pm 0.045) + 0.035(\pm 0.019)T_S \text{ (West)}$$

The correlation coefficients are $r = 0.289$ (East) and $r = 0.381$ (West). This indicates that even after the anomalous Argentine data are omitted there is a weak tendency for long-period amplitudes to be enhanced for late arrivals, but this is only apparent when the two provinces are isolated. The average long-period amplitude levels in Figure 5b only differ by 18%.

Several authors have noted that while S-wave travel time residuals have an overall variation 4 times greater than the P-wave residuals for North America, the short-period amplitudes have more comparable variations, with S-waves varying about twice as much as P-waves [Sengupta, 1975; Der et al., 1975, 1982; Lay and Helmberger, 1981]. The latter observation is consistent with the trend expected for attenuation-controlled amplitudes for predominantly shear losses [Lay and Helmberger, 1981]. The short-period S- and P-wave amplitude anomalies are compared in Figure 6. Figure 6a presents the data for South American earthquakes. The regression between the S and P (A_{SPP}) amplitudes is given by:

$$\log A_{SPS} = -0.397(\pm 0.059) + 1.926(\pm 0.338) \log A_{SPP}$$

This indicates a factor of two greater range in the S-wave anomalies and a relatively good degree of correlation ($r = 0.802$) for the southern azimuth. For the northwestern azimuth (Figure 6b) a similar relation is found:

$$\log A_{SPS} = -0.414(\pm 0.050) + 1.698(\pm 0.310) \log A_{SPP}$$

The correlation coefficient is $r = 0.767$. In both cases the amplitude anomalies have been determined for earthquakes spanning a fairly small range in azimuth from each station. Comparison of the S anomalies from the Sea of Okhotsk with the average P anomalies from all Russian test sites (which generally span a northern azimuth from each station) shows greater scatter (Figure 6c). The corresponding relation is:

$$\log A_{SPS} = -0.292(\pm 0.142) + 2.591(\pm 1.581) \log A_{SPP}$$

This increase in scatter ($r = 0.337$) may reflect the azimuthal sensitivity of the receiver structures beneath the WWSSN stations, or it

may indicate the greater variability of amplitude patterns for shallow high frequency events. The similarity of the relations for the northwestern and southern azimuths argues against the first alternative, whereas Butler and Ruff [1980] have shown that amplitude patterns for explosions at sites in as close a proximity as Northern and Southern Novaya Zemlya can have significant relative trends. This may be due to near source structure or contamination due to tectonic release.

Lay and Helmberger [1981] have shown that long-period P and SH amplitude patterns from South America track rather closely as well, with relative variations being consistent with attenuation variations assuming all losses are in shear. However, the long-period amplitude variations are so large that explaining them by frequency-independent Q variations predicts short-period amplitude patterns that are poorly correlated with and have a larger range than those observed. While frequency dependent models can be contrived to reconcile the data there is little correlation with geographic province or travel time anomalies. This indicates that receiver structure or propagational effects dominate the long-period amplitudes, as was proposed by Booth et al., 1974, and it is possible that part of the correlation in short-period amplitudes for P and SH is produced by receiver variations as well. Computation of amplification effects for plane layered receiver structures using the Haskell matrix techniques indicate that relative short-period P- and S-wave amplitudes can track closely for a wide range of models. It is also interesting to note that Δt^* estimates made from long-period body wave spectra do not accurately predict short- or long-period amplitude variations for North America [Lay and Helmberger, 1981], nor are they

well correlated with short-period travel time anomalies on a global scale [Mikami and Hirahara, 1981]. This may suggest that the Δt^* estimates at long periods are contaminated by three dimensional receiver structure or other effects not related to upper mantle attenuation.

The correlations shown above between short-period S amplitudes and travel times and short-period P and S amplitudes predict a correlation between P amplitudes and S travel times. This is in fact observed as shown in Figure 7. The P amplitude anomalies from the northwestern azimuth are compared with the S travel times from the Sea of Okhotsk, with the relation between them being

$$\log A_{SPP} = -0.001(\pm 0.043) - 0.026(\pm 0.017)T_S$$

A value of $r = -0.318$ was found for this comparison. Once again, it appears that a steplike shift in the amplitude level between the fast eastern (circles) and slow western (triangles) provinces is an equally valid interpretation.

Numerous studies have found that for North America S-wave travel time anomalies are roughly four times the corresponding P-wave anomalies [Doyle and Hales, 1967; Hales and Roberts, 1970; Sengupta, 1975]. This requires upper mantle variations preferentially affecting the rigidity [Hales and Doyle, 1967; Hales and Herrin, 1972]. On a global basis the relation between S and P anomalies appears to be different from that for North America, with a relative factor of 1.8 to 2.4, which does not require significant lateral variations in Poisson's ratio [Poupinet, 1977; Wickens and Buchbinder, 1980]. It has also been proposed that the relation for North America has been misinterpreted if more than one physical parameter varies in the upper mantle [Romanowicz

and Cara, 1980].

In Figure 8 we compare the S-wave travel time residuals from the Sea of Okhotsk and Argentina with the azimuthally dependent P-wave station anomalies (T_P) of Dziewonski and Anderson [1982], which have the form

$$T_P = A + B \cos(\phi-\phi_1) + C \cos[2(\phi-\phi_2)]$$

The azimuths, ϕ, used to compute the P residuals are the appropriate azimuths from each station to the Sea of Okhotsk and Argentine source regions. Figures 8a-8c show the northwestern azimuth comparison, with the first panel using the azimuthally independent term (A) of the P residual only; the second including the $\cos\phi$ term; and the third including the $\cos 2\phi$ term as well. Since not all 5 coefficients could be determined for each station there is a slight attrition as higher order terms are added. However, this does not account for the significant reduction in scatter of the correlations as the azimuthal terms are included ($r = 0.45, 0.62, 0.77$ in Figures 8a, 8b and 8c respectively). The value of the slope given by the major axis regression is indicated in each panel. Stations in western North America are indicated by triangles. Note that these are slow for both P and S, and there is little overlap between the provinces. The slope in Figure 8c is somewhat higher than the typical value of approximately 4, and the small scatter indicates that this may be significant. The lower value has always been determined using azimuthally averaged data, which may have resulted in an underestimation of the relative behavior, or it may be that the Sea of Okhotsk source region and/or lower mantle path effects account for the discrepancy.

The Argentine comparisons are shown in Figures 8d-8f. Here the reduction in number of stations with higher order P anomaly azimuthal terms is more severe, but there is again some indication that a slope significantly higher than 4 may be appropriate (r = 0.45, 0.45, 0.68 in Figures 8d, 8e and 8f respectively). The separation between the eastern and western provinces is not as clear as for the other azimuth, which results from the anomalous S and P travel time anomalies that affect the East Coast stations. The azimuthal variations are similar for both P and S for the latter stations, and are too strong to be produced at shallow depth in the upper mantle. It is likely that some of the lower mantle path anomaly detected in the S-waves by Lay [1982] has been mapped into the P-wave station anomalies for the southern azimuth. For both azimuths the correspondence between P and S travel time anomalies is quite good and there is little evidence for a baseline shift and decreased slope between the eastern and western provinces like those indicated by Romanowicz and Cara [1980]. The importance of azimuthal terms in the station anomalies is strongly supported by these data.

Discussion

By determining the relationships between travel time residuals, amplitude anomalies and attenuation variations it will ultimately be possible to constrain some important upper mantle processes, following approaches similar to that first employed by Solomon [1972]. This paper has shown that there is a clear, though weak, correlation between short-period P and S amplitude anomalies and S-wave travel time residuals. In general, western North America records low amplitudes and late arrivals relative to the east. While this result is qualitatively

consistent with many previous studies, it is the first to compare a large data set of short-period S amplitudes and travel times obtained from the same signals with P amplitudes that are similarly processed.

It is strongly indicated that a steplike change in amplitude level occurs across the Rocky Mountain front, with amplitudes within the eastern and western provinces being poorly correlated with travel time variations. The step between the average short-period S-wave amplitude levels is a factor of 2.4, which approximately corresponds to a $\Delta t^*_\beta = 0.8$ sec for the 2-4 sec periods of the observations [Lay and Helmberger, 1981]. Assuming all losses are in shear, this indicates $\Delta t^*_\alpha = 0.2$ sec, which produces a factor of two variation in amplitude at 1 sec period. This is consistent with the average Δm_b (0.26) value between the provinces [Booth et al., 1974; Der et al., 1975], and with average differences in Δt^*_α from high frequency spectral analysis [Der et al., 1982]. The long-period S-wave amplitude variation predicted for $\Delta t^*_\beta = 0.8$ sec is about 20% [Lay and Helmberger, 1981], which is consistent with the 18% variation found in Figure 5b. The associated S-wave travel time step is about 4 sec. Superimposed on this attenuation-controlled amplitude variation are many individual station variations that are not associated with travel time anomalies and presumably reflect receiver structure or scattering effects within the mantle. These amplitude variations are comparable to those produced by attenuation variations. The long-period SH-wave amplitudes show no overall correlation with travel time anomalies, though within each province there is a tendency for later arrivals to be enhanced, thus it is probable that receiver structure or other propagation effects are

responsible for much of the substantial variation in long-period amplitudes. There is recent work using body waves that shows that lateral variations in upper mantle shear velocity structure beneath North America are distributed throughout the upper mantle to a depth of 400 km [Grand and Helmberger, 1983]. Future work with body waves will be needed to determine whether the variations in Q are similarly distributed or concentrated in a narrow channel.

The relative variation of S and P residuals may have a steeper slope than previously found in studies which neglect the azimuthal variations in station anomaly terms. If this proves generally valid, even more dramatic variations in rigidity in the upper mantle are required, or possibly alternate mechanisms such as anisotropy.

Acknowledgments

This research was supported in part by the National Science Foundation under grant NSF EAR 810-8616, and by the Advanced Research Projects Agency of the Department of Defense and was monitored by the Air Force Office of Scientific Research under Contract No. F49620-81-C-0008. Contribution No. 3852, Division of Geological and Planetary Sciences, California Institute of Technology, Pasadena, California, 91125, USA.

References

Booth, D. C., P. D. Marshall and J. B. Young, Long and short period P-wave amplitudes from earthquakes in the range 0^{o}-114^{o}, Geophys. J. Roy. Astr. Soc., 39. 523-537, 1974.

Butler, R. and L. Ruff, Teleseismic short-period amplitudes: source and receiver variations, Bull. Seism. Soc. Am., 70, 831-850, 1980.

Butler, R., L. J. Ruff, R. S. Hart and G. R. Mellman, Seismic waveform analysis of underground nuclear explosions, Technical Report, SGI-R-79-011, 1979.

Cleary, J., Analysis of the amplitudes of short-period P-waves recorded by Long Range Seismic Measurements stations in the distance range 30^{o} to 102^{o}, J. Geophys.Res., 72, 4705-4712, 1967.

Der, Z. A., R. P. Masse and J. P. Gurski, Regional attenuation of short-period P- and S-waves in the United States, Geophys. J. Roy. Astr. Soc., 40, 85-106, 1975.

Der, Z. A. and T. W. McElfresh, The relationship between anelastic attenuation and regional amplitude anomalies of short-period P-waves in North America, Bull. Seism. Soc. Amer., 67, 1303-1317, 1977.

Der, Z. A., T. W. McElfresh, C. P. Mrazek, Interpretation of short-period P-wave magnitude anomalies of selected LRSM stations, Bull. Seism. Soc. Amer., 69, 1149-1160, 1979.

Der, Z. A., T. W. McElfresh, A. O'Donnell, An investigation of the regional variations and frequency dependence of anelastic attenuation in the mantle under the United States in the 0.5-4.0 Hz band, Geophys. J. Roy. Astr. Soc., 69, 67-99, 1982.

Doyle, H. A. and A. L. Hales, An analysis of the travel times of S-waves to North American stations, in the distance range 28^{o} to 82^{o}, Bull. Seism. Soc. Amer., 57, 761-771, 1967.

Dziewonski, A. M. and D. L. Anderson, Travel times and station corrections for P-waves at teleseismic distances, J. Geophys. Res., submitted 1982.

Evernden, J. F. and D. M. Clark, Study of teleseismic P II-amplitude data, Phys. Earth. Planet. Int., 4, 24-31, 1970.

Grand, S. and D. V. Helmberger, Modeling upper mantle structure using SS, in preparation, 1983.

Hales, A. L. and H. A. Doyle, P and S travel time anomalies and their

interpretation, Geophys. J. Roy. Astr. Soc., 13, 403-415, 1967.

Hales, A. L. and E. Herrin, Travel times of seismic waves in nature of the solid Earth, pp. 172-215, ed. Robertson, E. C. McGraw-Hill, New York, 1972.

Hales, A. L. and J. L. Roberts, The travel times of S and SKS, Bull. Seism. Soc. Amer., 60, 461-489, 1970.

Hales, A. L., J. R. Cleary, H. A. Doyle, R. Green and J. Robert, P-wave station anomalies and the structure of the upper mantle, J. Geophys. Res., 73, 3885-3896, 1968.

Herrin, E. and J. Taggart, Regional variations in Pn velocity and their effect on the location of epicenters, Bull. Seism. Soc. Amer., 52, 1037-1046, 1962.

Lay, T., Localized velocity anomalies in the lower mantle, Geophys. J. Roy. Astr. Soc., 1983, in press.

Lay, T. and D. V. Helmberger, Body wave amplitude patterns and upper mantle attenuation variations across North America, Geophys. J. Roy. Astr. Soc., 66, 691-726, 1981.

Marshall, P. D., D. L. Springer and H. C. Rodean, Magnitude corrections for attenuation in the upper mantle, Geophys. J. Roy. Astr. Soc., 57, 609-638, 1979.

Mikami, N. and K. Hirahara, Global distribution of long-period P-wave attenuation and its tectonic implications, J. Phys. Earth, 29, 97-117, 1981.

North, R. G., Station magnitude bias: Its determination causes and effects, Report No. ESD-TR-77-85, Lincoln Laboratory, Lexington, Massachusetts, 1977.

Poupinet, G., Heterogeneities du manteau terrestre deduites de la propagation des ondes de volume: implication geodynamique, Thèse présentée à l'Université Scientifique et Médicale de Grenoble, 1977.

Romanowicz, B. A. and M. Cara, Reconsideration of the relations between S and P station anomalies in North America, Geophys. Res. Letters, 7, 417-420, 1980.

Romney, C., B. C. Brooks, R. H. Mansfield, D. S. Carter, J. N. Jordan and D. W. Gordon, Travel times and amplitudes of principal body phases recorded from Gnome, Bull. Seism. Soc. Amer., 52, 1057-1074, 1962.

Sengupta, M. K., The structure of the earth's mantle from body wave observations, ScD thesis, Massachusetts Institute of Technology, 578pp., 1975.

Shore, M. J., Seismic travel-time anomalies from events in the western Soviet Union, Bull. Seism. Soc. Amer., 72, 113-128, 1982.

Solomon, S. C., Seismic wave attenuation and partial melting in the upper mantle of North America, J. Geophys. Res., 77, 1483-1502, 1970.

Wickens, A. J. and G. G. R. Buchbinder, S-wave residuals in Canada, Bull. Seism. Soc. Amer., 70, 809-822, 1980.

York, D., Least-squares fitting of a straight line, Canadian J. of Phys., 44, 1079-1086, 1966.

Table 1

	Sea of Okhotsk			Argentina			
STA	A_{SPS}	A_{LPS}	T_S	A_{SPS}	A_{LPS}	T_S	
AAM	0.63	0.50	-2.87	0.69	0.53	-1.86	E
ALE	0.77	0.63	-2.28	----	----	----	E
ALQ	0.26	0.60	2.81	0.32	0.40	0.62	W
ATL	0.28	0.45	-2.71	0.22	0.39	-3.29	E
BEC	----	----	----	0.59	0.54	0.87	E
BKS	0.38	0.61	3.62	0.32	0.63	2.91	W
BLA	0.73	0.64	-1.23	0.67	0.64	0.85	E
BLC	----	0.67	-3.04	----	----	----	E
BOZ	0.18	0.61	1.50	0.10	0.29	1.00	W
CMC	1.19	1.30	-1.31	----	----	----	E
COR	0.38	0.54	3.36	----	----	----	W
DAL	0.66	0.40	-1.98	2.43	0.79	0.26*	E
DUG	0.33	0.61	4.36	0.13	0.46	3.39	W
EDM	0.63	0.71	-0.88	----	----	----	E
FBC	0.51	0.55	-5.43	----	----	----	E
FCC	0.93	0.72	-1.62	----	----	----	E
FFC	1.04	0.65	-0.10	----	----	----	E
FLO	0.79	0.51	-3.26	0.69	0.24	-3.81*	E
FSJ	0.96	0.65	2.58	----	----	----	W
GEO	0.29	0.53	-2.33	0.31	0.64	1.89*	E
GOL	0.18	0.47	1.92	0.16	0.46	1.41	W
GSC	0.22	0.47	1.78	0.30	0.46	3.12	W
GWC	1.31	0.73	-4.19	0.70	----	-0.62*	E
HAL	----	0.39	-1.91	0.53	0.81	0.50*	E
INK	----	0.71	-1.61	----	----	----	E
JCT	0.34	0.51	-1.12	0.72	0.54	-0.34	E
LHC	0.37	0.49	-4.80	0.54	0.50	-2.61	E
LND	----	----	----	0.39	1.42	-1.64	E
LON	0.09	0.56	0.77	----	----	----	W
LUB	0.40	0.57	0.26	1.03	0.59	-1.26	E
MBC	0.76	0.73	-1.00	----	----	----	E
MNT	0.36	0.79	-1.62	0.15	0.23	1.49*	E
OGD	0.34	0.37	-3.12	0.22	0.61	2.40*	E
OTT	1.06	0.54	-4.61	0.53	0.49	0.24*	E
OXF	2.69	0.55	-1.42	0.86	0.32	-3.59*	E
PHC	----	0.56	2.16	----	----	----	W
PNT	----	0.56	-0.53	----	----	----	W
RCD	1.15	0.70	1.21	0.69	0.36	1.26	E
RES	0.41	0.76	-0.23	----	----	----	E
SCB	----	0.60	-4.66	----	----	----	E
SCH	0.36	0.44	-2.40	0.33	0.52	-0.20*	E
SCP	0.75	0.45	-3.44	0.59	0.85	3.06*	E

SES	0.90	0.75	2.80	----	----	----	W
SFA	0.79	0.55	-2.69	0.69	0.71	1.95*	E
SHA	2.39	0.97	2.00	1.01	0.61	-2.64*	E
STJ	----	0.76	-0.54	0.81	0.79	0.97*	E
TUC	0.17	0.39	2.42	0.14	0.28	1.17	W
VIC	0.46	0.49	1.38	----	----	----	W
WES	0.54	0.53	-1.72	0.22	0.36	1.97*	E
YKC	0.45	0.59	-1.64	----	----	----	E

*Argentine data with anomalous travel times.

Figure Captions

Figure 1. Azimuthal equidistance projections centered on the Argentine (left) and Sea of Okhotsk (right) source regions. The locations of the intermediate and deep focus event epicenters and recording stations used in this study are shown. The stations with an asterisk are designated as stations within the western tectonic province. GSC, RCD and SCH are approximately 80° from the Argentine source region. SHA ranges from 78° to 88° from the Sea of Okhotsk events used.

Figure 2. Short- and long-period SH components and amplitude ratios of the Argentine event of January 17, 1967 recorded at North American WWSSN stations.

Figure 3. Top: The mean and standard error of the mean of the S-wave JB residuals at North American stations for the Sea of Okhotsk and South American source regions. Only those stations at which anomalies could be determined for both azimuths are shown. Source region baseline corrections have been determined using the first 11 stations from the left. Bottom: Comparison of the station amplitude anomalies from the Sea of Okhotsk and Argentina short-period SH data. The relative amplitudes have been adjusted to minimize the scatter at each station following the procedure described in Lay and Helmberger [1981].

Figure 4. (a) Comparison of short-period S-wave amplitude anomalies and station S-wave residuals in North America for the Sea of Okhotsk (empty symbols) and Argentina (filled symbols) source regions. (b) A similar comparison for long-period S-wave amplitude anomalies and S residuals. The curves are major axis regressions assuming equal weighting.

Figure 5. (a) Comparison of short-period S-wave amplitude anomalies and S residuals after anomalous East Coast and Mississippi Valley observations from Argentina are removed. Tectonic province stations are indicated by triangles. The squares indicate the mean travel time and amplitude values for the eastern and western provinces. The solid curve is a major axis regression for the whole data set, and the dashed curves are for the two provinces separately. (b) Same as in (a) but for the long-period S wave amplitudes.

Figure 6. Comparison between short-period WWSSN S and P amplitude anomalies for (a) South American earthquakes; (b) northwestern azimuth earthquakes; and (c) Sea of Okhotsk earthquakes (S) and Russian nuclear tests (P). Solid symbols indicate western U.S. stations.

Figure 7. Comparison between P wave amplitude anomalies and S wave travel time residuals for the northwestern azimuth. Triangles indicate western North America stations.

Figure 8. S and P travel time residuals for the Sea of Okhotsk azimuth (a)-(c) and the Argentina azimuth (d)-(f). The P-wave station anomalies of Dziewonski and Anderson [1982] are used with the azimuthally independent term alone (a),(d); inclusion of the first $\cos\phi$ term (b),(e); and inclusion of both the $\cos\phi$ and $\cos 2\phi$ terms (c),(f). The value of the slope in the regression $T_S = a + bT_P$ is given for each panel. Triangles indicate stations in the western tectonic province.

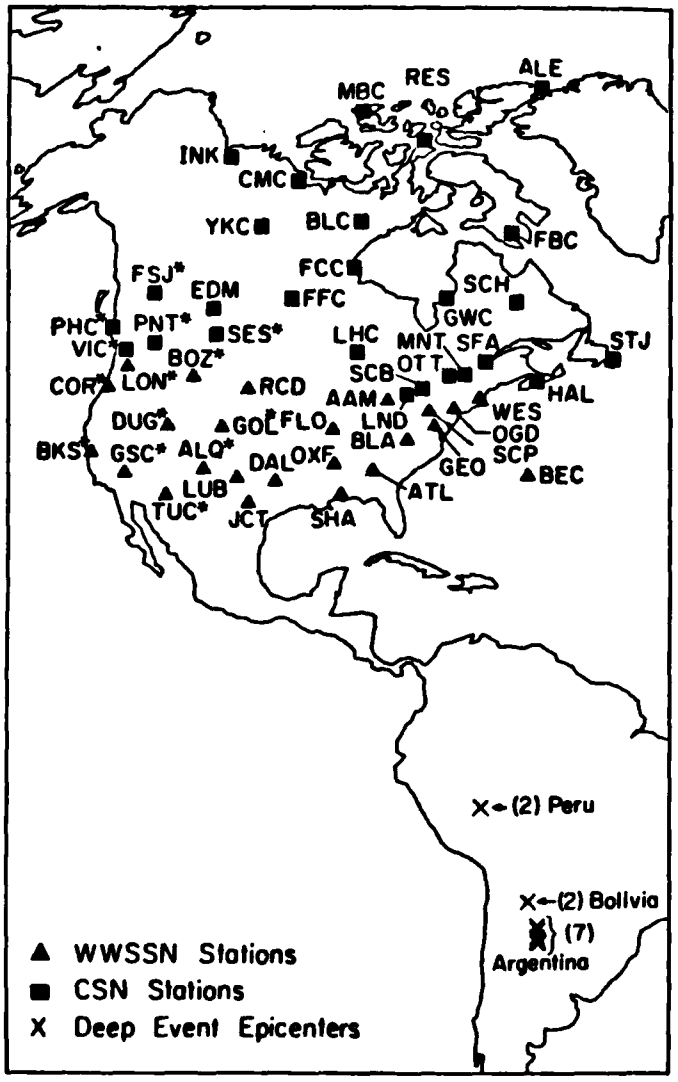
MBC
RES
ALE
INK
CMC
YKC
BLC
FBC
FSJ*
EDM
FCC
FFC
SCH
GWC
PHC*
PNT*
SES*
LHC
MNT
SFA
STJ
VIC*
BOZ*
OTT
COR*
LON*
RCD
SCB
HAL
AAM
WES
DUG*
GOL*
FLO
LND
OGD
BKS*
GSC*
ALO*
BLA
SCP
DAL
OXF
GEO
BEC
LUB
ATL
TUC*
JCT
SHA
X←(2) Peru
X←(2) Bolivia
(7)
Argentina
▲ WWSSN Stations
■ CSN Stations
X Deep Event Epicenters

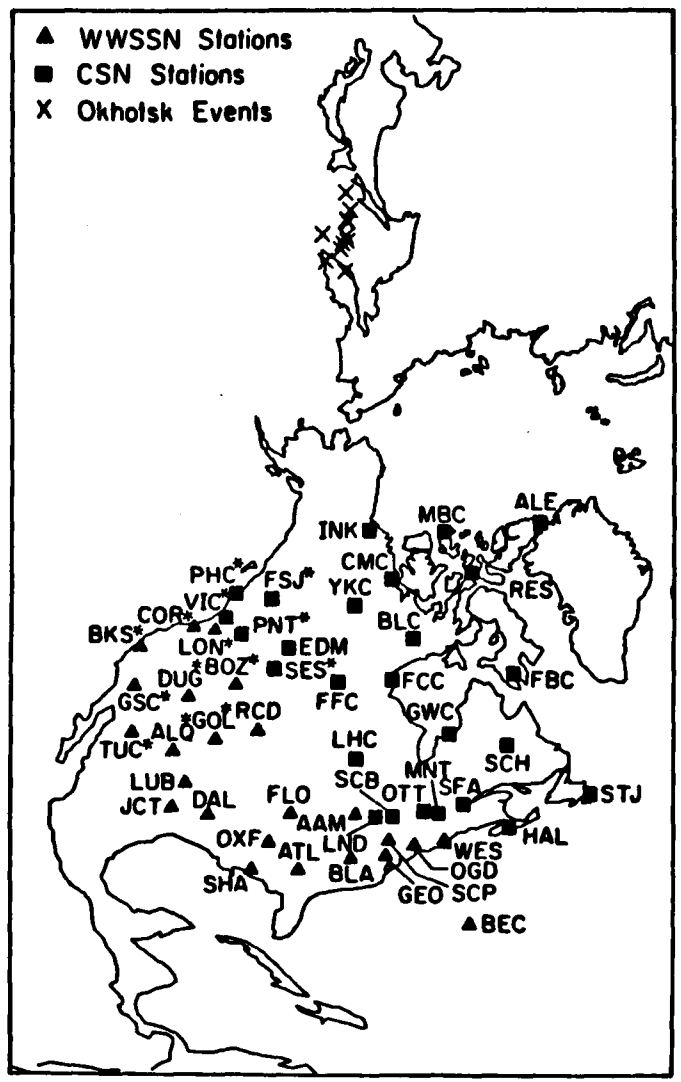
▲ WWSSN Stations
■ CSN Stations
X Okhotsk Events
INK
MBC
ALE
CMC
PHC*
FSJ*
YKC
RES
VIC*
COR*
PNT*
BLC
BKS*
LON*
EDM
BOZ*
SES*
DUG*
FCC
FBC
GSC*
FFC
RCD
GWC
GOL*
ALO*
TUC*
LHC
SCH
LUB
SCB
MNT
JCT
DAL
FLO
OTT
SFA
STJ
AAM
OXF
LND
HAL
ATL
WES
OGD
SHA
BLA
GEO
SCP
BEC

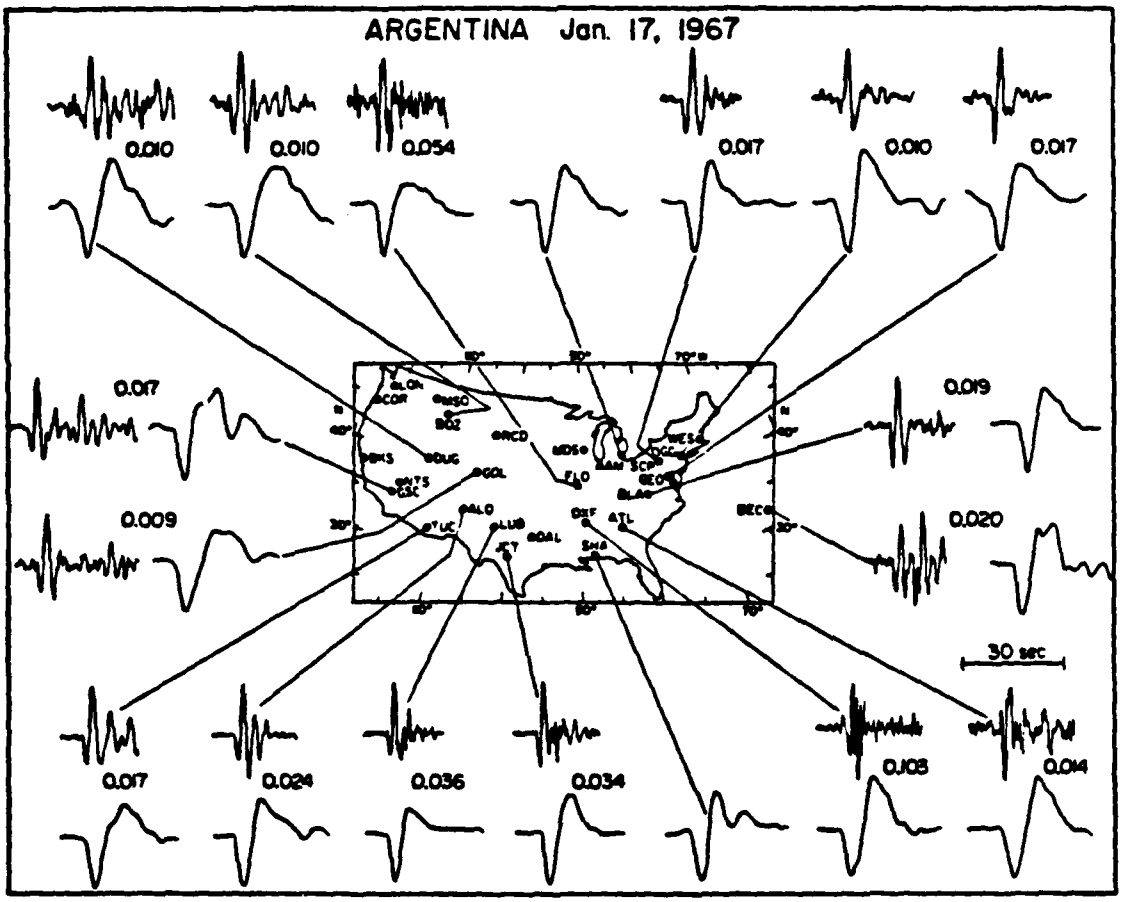
ARGENTINA Jan. 17, 1967
0.010
0.010
0.054
0.017
0.010
0.017
0.017
0.019
0.009
0.020
30 sec
0.017
0.024
0.036
0.034
0.108
0.014

Fig. 2.

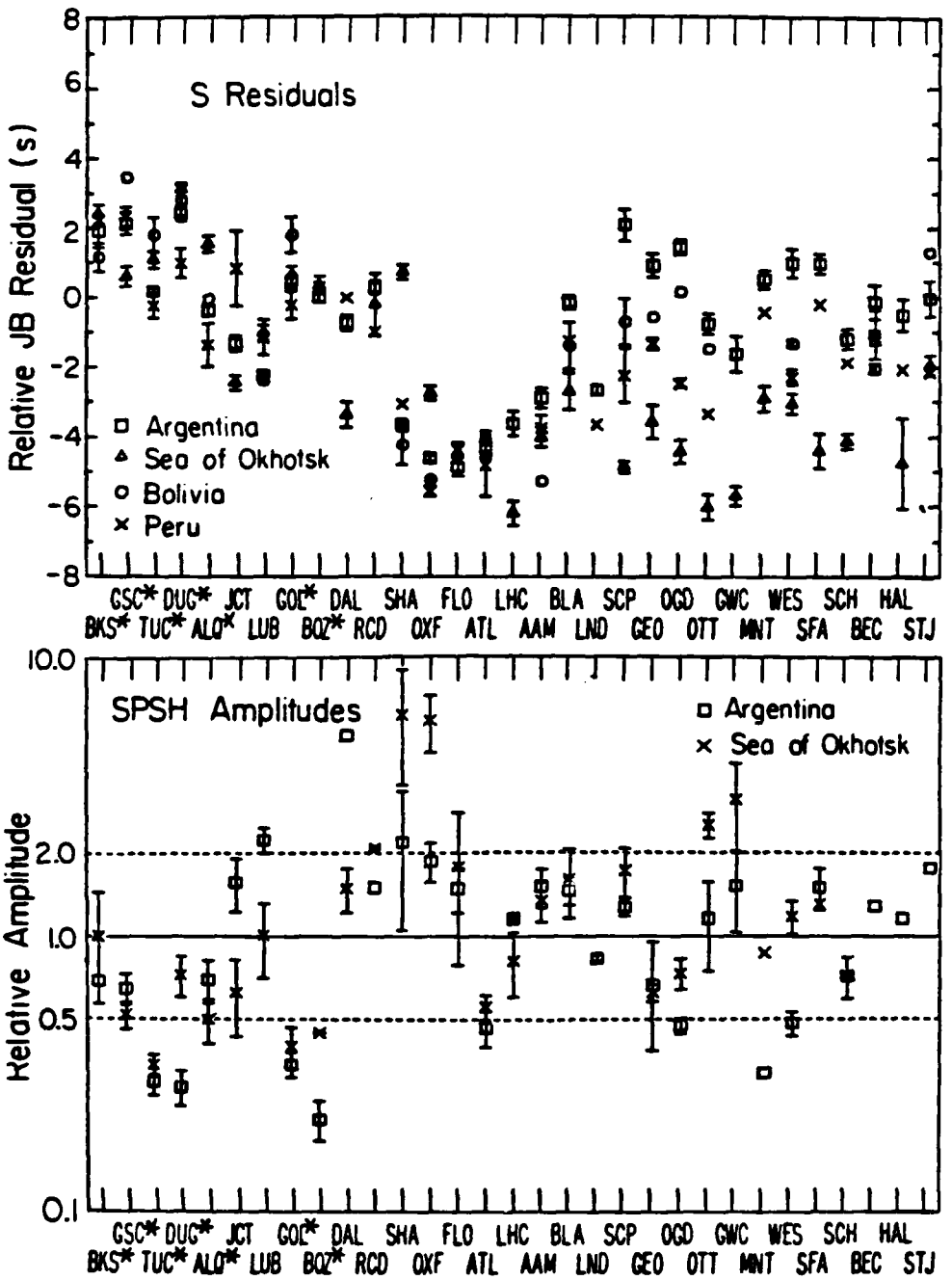
S Residuals
Relative JB Residual (s)
8
6
4
2
0
-2
-4
-6
-8
Argentina
Sea of Okhotsk
Bolivia
Peru
GSC* DUG* JCT GOL* DAL SHA FLO LHC BLA SCP OGD GWC WES SCH HAL
BKS* TUC* ALQ* LUB BOZ* RCD OXF ATL AAM LND GEO OTT MNT SFA BEC STJ
SPSH Amplitudes
Relative Amplitude
10.0
2.0
1.0
0.5
0.1
Argentina
Sea of Okhotsk
GSC* DUG* JCT GOL* DAL SHA FLO LHC BLA SCP OGD GWC WES SCH HAL
BKS* TUC* ALQ* LUB BOZ* RCD OXF ATL AAM LND GEO OTT MNT SFA BEC STJ

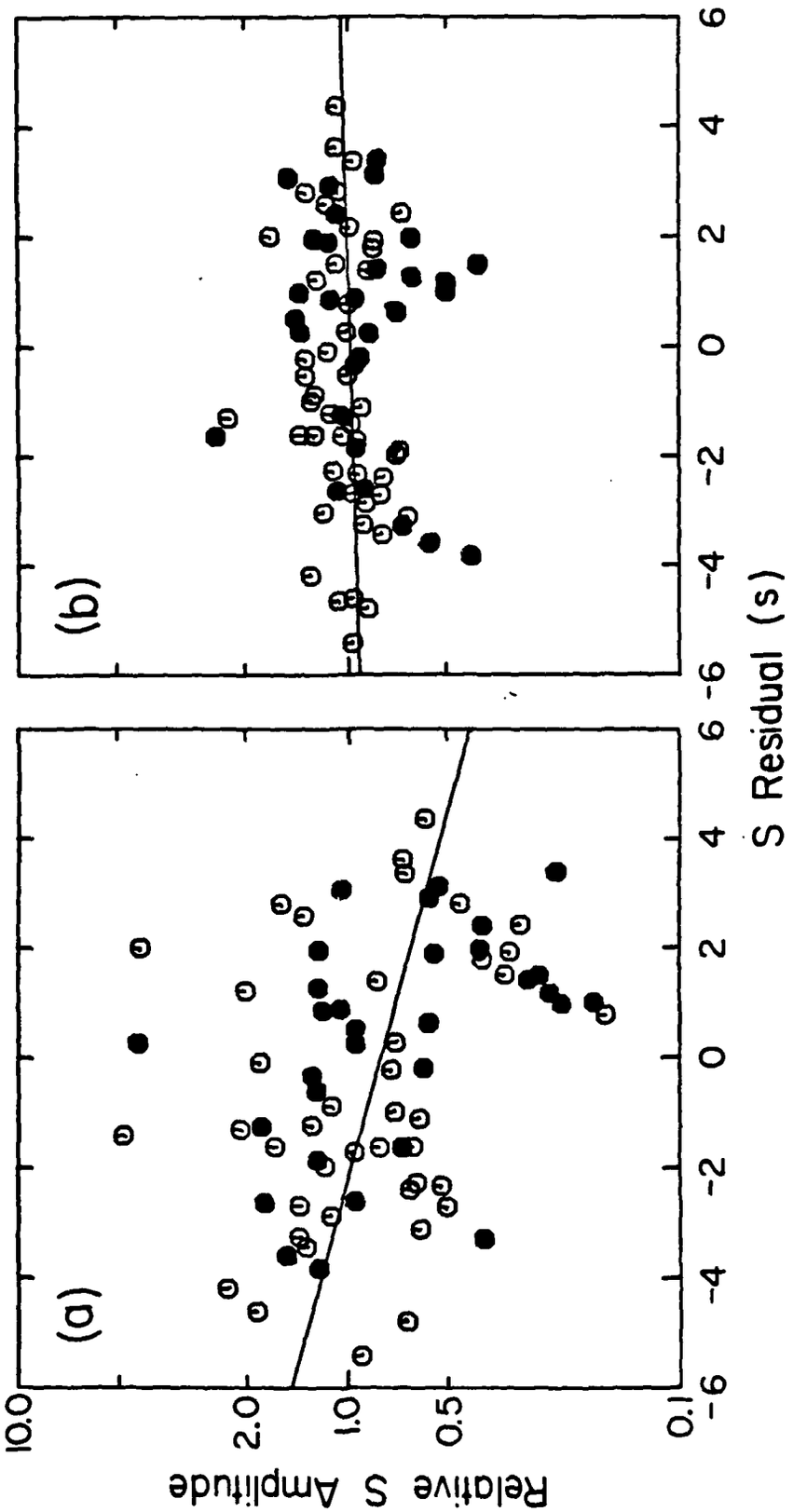
(a)
(b)
Relative S Amplitude
10.0
2.0
1.0
0.5
0.1
S Residual (s)
6
4
2
0
-2
-4
-6

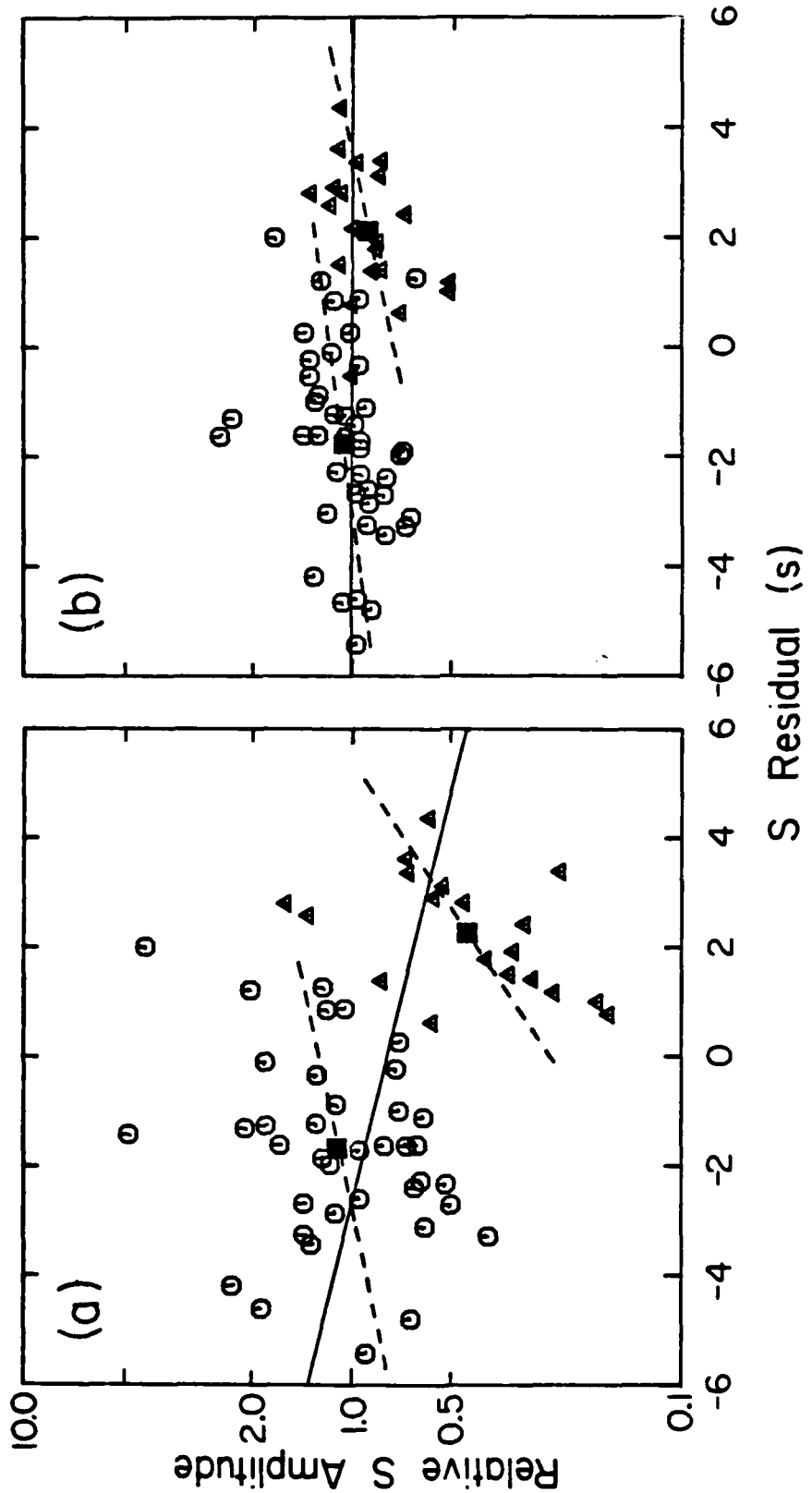
(a)
(b)
Relative S Amplitude
10.0
2.0
1.0
0.5
0.1
-6
-4
-2
0
2
4
6
S Residual (s)

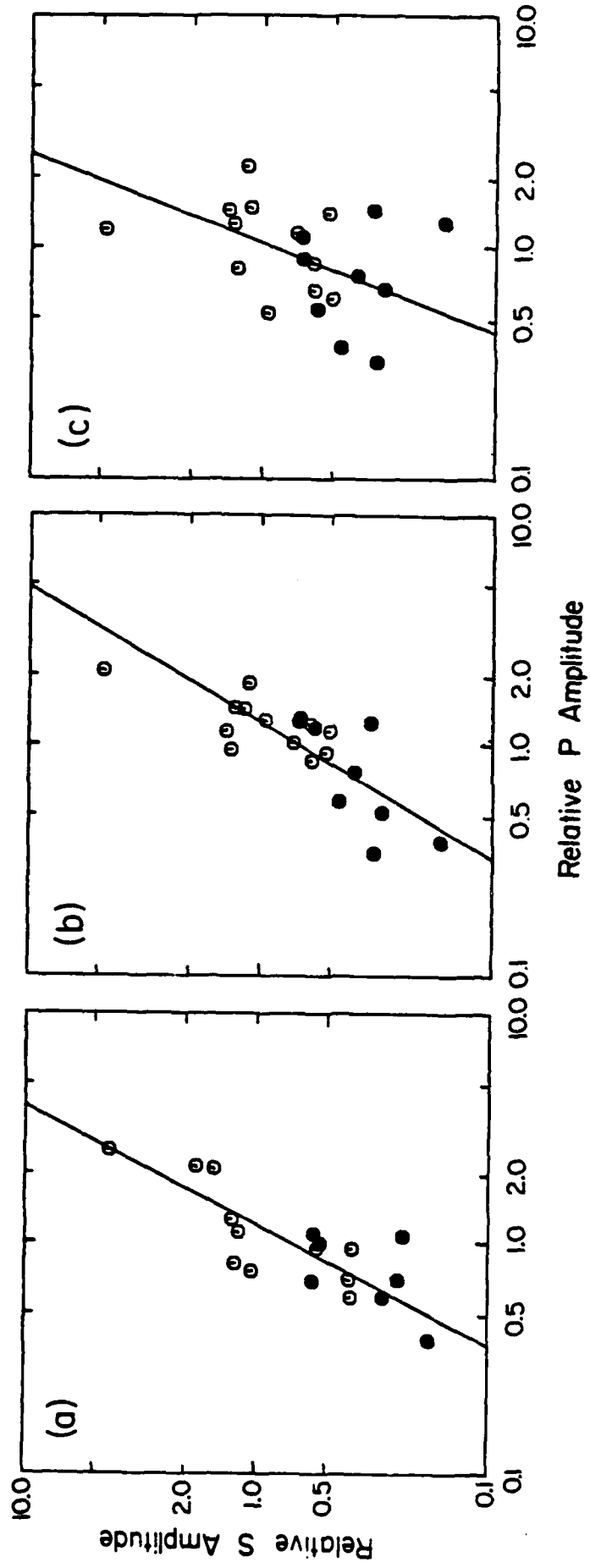
(a)
(b)
(c)
Relative S Amplitude
Relative P Amplitude
10.0
2.0
1.0
0.5
0.1

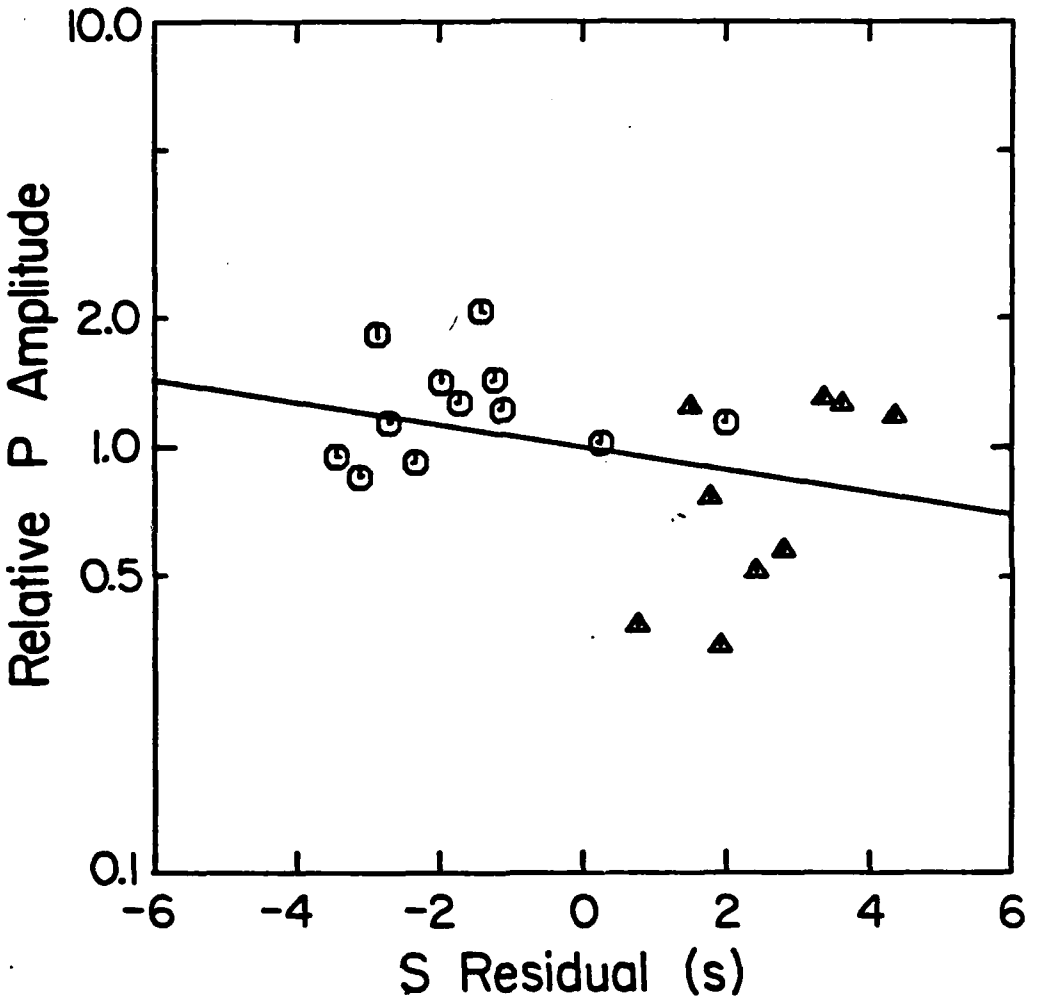
10.0
2.0
1.0
0.5
0.1
Relative P Amplitude
-6
-4
-2
0
2
4
6
S Residual (s)

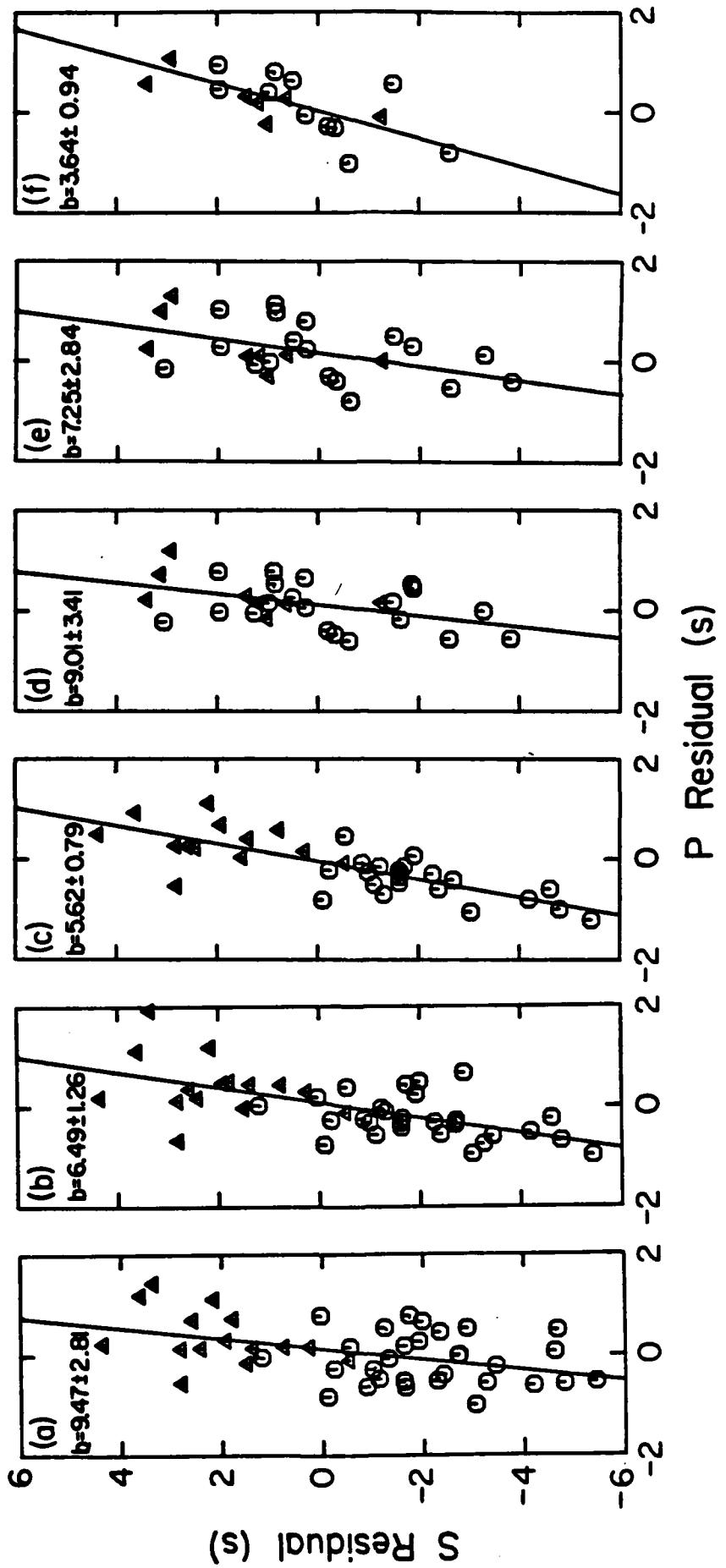
(a)
b=9.47±2.81
(b)
b=6.49±1.26
(c)
b=5.62±0.79
(d)
b=9.01±3.41
(e)
b=7.25±2.84
(f)
b=3.64±0.94
S Residual (s)
P Residual (s)

IV

EVIDENCE OF TECTONIC RELEASE FROM UNDERGROUND NUCLEAR EXPLOSIONS IN LONG-PERIOD P-WAVES

by

Terry C. Wallace

Don V. Helmberger

Gladys R. Engen

Seismological Laboratory

California Institute of Technology

Pasadena, California 91125

July 31, 1982

revised October 11, 1982

(to be submitted to Bull. Seism. Soc. Am.)

ABSTRACT

In this paper we study the long-period body waves at regional and upper mantle distances from large underground nuclear explosions at Pahute Mesa, Nevada Test Site. A comparison of the seismic records from neighboring explosions shows that the more recent events have much simpler waveforms than those of the earlier events. In fact, many of the early events produced waveforms which are very similar to those produced by shallow, moderate-size, strike-slip earthquakes; the phase sP is particularly obvious. The waveforms of these explosions can be modeled by assuming that the explosion is accompanied by tectonic-release represented by a double couple. A clear example of this phenomenon is provided by a comparison of GREELEY (1966) and KASSERI (1975). These events are of similar yields and were detonated within 2 km of each other. The GREELEY records can be matched by simply adding synthetic waveforms appropiate for a shallow strike-slip earthquake to the KASSERI observations. The tectonic release for GREELEY has a moment of 5×10^{24} dyne-cm and is striking approximately 340^{o}. The identification of the sP phase at upper-mantle distances indicates that the source depth is 4 km or less. The tectonic release time function has a short duration (less than one second). A comparison of these results with well studied strike-slip earthquakes on the west coast and eastern Nevada indicate that, if tectonic release is triggered fault motion, then the tectonic release is relatively high stress drop, on the order of several hundred bars. It is possible to reduce these stress-drops by a factor of two if the tectonic release is a driven fault; that is, rupturing with the P velocity. The region in which the stress is released for a megaton event has a radius of about 4 km.

Pahute Mesa events which are detonated within this radius of a previous explosion have a substantially reduced tectonic release.

INTRODUCTION

It is well documented that certain underground nuclear explosions require sources which have substantial non-isotropic components (Press and Archambeau, 1962; Toksoz, Ben-Menaham and Harkrider, 1964; Toksoz and Kehrer, 1971; among others). The surface-wave observations provide the evidence which is most commonly cited for this source asymmetry. For example, for the explosion GREELEY, the observed ratio of the Love to Rayleigh wave excitation is much larger than would be predicted for a pure explosion source and scattering in a simple layered earth. In addition, the Rayleigh waves display a radiation pattern (Toksoz and Kehrer, 1972). In the case of the Shagan river region of the Eastern Kazakh Test site, explosions which are only kilometers apart produce Rayleigh waves which are 180^{o} out of phase (North and Fitch, 1981; Goforth 1982). As for body waves, SH waves at teleseismic distances are a fairly common observation (Nuttli, 1969). Similarly, in the near field, there are tangential accelerograms which are much too large to be explained by simple scattering (Aki et al., 1969).

A widely accepted explanation for the phenomenon of SH-type seismic wave generation by explosions is the release of tectonic strain. Considering the abundance of examples for the influence of tectonic release on SH and surface waves, it is somewhat surprising that there is very little documentation of its influence on P waves. Johnson et al. (1982) have shown that moment tensor inversion of three-component, strong-motion data (the data encompasses both P and S waves) can be interpreted in terms of an explosion plus a double couple, although the effect of the tectonic release on the P waves is not obvious. No one has presented a set of teleseismic short-period P waves which are

clearly distorted by tectonic release. One of the more widely accepted explanations for the lack of an obvious tectonic release signature on short-period P-waves is that tectonic release is a low stress-drop phenomenon (Bache, 1976). In the case of NTS, the low stress-drop would conspire with the strike-slip radiation pattern (which does not radiate P-waves efficiently to teleseismic distances) predicted for tectonic release from the surface waves to make the short-period signature very difficult to observe in the far-field body waves. In this paper we present a suite of long-period P waveform distortions which we have modeled as tectonic release. An unexpected result of our modeling analysis is that, if the tectonic release is interpreted in terms of a triggered earthquake, very high stress drops are required. This apparent inconsistency with the short-period data may help resolve the mechanism of tectonic release.

The data set which we use is the long-period WWSSN recordings at regional and upper-mantle distances from megaton explosions at Pahute Mesa. At regional distances (less than 12^{o}), the long-period body waves are essentially crustal reverberations and very little diving ray energy is present. Fairly complete azimuthal station coverage at regional distances allows the determination of a radiation pattern and moment for the double couple. Beyond regional distances the dominant body-wave arrivals are diving rays (rays bottoming below the Moho) and the phase sP can be identified and used to determine source depth and duration. The purpose of this report is to qualify the effects of tectonic release for these large explosions with this data set.

COMPARISON OF EXPLOSIONS AND EARTHQUAKES

The set of observations that first lead us to suggest that there is a tectonic release signature on the long-period P waves is the striking similarity between the seismograms of certain NTS events and shallow, moderate-size earthquakes. Fortunately, long-period seismograms for earthquakes of this size are fairly well understood at regional through teleseismic distances. The use of synthetic seismograms allows the separation of the travel path and source effects and it is possible to identify the various phases such as P, pP and sP. A comparison of the well understood earthquake waveforms and those of an explosion can be used to isolate S-wave energy in the source. An earthquake of particular importance to this study occurred in eastern Nevada (m_b = 5.6, ISC) on August 16, 1966. The proximity of this event to NTS ($\sim$200 km due east) allows us to calibrate the travel paths. In addition, the fault orientation is roughly consistent with that predicted for the tectonic release at NTS. Appendix I gives the detailed analysis of the regional waveforms for the source parameters of this earthquake.

Figure 1 shows a comparison of the tangential records for the Nevada earthquake and the nuclear explosion GREELEY (12/20/66). The stations shown here (YKC, CMC and MBC) have source-station separations which are almost identical for the explosion and the earthquake. These stations are also very close to being naturally rotated, which makes it possible to compare the SH and Love waves for both sources directly on the E-W component. In Figure 1 the records are aligned on the SH arrival. Although the record from GREELEY is noisier, the coherence between the explosion and earthquake is remarkable. The earthquake

depth is on the order of 6 km (see Appendix I) while the explosion detonation was at 1.2 km depth. Considering this difference in depth, the coherence of the surface waves is also quite good. The SH pulses at MBC have been enlarged and very nearly overlay. The similarity between these seismograms suggests that the time function and mechanism associated with the GREELEY tectonic release must be similar to that of the earthquake. This leads us to believe that the long-period P waves from the GREELEY tectonic release should be visible wherever the earthquake's P waves are apparent. On the basis of the comparison in Figure 1, it is possible to place a lower bound on the moment for the tectonic release of 4.5×10^{24} dyne-cm. This lower bound is based on the fact that the northern azimuth is in a similar part of the SH radiation pattern for both the earthquake and tectonic-release orientations, within 20^{o} of the maximum.

Another earthquake which provides an interesting comparison with Pahute Mesa explosions occurred in Northern Baja on December 22, 1964. The earthquake has a strike-slip orientation (see Appendix I for the detailed source parameters) such that ALQ and LUB are near the positive P-wave radiation lobe. The tectonic-release orientation predicted for NTS on the basis of surface waves (right lateral strike-slip) also puts these two stations in the positive lobe. A comparison of the waveforms for the Baja earthquake and BOXCAR is shown in Figure 2. At the regional distance of ALQ, the waveform is essentially crustal reverberations. There is very little mantle ray energy present because the distance range is in the shadow of a low-velocity zone. At the slightly larger distance range represented by the LUB records, the shadow zone has been passed and diving rays play an important role in

the waveform.

A comparison of the explosion and earthquake records at ALQ shows that they are similar. The PL from BOXCAR has a higher frequency content than that from the Baja event as would be expected from the higher frequency of the time function of the explosion. Although the larger distance for the earthquake makes the waveform slightly more dispersed, the long-period content is fairly coherent. At LUB, the PL on the earthquake record is again longer period than that of the explosion. In the beginning part of the record there is a clear separation of arrivals. For the earthquake we can model the second arrival as sP. Note that there is a similar separation of arrivals for BOXCAR, which is suggestive of a similar phenomenon. The shallower depth of the explosion (1.2 km compared to 8 km) can explain the less dramatic separation, but it appears that there is significant S-wave energy present in the explosion time function.

Figure 3 shows a profile of synthetic seismograms for a strike-slip fault. The earth model wich was used is a single layer crust over the T7 (Burdick and Helmberger, 1978) mantle. The ALQ seismogram for the Baja event corresponds to the record at 900 km while the LUB seismogram corresponds to the record at 1300 km. Our ability to predict the earthquake waveforms assures that we are correctly identifying sP. In the synthetic profile the effect of the low-velocity zone is fairly obvious; the seismogram at 800 km is clearly in the shadow while 1000 km is out of the shadow.

ANALYSIS

The megaton explosions at Pahute Mesa provide a good data set for a systematic analysis of tectonic release. The large size of the events produced usable long-period P waves out to 30°. Figure 4 is a base map of Pahute Mesa showing the location of some of the larger explosions. The outline of the Silent Valley Caldera, which is an important geological feature on Pahute Mesa, is also shown. The explosions in the western half of the caldera are the most important for this study. The sizes and depths of burial for these events are comparable (see Table 1) which allows us to assume that the explosion time function is constant. The close spatial relationship of the detonations suggests that the near-source structure is also similar for all the events (at least in the long-period pass band). Therefore, we can interpret differences in the waveforms for several explosions in terms of tectonic release. It is particularly interesting to compare events which are very close in space but separated in time such as GREELEY and KASSERI or BOXCAR and COLBY.

Upper-Mantle Records: Ideally, at upper-mantle distances the waveforms from explosions should simply be the product of the interaction of the source time function, the rays P and pP and the earth structure. The addition of a component of tectonic release adds another time function convolved with the set of rays P, pP and sP. If the NTS tectonic release has the strike-slip mechanism as indicated by the surface waves, then the most important phase at upper mantle distances should be sP. Figure 5 shows the long-period vertical seismograms for eight of the Pahute shots at the WWSSN station SHA ($\Delta \sim 24^{\circ}$). All the records are plotted on the same amplitude scale. The records have been

ordered according to the importance of the second upswing relative to the first upswing. About 4 1/2 minutes after the P wave is a long-period arrival whose timing corresponds to the travel time of SV. There is a strong correlation between the ratio of the second and first upswings in the P-wave signal and the size of SV (compare the first swing, or a-b P amplitudes to the SV amplitudes). This strongly suggests that the second upswing in the P wave train is controlled by an S wave, namely sP. Given this interpretation, the records in Figure 5 are ordered from least to most tectonic release. Note that KASSERI has a much smaller tectonic release than GREELEY which was detonated nine years earlier.

On the basis of the SHA comparison, BENHAM would be assigned the largest tectonic release. On the other hand, Toksoz and Kehrer (1972) assign an F factor of 1.6 for GREELEY compared to 0.85 for BENHAM. The F factor is the relative strength of the double-couple (tectonic release) and explosion as determined by the ratio of the Love-wave to Rayleigh-wave amplitude. The difference between our assessment of the importance of tectonic release and that determined by the F factors is that Toksoz and Kehrer assume a pure strike-slip mechanism for the tectonic release. In the case of BENHAM, preliminary modeling of the SV pulse suggests that there is a small, but detectable (15-20 per cent), component of dip-slip motion. This also agrees with observations of surface faulting (Bucknam, 1969; Hamilton and Healy, 1969). Even a ratio of 1-to-5 for dip-slip to strike-slip motion is important since the dip-slip motion is much more efficiently radiated to teleseismic distances.

The differences in the P waveforms, such as were discussed for SHA

in Figure 5, are the types of waveform distortions we qualitatively model as tectonic release at upper-mantle distances. There is a well aligned profile of stations in the southern United States which simplifies the analysis. The stations LUB, JCT, DAL, OXF, and SHA only vary by about 10^{o} in azimuth from NTS. This constant azimuth means that the effects of radiation pattern can be neglected. Also, this station profile is very close to the radiation lobe of sP as predicted by the surface-wave orientation for the double couple. The type of analysis we do is to compare the waveform of a low tectonic-release event with one which is high. Figure 6 is an example of this process. Shown are the COLBY and BOXCAR records at LUB ($\Delta \sim 12.4^{o}$). The main difference in waveform for these events is the second upswing. The latter part of the records are quite similar. This similarity suggests that one could simply add a component of tectonic release to the COLBY record and simulate the BOXCAR record. Shown below the BOXCAR record in Figure 6 is such a simulation. In this case the tectonic-release synthetic has a strike-slip orientation where the earth model used is a single layer crust over the upper-mantle T7. This synthetic includes the large number of rays for the crustal waveguide (the $P_{n\ell}$ response) plus the diving rays in the upper mantle. There is a one-second time delay between the double-couple component and the explosion, although the S-velocity of the source region is larger (3.5 km/sec) than would be expected for a shallow source (the crust is modeled as a single layer). There is a tradeoff between the relative timing of the explosion and double-couple and the S-velocity, but this aside, the prediction of the BOXCAR waveform is quite remarkable. Peak for peak, the prediction and observation of BOXCAR correspond back into the PL arrivals. The time

function for the synthetic has a 0.6 second duration. The moment that is required for this fit is 5 x 10^{24} dyne-cm. This is a minimum estimate for a pure strike-slip orientation. Although there is very little seismic evidence for much dip-slip component in the BOXCAR tectonic release, a small component of dip-slip motion could lower the overall moment to 4.0 x 10^{24} dyne-cm (any larger component of dip-slip motion degrades the synthetic fit at LUB). Although there is not much resolution on the depth of the tectonic double couple, which may have some effect on the time function duration, even the least favorable case of the ratio of source duration to moment implies a high stress-drop (hundreds of bars) if the tectonic release is triggered fault motion.

The best example of this type of comparison analysis is for GREELEY and KASSERI. In this case there are four stations in the southern profile which are available for comparison. Figure 7 shows the records at LUB, JCT, DAL and SHA. The records are very similar for the two events with the exception of the very strong second upswing on all the GREELEY records. The similarity of waveforms allows us to perform the same kind of exercise of adding a double-couple synthetic to the KASSERI records to simulate the GREELEY records. In this case we chose a mechanism for the tectonic release which has a small component of dip-slip motion (strike-slip to dip-slip ratio of 5-to-1). The dip-slip component was used to lower the seismic moment required to get the very strong, second upswing at SHA. Figure 8 summarizes the results of this synthysis. Again there is a one-second time lag between the explosion and the tectonic release. The moments which were used for the double couple were 5 x 10^{24} dyne-cm for the strike-slip component and 1 x 10^{24} dyne-cm for the dip-slip component. The time-function has a source

duration of 0.6 seconds (a triangle with 0.3 second rise and fall). The overall fit of the simulations to observations is quite good considering the large range of Δ's. At LUB there is very little diving ray energy present, but at the distance of JCT the predominant arrivals are diving and there is still coherence between the observation and prediction. At DAL an arrival associated with the 400 km discontinuity is quite important, but the GREELEY record is still well predicted (the 400 km discontinuity causes the very strong second downswing). Finally, the waveform at SHA is fairly simple and the effect of the tectonic release sP is obvious. A slightly longer time function would improve the fits at LUB and JCT (a time function of 1.0 second duration brings out the interference in the second pulse at JCT quite well) but degrades the fit at DAL and SHA. If we increase the length of the time funtion by 25 per cent the stress drop decreases by a factor of 2, still a very high value for triggered fault motion.

The comparison of records over this southern profile of stations results in a consistent picture; the distortion of the waveforms can be explained by the addition of a double couple to simulate the tectonic release. Unfortunately, there is not another profile of stations along constant azimuth with which we can conduct a similar analysis, so it is difficult to constrain the strike direction of the double couple on the basis of the upper-mantle records alone. We can do a comparison of RCD with LUB, which is approximately the same distance from NTS, but should be in the opposite quadrant (negative) for the double couple. Figure 9 shows a comparison of GREELEY at LUB and RCD. Also shown is the RCD seismogram for the 8/16/66 Nevada earthquake. The two explosion records are quite similar, but appear to have the long-period content of the

waveforms reversed in polarity. We have attempted to simulate the GREELEY waveform at RCD by assuming that the Nevada earthquake waveform is representative of the tectonic release. The earthquake waveform was added to an explosion source synthetic. This sum is shown below the GREELEY waveform. Although the waveform fit is not as good as that for the single-station comparisons, where the explosions have the same source structure and travel path, it is still good enough to be suggestive of several things. The long-period signature is fit quite well in that the ratio of the downswing to upswing amplitude for the second pulse is roughly correct. The difference in travel path length makes the earthquake waveform slightly too dispersed. The orientation of the Nevada earthquake is similar to that which we would expect for the tectonic release, so the approximate fit of the composite seismograms to the RCD GREELEY record supports the hypothesis that RCD and LUB are in opposite radiation quadrants.

Regional Distance Records: At regional distances the seismograms are very complicated due to the waveguide nature of the crust. The mode conversions (S-to-P and P-to-S) at the surface and Moho are very important to the $P_{n\ell}$ waveform. Since the waveform is sensitive to both P and SV it contains a large amount of information about the seismic source. By making certain assumptions about the crustal structure it is possible to invert the $P_{n\ell}$ waveforms of shallow, moderate-size earthquakes to determine the fault orientations (Wallace et al. 1981a). On the other hand, a pure explosion source has a $P_{n\ell}$ waveform which is quite distinct from those of earthquakes. The absence of S in the source and the very high frequency time function result in seismograms which "ring". Under favorable circumstances, if a double couple is

superimposed on an explosion source, the waveforms are distorted in such a fashion that it is possible to recover the orientation of the fault.

Certain systematic effects emerge for some of the seismograms from the Pahute Mesa explosions. For example, the $P_{n\ell}$ waveforms recorded at ALQ and TUC appear much more like those produced by earthquakes than explosions. Figure 10 is a composite of different explosions recorded at regional stations. These long-period seismograms have been convolved with a filter whose impulse response is a triangle with a 2 second rise and fall. Shown below the observations are a pair of synthetics which have been similarly filtered. The synthetics were generated with generalized rays using the crustal model in Table 1 in Appendix I. For each synthetic pair, the top trace is for an explosion source, while the lower trace is for a double couple source which has a strike-slip mechanism. The orientation of the fault was taken from the surface wave-work of Toksoz and Kehrer (1972): right lateral motion on a plane striking N15^{o}W. ALQ and TUC are in the radiation lobe for the tectonic release $P_{n\ell}$, while LON, which is in good agreement with the explosion synthetic, is near a node. DUG, which is in the negative quadrant, has a greatly reduced P amplitude. The first P pulse at DUG is only two thirds that which would be predicted on the basis of HANDLEY records at LON. This is significant in that the DUG P amplitude is not systematically small. For a low tectonic-release event (COLBY) the amplitude is larger than would be predicted on the basis of LON. Although Figure 10 is a composite and no doubt the tectonic release varies from shot to shot, it is highly suggestive that there is a significant tectonic release signature on the $P_{n\ell}$ waveforms.

FAULTLESS was detonated about 100 km north of Pahute Mesa at Hot

Creek Valley, Nevada. In contrast to the Pahute explosions, the FAULTLESS P waveforms show much less evidence of tectonic release. Figure 11 shows the regional long-period records. Again the waveforms have been filtered as described above. Shown below each observation is a synthetic for an explosion source. Although TUC is not fully explained by an explosion alone, the tectonic release must be down by a factor of 3 in comparison to GREELEY or a factor of 2 compared to BOXCAR.

In this analysis it was assumed that differences between the observed explosion and the explosion synthetics can be isolated in the source. To determine the importance of the tectonic release, a double couple was added to the explosion synthetics until the fit to the observations was maximized. The attempt here is to qualify the nature of the tectonic release, so each record was fit independently although the orientation of the double couple was constrained to be the same for all the records. The explosion synthetics were constructed using a source time function described by Helmberger and Hadley (1981). They used their source time function to model both the near-in velocity records and the far-field displacements for HANDLEY, one of the explosions considered in this report, so the values they determined for rise time and overshoot ($k = 5$, $B = 2$) were assumed for all the modeling. Changing the values of k and B within reasonable limits has little effect on the filtered synthetics. This is similarly true if we had used a Haskell (1967) source or a Von Seggern and Blandford (1972) source.

Strike-slip orientations have the largest effect on the P_{nl} waveforms for explosions. The displacement response from dip-slip

faulting is higher frequency than that for strike-slip motion (this is a result of excitation) and generally adds or subtracts to the explosion waveform without substantially changing it. Since the ratio of dip-slip to strike-slip motion is small on the basis of upper mantle records, only the orientation of the strike-slip component was determined. Different orientations for the strike were tested for compatability with the observations. Figure 12 summarizes the analysis. Shown are the same explosions as in Figure 10 and synthetics generated for a combination of double couple and explosion. The LON and COR records have a profound effect on the strike of the double couple. The contribution of the explosion to the waveform is much greater than that of the double couple implying that these stations are near the node of the radiation pattern. This is particularly true of LON for nine different explosions. The best fitting strike-slip fault has a strike of N20^{o}W, not significantly different from that of Toksoz and Kehrer (1972). The numbers to the right of each seismogram pair in Figure 12 give the ratio of Pn displacement caused by the explosion contribution to that caused by the strike-slip dislocation. Since different explosions were used in the composite figure, no absolute moments are given. Rather, these ratios give a measure of the importance of tectonic release for a given azimuth.

DISCUSSION

The main interpretation of the previous sections is that tectonic release has a significant effect on the signature of long-period P waves. What now must be done is to integrate this observation with the

previous work on surface waves and teleseismic short-period P waves. There are two basic theories for the release of pre-existing tectonic stress by an explosion. The first, summarized by Aki and Tsai (1972), is the triggering of a dislocation along a nearby fault. The second, is stress relaxation from the highly fractured zone immediately around the detonation point (Archambeau, 1972). Most of the previous work on tectonic release has relied on the surface-wave amplitude to determine the moment which in turn was used to obtain the stress-drop by relating the moment to the fault dimensions (as determined from aftershocks) or the volume of pulverized material. Aki and Tsai (1972) argue that the ratio of the fault dimensions to moment (the moments they obtain are smaller although roughly consistent with those in this study) requires low stress-drops; on the order of 10 bars. Since the surface waves that are used in this analysis have periods longer than 10 seconds there is little resolution of the time function. The shape of the time function can be used as another measure of stress-drop. In most fault models the time function is some convolution of a dislocation function and source finiteness. Therefore, the time funtion is dependent on the area of rupture as well as the average displacement on the fault. Assuming certain average properties about the rupture and displacement history, it is possible to relate the source duration to stress drop. We use a simple model in which the length of faulting is approximately the product of the source duration and the rupture velocity. Therefore, the stress drop is proportional to the time function (for a given moment, a time function which has a shorter duration has a higher stress drop than one which has a longer duration). We can calculate a fault length for GREELEY and BOXCAR on the basis of the time functions

required to fit the upper mantle observations. Assumming a S-velocity of 3 km/sec and rupture velocity of .8 , then the fault length is on the order of 1.5 to 2 km. Using the formula (Kanamori and Anderson, 1975)

$$\Delta\sigma = \frac{7}{16} \left\{ \frac{M_o}{a^3} \right\} \qquad (1)$$

where a is the radius of rupture would give a stress-drop between 300 and 600 bars. This is an order of magnitude larger than Aki and Tsai's values. We can also compare this result to a number of recent studies which investigate the relationship between source duration of earthquakes and seismic moment (Ebel et al., 1978; Liu and Kanamori, 1980; Cohn et al., 1982). In all cases, the short duration of the tectonic release translates into a stress drop which is an order of magnitude larger than would be expected for an earthquake of similar moment.

If tectonic release is a triggered earthquake, the frequency dependence of the stress-drop is not without precedent. Numerous authors (Hart et al., 1977; Lay and Kanamori, 1980; Ebel, 1980; Boatwright, 1980; among others) have noted a large discrepancy between the moment computed with the body and the surface waves. The asperity model suggests that this phenomenon results from the body waves being radiated from small, strongly coupled, isolated regions while the fault as a whole radiates the surface waves. A similar argument can be made for stress-drop; the asperities have a high stress-drop. It is becoming apparent that for most earthquakes which are studied in detail in both the near-field and far-field, faulting often involves high stress-drop asperities (Hartzell and Helmberger, 1982; Wallace et al., 1981b; Liu and Helmberger, 1982). If this is the case for tectonic release, the question is not so much how to rectify the long-period P

waves and the surface-wave stress drops, but rather, should there be a strong short-period signature.

The 8/16/66 Nevada earthquake appears to be very similar to the tectonic release from GREELEY, although the stress drop appears to be a factor of two smaller. For this earthquake there were significant teleseismic short periods at 30°, in particular on the east coast of the U.S. Beyond 40° the short-periods were rarely visible on the WWSSN network. This is an expression of the strike-slip orientation; P waves are not efficiently radiated to teleseismic distances. The higher stress drop from the tectonic release probably would cause records to be written at larger distances. Since the main phase radiated is sP there would be only a very small change in the a-b amplitude of an explosion with a tectonic release time function similar to those in this study. T. Lay (personal communication) has shown that at a distance of 50° a strike-slip mechanism with a moment of 5×10^{24} dyne-cm will effect the a-b amplitude by about 10 percent between maximum radiation lobes. On the other hand, the part of the waveform which corresponds to the arrival of sP has distinguishable differences. A comparison of short-period waveforms on the east coast show only minor differences between high and low tectonic release events. This leaves two possible conclusions: (1) the stress-drop must be lower, or (2) the spectra of the time function is peaked at 2-3 seconds. The stress-drops can be reduced by a factor of 2 by assuming that the rupture velocity of the tectonic release is approximately the P-velocity. In this case, the mechanism of tectonic release is fault motion driven by the explosion. Even with this reduced stress drop, the waveforms for high and low tectonic release events recorded on the east coast stations should show

more variance than is observed. Although it if difficult to construct a time function which is strongly peaked at the pass band of the long-period P waves, the direction of rupture can produce a frequency dependent effect. The very strong similarity of the GREELEY SH waves with those of the Nevada earthquake suggests that the point source location of the tectonic release is deeper than the working point. Similarly, the time lag for the summing process in Figure 8 suggests that the best point source hypocenter of the tectonic release is on the order of 4 km. If we assume that the fault is driven by the explosion, then the rupture starts at the working point and is driven downward. Liu and Helmberger (1982) have shown that the short-period sP is greatly reduced compared to the long-period sP for a strike-slip event rupturing downward. This type of phenomenon could explain the apparent inconsistancy between the long and short-period data.

The fact that tectonic release is significantly reduced for explosions which are detonated close to the site of a previous explosion can be used to estimate the dimensions of the crust in which the stresses are relieved. On the basis of FONTINA and BOXCAR, the minimum radius of area affected by a megaton explosion is on the order of 3 km. On the other hand, CAMEMBERT is about 4 km from KASSERI and GREELEY but shows substantial tectonic release. Similarly BOXCAR and GREELEY are about 4.5 km apart and are apparently unaffected by each other. Assuming that 4 km is the outer radius at which stress relaxes for megaton events, it is possible to calculate the stress drop expected in the Archambeau (1972) cavity model. Using the elastic parameters given in Bache (1976) the stress drop must be at least 500 bars. This is in agreement with the time function found in this study, but again

stress-drops this large should radiate sufficent short-period seismic energy to cause obvious waveform distortion.

It is apparent that the tectonic-release parameters determined from the long-period P waveforms does not fit neatly in either theory for tectonic release. We prefer a driven fault model, with the bulk of the tectonic release occurring deeper than the working point of the explosion. This type of stress release mechanism incorporates features from both the cavity and triggered earthquake models. It is interesting to note that CAMEMBERT and MUENSTER are smaller than most of the other explosions studied here, but still showed significant tectonic release. It is also true that these two explosions have a high ratio of depth of burial to yield.

CONCLUSIONS

Certain megaton explosions on Pahute Mesa have a long-period body waveform distortion which can be modeled as the signature of tectonic release. The tectonic release can be sufficiently represented as a double couple. Long-period WWSSN data at regional and upper-mantle distances constrain the double couple to be primarily strike-slip, which is in agreement with previous work on NTS surface waves. The events with the largest tectonic release (BENHAM and GREELEY) have double couples with moments on the order of 5×10^{24} dyne-cm. In the case of megaton explosions, detonations within a 4 km radius of previous large explosions result in a substantially reduced component of tectonic release.

The modeling of the sP phase from the double couple requires a time

function which has a short duration. The moments determined both from the sP and SH amplitudes require very high stress-drops if the short duration time functions are interpreted in terms of a triggered fault. Similarly, the cavity model would also predict high stress-drops. It seems likely that stress drops higher than 300 bars should produce a detectable short-period tectonic release signature. Since, at this time, the evidence for short-period distortions is lacking, the long-period P-wave data does not easily fit either the triggered fault or cavity mechanism for stress release. Fault motion which is driven by the explosion and ruptures downward could account for the observed long-period and short-period data. A driven fault would be in better agreement with the observations.

Acknowledgements

The authors wish to thank Thorne Lay and Larry Burdick for reviewing this manuscript and offering constructive criticism. This research was supported by the Advanced Research Projects Agency of the Department of Defense and was monitored by the Air Force Office of Scientific Research under contract F49620-81-C-0008. Contribution 3817, Division of Geological and Planetary Sciences, California Institute of Technology.

REFERENCES

Aki, K. and Y.B. Tsai (1972). Mechanism of Love wave excitation by explosion sources, J. Geophys. Res.,77, pp 1452-1475.

Aki, K., P. Reasenberg, T. DeFazio and Y. Tsai (1969). Near-field and far-field seismic evidence for triggering of an earthquake by the Benham explosion, Bull. Seism. Soc. Am, 59, pp 2197-2209.

Archambeau, C.B. (1972). The theory of stress wave radiation from explosions in prestressed media, Geophys. J., 29, pp 329-366.

Bache, T.C. (1976). The effect of tectonic stress release on explosion P-wave signatures, Bull. Seism. Soc. Am, 66, pp 1441-1457.

Boatwright, J. (1980). Preliminary body wave analysis of the St. Elias Alaska, earthquake of February 28, 1979, Bull. Seism. Soc. Am., 70, pp 419-436.

Buckhnam, R.C. (1969). Geologic effects of the Benham underground nuclear explosion, Nevada Test Site, Bull. Seism. Soc. Am., 59, pp 2209-2220.

Burdick, L. and D. Helmberger (1978). The upper mantle P velocity structure of the western United States, J. Geophy. Rev., 83, pp 1699-1712.

Cohn, S.N, T.L. Hong and D.V. Helmberger (1982). The Oroville earthquakes; a study of source characteristics and site effects, J. Geophys. Res., 87, pp 4585-4594.

Dahlman, O. and H. Israelson (1977). Monitoring Underground Nuclear Explosions, Elsevier, New York, 440 p.

Ebel, J.E. (1980). Source processes of the 1965 New Hebrides Island earthquakes inferred from teleseismic waveforms, Geophys. J., 63, pp 381-403.

Ebel, J.E., L.J. Burdick and G.S. Stewart (1978). The source mechanism of the August 7, 1966, El Golfo earthquake, Bull. Seism. Soc. Am, 68, pp 1281-1292.

Goforth, T. (1982). Anomalous Rayeigh waves from presumed explosions at the Shagan River test site-A, abstract, DARPA symposium, Hampton, Va.

Hamilton, R.M. and J.H. Healy (1969). Aftershocks of the Benham nuclear explosion, Bull. Seism. Soc. Am., 59, pp 2271-2281.

Hart, R.S., R. Butler and H. Kanamori (1977). Surface wave constraints on the August 1, 1975 Oroville earthquake, Bull. Seism. Soc. Am., 67, 1281-1292.

Hartzell, S. and D.V. Helmberger (1982). Strong-motion modeling of the Imperial Valley earthquake of 1979, Bull. Seism. Soc. Am., 72, pp 571-596.

Haskell, N.A. (1967). Analytic approximations for the elastic radiation from a contained underground explosions, J. Geophys. Res., 72, pp 2583-2587.

Helmberger, D.V. and G.R. Engen (1980). Modeling the long-period body waves from shallow earthquakes at regional ranges, Bull. Seism. Soc. Am., 70, pp 1699-1714.

Helmberger, D.V. and D.M. Hadley (1981). Seismic source functions and attenuation from local and teleseismic observations of the NTS events Jorum and Handley, Bull. Seism. Soc. Am., 71, pp51-67.

Johnson, L.R., T.V. McEvilly and K.L. McLaughlin (1982). Near-field recordings of ground accelerations from the Harzer explosion, abstract, EOS, 62, p 971.

Kanamori, H. and D.L. Anderson (1975). Theoretical basis of some empirical relations in seismology, Bull. Seism. Soc. Am., 65, 1073-1095.

Lay, T. and H. Kanamori (1980). Earthquake doublets in the Solomon Islands, Phys. Earth Plant. Inter., 21, pp 283-304.

Liu, H.L. and H. Kanamori (1980). Determination of source parameters of mid-plate earthquakes from the waveforms of body waves, Bull. Seism. Soc. Am., 70, pp 1989-2004.

Liu, H.L. and D.V. Helmberger (1982). The near-source ground motion of the August 6, 1979 Coyote Lake California Earthquake, Bull. Seism. Soc. Am., submitted.

Nuttli, O.W. (1969). Travel times and amplitudes of S waves from nuclear explosions in Nevada, Bull. Seism. Soc. Am., 59, pp 385-398.

Press, F. and C.B. Archambeau (1962). Release of tectonic strain by underground nuclear explosions, J. Geophys. Res., 67, pp 337-343.

Smith, R.B. and M.L. Sbar (1974). Contemporary tectonics and seismicity of the Western United States with emphasis on the Intermountain seismic seismic belt, Geol. Soc. Am. Bull., 85, pp 1205-1218.

Toksoz, M.N. and H.H. Kehrer (1972). Tectonic strain release by underground nuclear explosions and its effect on seismic discrimination, Geophys. J., 31, pp 141-161.

Toksoz, M.N. and H.H. Kehrer (1971). Underground nuclear explosions; tectonic utility and dangers, Science, 173, pp 230-233.

Toksoz, M.N., A. Ben-Menahem and D.G. Harkrider (1964). Determination of source parameters by amplitude equalization of seismic surface waves, 1. underground nuclear explosions, J. Geophys. Res, 69, pp 4355-4366.

Von Seggren, D., and R. Blandford (1972). Source time functions and spectra for underground nuclear explosions, Geophys. J., 31, pp 83-97.

Wallace, T.C., D.V. Helmberger and G.R. Mellman (1981a). A technique for the inversion of regional data in source parameter studies, J. Geophys. Res., 86, pp 1679-1685.

Wallace, T.C., D.V. Helmberger and J.E. Ebel (1981b). A broadband study of the 13 August 1978 Santa Barbara earthquake, Bull. Seismo. Soc. Am., 71, pp 1701-1718.

APPENDIX I

A moderate size earthquake (m_b = 5.6, ISC) which occurred on August 16, 1966 (OT; 18:02) near the Nevada-Utah border (epicentral coordinates: 37.4°N, 114.2°W) produced good regional waveforms at five WWSSN stations. Using the crustal model in Table 1 it is possible to invert these waveforms to obtain the source mechanism (see Wallace et al., 1981, for a description of the technique). Figure I-1 summarizes the analysis. Shown are the vertical and radial $P_{n\ell}$ observations and below are the synthetics computed for the inversion source. Both the observations and the synthetics have been lightly filtered. The fault parameters determined from the waveforms are a strike of N17°E dipping 80° to the east. The rake (defined as the sense of motion of the hanging wall relative to the foot wall; e.g. pure normal fault motion has a rake of -90°) is 190°, or nearly pure right-lateral strike-slip. This solution is in close agreement with that of Smith and Sbar's (1974) which was determined on the basis of local first motions; strike = N14°E, dip = 80°W, rake = 170°. The moment of the earthquake can be determined by comparing the amplitude of the observations and the synthetics. The ratio of the moment determined from each seismogram to the average moment is shown in Figure I-1 to the right of each trace.

The teleseismic short-periods at nine stations were modeled for source depth and time-function. The separation of P and sP indicates that the hypocenter is on the order of 6 km deep. Six of these records are shown in Figure I-2. In the short-period modeling it was assumed that the source orientation is known; depth and time function are the only unkowns. In Figure I-2 the depth phase sP is often the largest arrival. For example, the OGD waveform has a small, but clear, P and pP

followed by a large sP. There obviously is some uncertainy in depth, but the event probably can not be shallower than 4 km or deeper than 8 km. The short-period time function was a trapezoid with a 0.4 second rise, 0.5 second top and 0.4 second fall. The short-period amplitudes give a moment of 4.2×10^{24} dyne-cm, consistent with the long-period analysis. The 8/16/66, Nevada earthquake is very similar to a strike-slip event which occurred near Coyote Lake, California on August 6, 1979. Liu and Helmberger (1982) give a moment of 3.5×10^{24} dyne-cm for this event, and the analysis of the strong-ground motion data indicates that the event is high stress-drop. The primary rupture occurred along a patch 2 km long and the stress-drop was 150 bars. A comparison of the teleseismic short-period records for the Nevada and Coyote Lake events shows that they are systematically larger for the Nevada event. This implies that the Nevada event is at least as high stress-drop as the Coyote Lake earthquake.

The December 22, 1964, Baja Norte, Mexico earthquake (m_b = 5.6, PAS) occurred on the San Miguel Fault zone (OT; 20.54, epicentral coordinates; 31.8°N, 117.1°W). The fault zone strikes N50°W and is right lateral strike-slip. The date of the event coincides with operation of a large number of LRSM stations in the southwestern U.S., which provided 15 $P_{n\ell}$ waveforms used in the inversion for source parameters. The analysis is summarized in Figure I-2. As before the observation (verticals only) are shown above the synthetic computed for the fault model. The fault parameters are strike = 312°, dip = 85° and rake of 177°. The moment is 8×10^{24} dyne-cm. The depth of the event is not well constrained but is between 2 and 8 km.

FIGURE CAPTIONS

Figure 1: A comparison between the SH Love waves for the nuclear explosion GREELEY (12-20-66) and an earthquake in eastern Nevada (8-16-66). The stations are naturally rotated. The seismograms are lined up on the S arrival and the amplitude scale is the same for both the earthquake and explosion. The time scale of the enlarged SH wave at MBC is one half that of the other traces.

Figure 2: A comparison between the regional body waves of the nuclear explosion BOXCAR (top trace for both stations) and the San Miguel earthquake (12-22-64). The seismograms are the vertical components.

Figure 3: Profiles of synthetic strike-slip responses without instrument (left) and with a WWSSN long-period instrument (right) computed for a crustal layer over the T7 upper mantle. The distances before 900 km are in the shadow of the low velocity zone, while beyond a 1000 km strong diving ray energy is present. The clear separation of arrivals beyond 1000 is due to sP and P.

Figure 4: A base map of the Pahute Mesa test site and the location of some of some of the larger explosions.

Figure 5: The vertical component records for 8 large Pahute Mesa explosions at the WWSSN station SHA. These are long-period seismograms which are arranged according to the importance of the second upswing in the P wave. About 4 1/2 minutes after the P-arrival is the SV wave.

Figure 6: A comparison of the P and PL waves for BOXCAR and COLBY at LUB. Shown below is the COLBY waveform summed with a synthetic seismogram to simulate the tectonic release. The double couple has a pure strike-slip orientation. The time function is a triangle with a 0.6 second duration. The seismic moment for the double couple required to obtain the fit is 5×10^{24} dyne-cm.

Figure 7: A comparison of the waveforms for GREELEY and KASSERI. Shown are LUB, JCT, DAL, and SHA. The two explosions look very similar with the exception of the large second arrival for GREELEY.

Figure 8: A comparison of the GREELEY waveforms with those predicted by KASSERI plus tectonic release. The tectonic release time function

is a triangle with a 0.6 second duration. The fault orientation is a 5-to-1 ratio of strike-slip to dip-slip motion. The total moment is 6 x 10^{24} dyne-cm.

Figure 9: A comparison of the GREELEY waveforms at LUB and RCD. Also shown is the waveform of the 8-16-66 earthquake. This earthquake was used to simulate the GREELEY record by summing with a synthetic explosion waveform.

Figure 10: The P_{nl} waveforms for several Pahute Mesa explosions (top trace at each station) and synthetics for an explosion source (middle trace) and a double couple (bottom trace) source. Both the observations and synthetics were lightly filtered. The fault orientation for the double couple is strike-slip; the nodal planes are sketched on the location map.

Figure 11: A comparison of the P_{nl} waveforms for the explosion FAULTLESS (top trace) and synthetics computed for an explosion source. Both observations and synthetics have been lightly filtered.

Figure 12: A comparison of the P_{nl} waveforms of the same explosions as in Figure 10 and synthetic explosion waveforms with a component of tectonic release. Both observations and synthetics have been lightly filtered. The numbers to the right of each seismogram pair give the ratio of Pn amplitude due to the double couple.

Figure I-1: Location of the 8-16-66 Nevada earthquake (star) can recording stations. Both radial and vertical components are shown. For each seismogram pair the top trace is the observation while the lower trace is a synthetic computed with the source orientation given by the inversion. The moment of the event is 4.1 x 10^{24} dyne-cm. The numbers to the right of each seismogram pair give the ratio of the moment determined from that trace to the average moment.

Figure I-2: A comparison of the short-period seismograms (top trace) and synthetics calculated with the fault orientation given by the regional waveforms. The depth is 6 km.

Figure I-3: Location of the 12-22-64 San Miguel earthquake (star) and the recording stations. The stations with two and four letter designations are LRSM while those with three letters are WWSSN. Also shown are the vertical component (top trace) and synthetics (bottom trace) computed with the inversion fault orientation. The

moment of the event is 8×10^{24} dyne-cm.

Table 1: Large Pahute Mesa Explosions

Name	Date	OT	Lat (N)	Long (W)	dep	Est Yield† (kt)
GREELEY	12-20-1966	15:30	37.30	116.41	1215	830
BOXCAR	04-26-1968	15:00	37.29	116.46	1158	1000
BENHAM	12-19-1968	16:30	37.23	116.47	1402	1000
JORUM	09-16-1969	14:30	37.31	116.46	1158	700
HANDLEY	03-26-1970	19:00	37.30	116.53	1206	1900
ALMENDRO	06-06-1973	13:00	37.24	116.35	1064	570
MAST	06-19-1975	13:00	37:35	116.32	912	520
CAMEMBERT	06-26-1975	12:30	37.28	116.37	1311	750
KASSERI	10-28-1975	14:30	37.29	116.41	1265	1200
INLET	11-20-1975	15:00	37.22	116.37	817	500
MUENSTER	01-03-1976	19:15	37.30	116.33	1451	600
FONTINA	02-12-1976	14:45	37.27	116.49	1219	900
COLBY	03-14-1976	12:30	37.31	116.47	1273	900
POOL	03-17-1976	14:15	37.26	116.31	879	500

† From Dahlman and Iserelson (1977)

APPENDIX I

TABLE 1 - CRUSTAL MODEL

P_{VEC}	S_{VEC}	DENSITY	LAYER THICKNESS
6.2	3.5	2.7	32.
8.2	4.5	3.4	

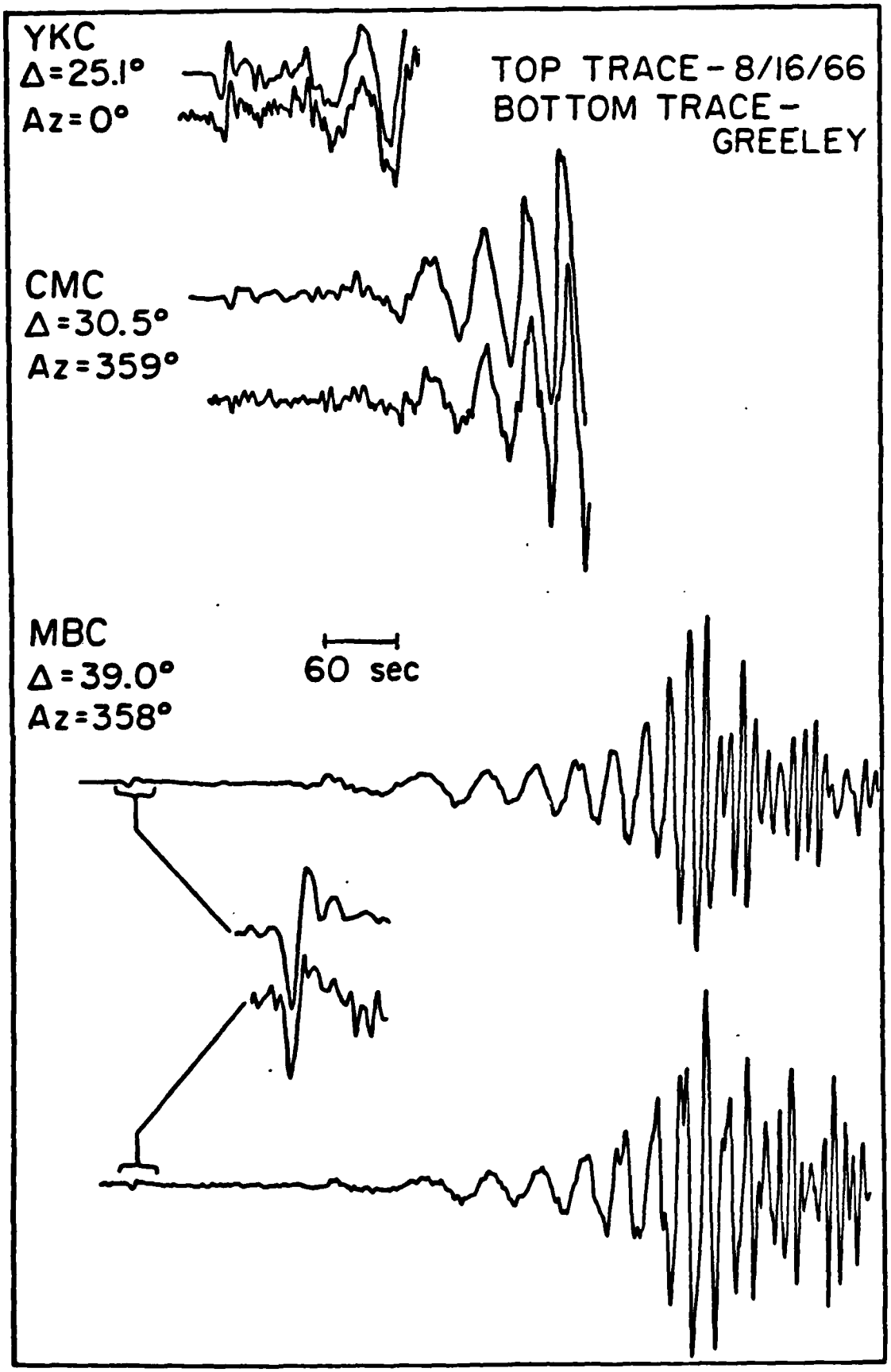
YKC
Δ=25.1°
Az=0°
TOP TRACE - 8/16/66
BOTTOM TRACE -
GREELEY
CMC
Δ=30.5°
Az=359°
MBC
Δ=39.0°
Az=358°
60 sec

Figure 1

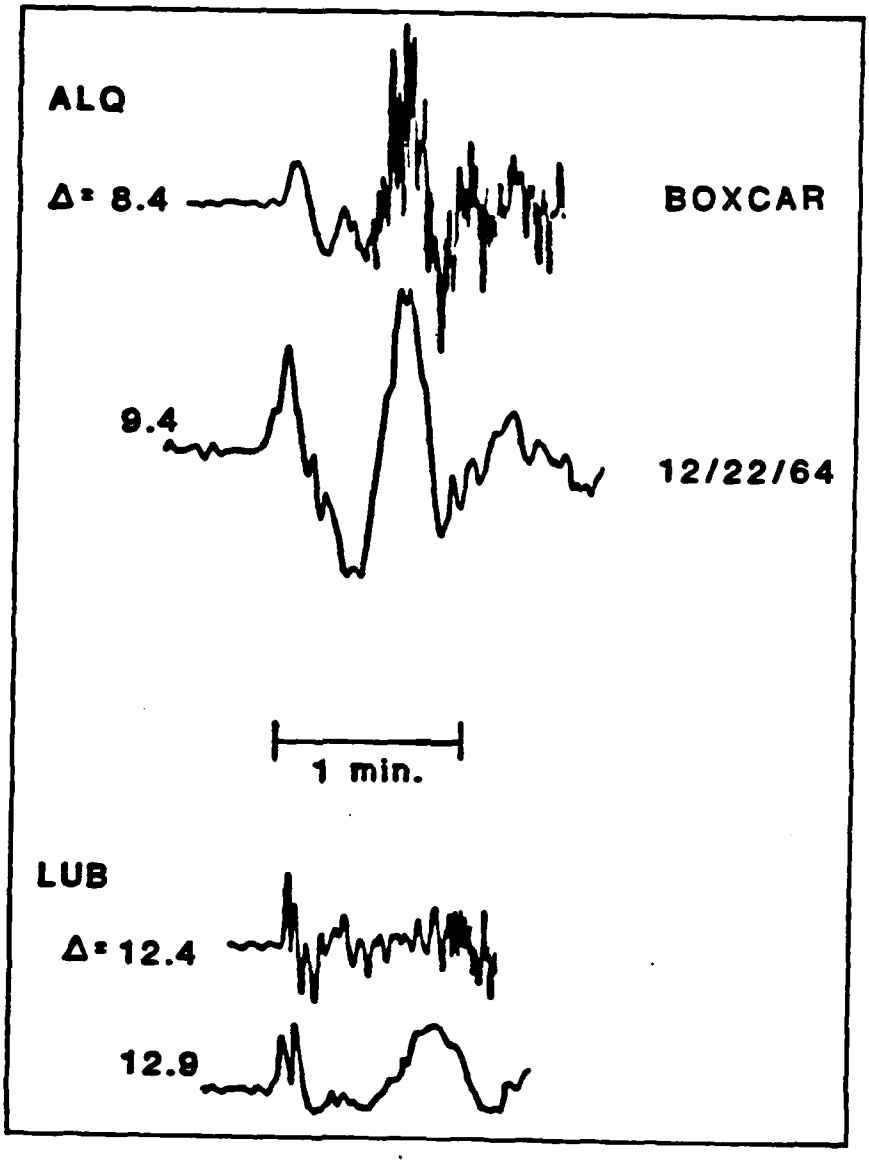

Figure 2

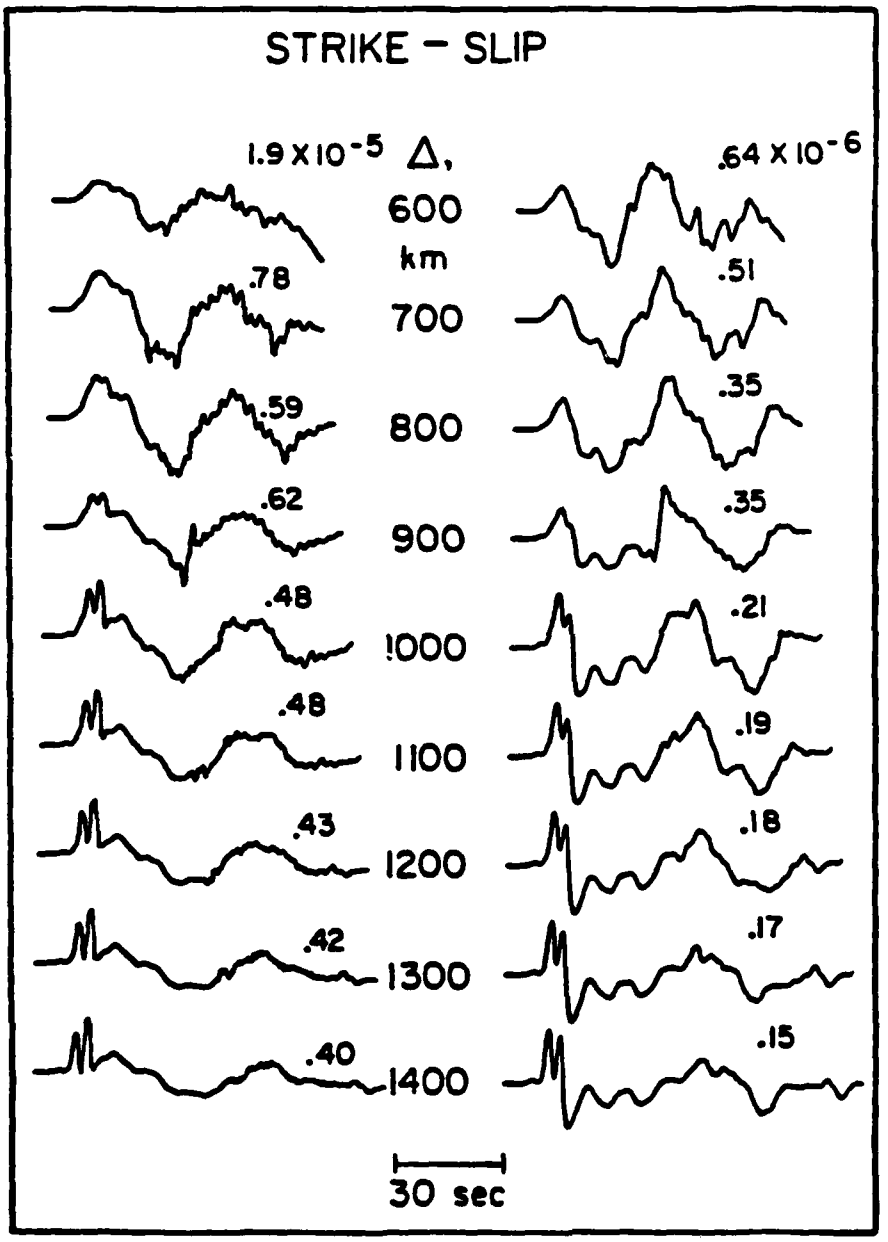
STRIKE – SLIP
1.9 X 10⁻⁵
Δ,
km
.64 X 10⁻⁶
600
.78
700
.51
.59
800
.35
.62
900
.35
.48
1000
.21
.48
1100
.19
.43
1200
.18
.42
1300
.17
.40
1400
.15
30 sec

Figure 3

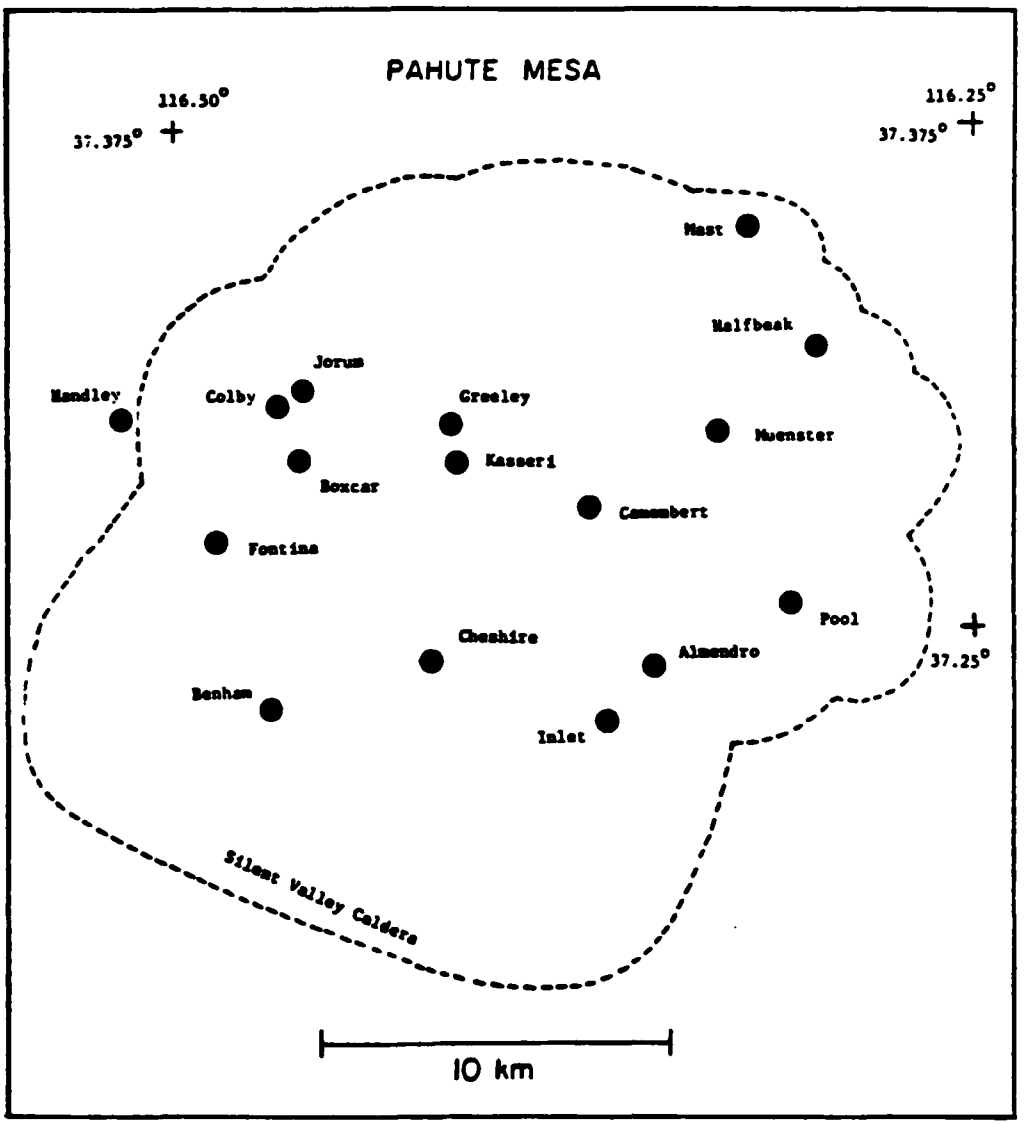
PAHUTE MESA
116.50°
37.375°
116.25°
37.375°
37.25°
Mast
Halfbeak
Jorum
Colby
Handley
Greeley
Muenster
Kasseri
Boxcar
Camembert
Fontina
Pool
Cheshire
Almendro
Benham
Inlet
Silent Valley Caldera
10 km

Figure 4

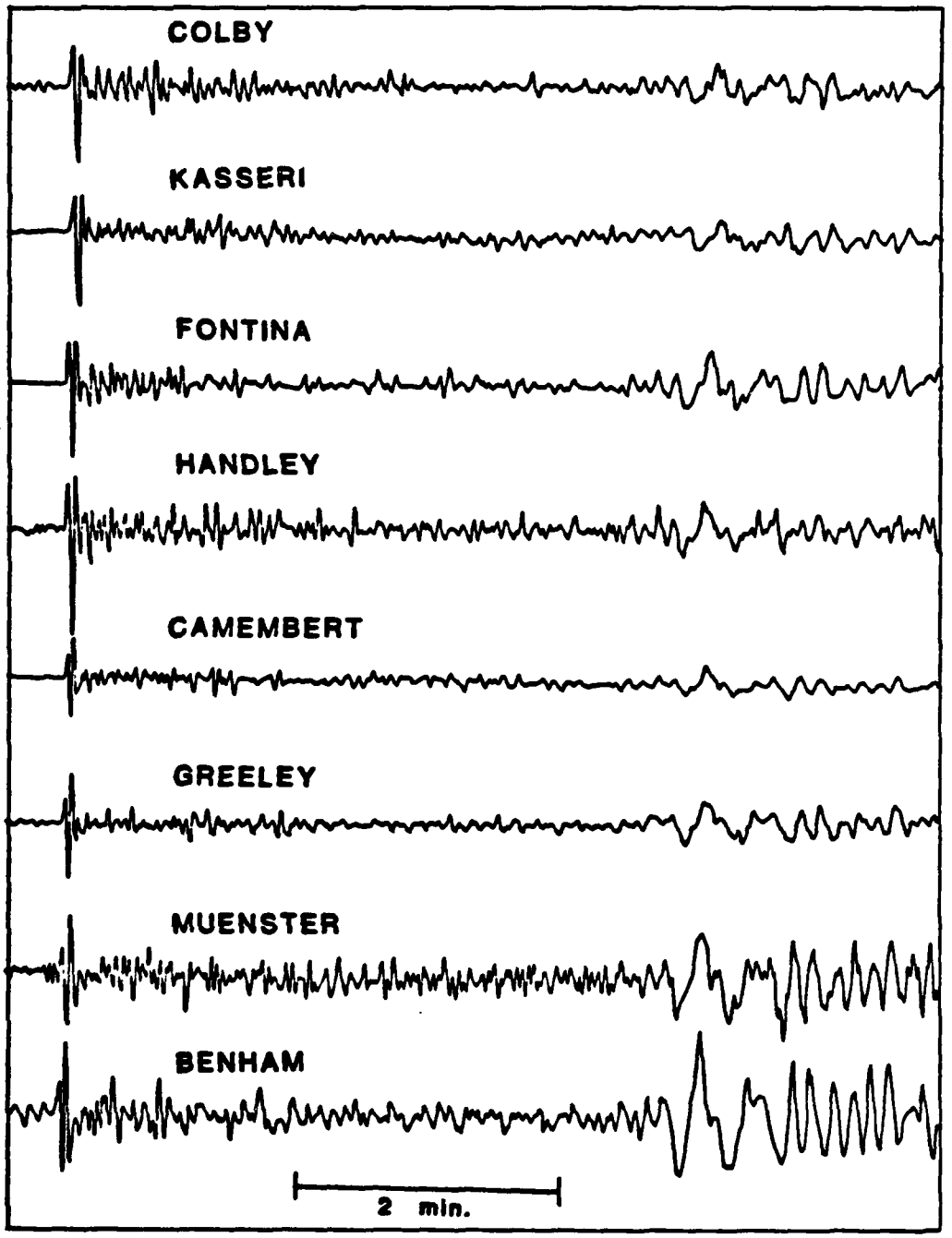
COLBY
KASSERI
FONTINA
HANDLEY
CAMEMBERT
GREELEY
MUENSTER
BENHAM
2 min.

Figure 5.

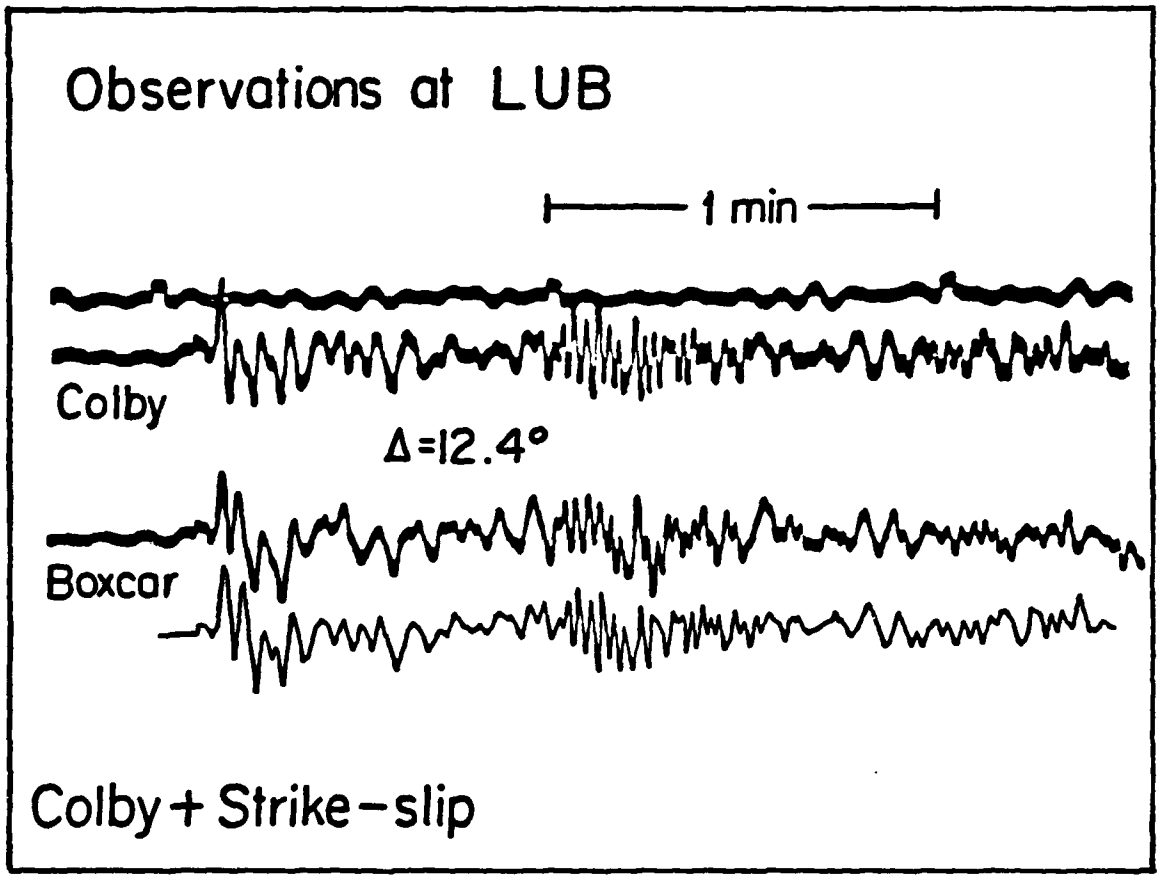
Observations at LUB
1 min
Colby
Δ=12.4°
Boxcar
Colby + Strike-slip

Figure 6

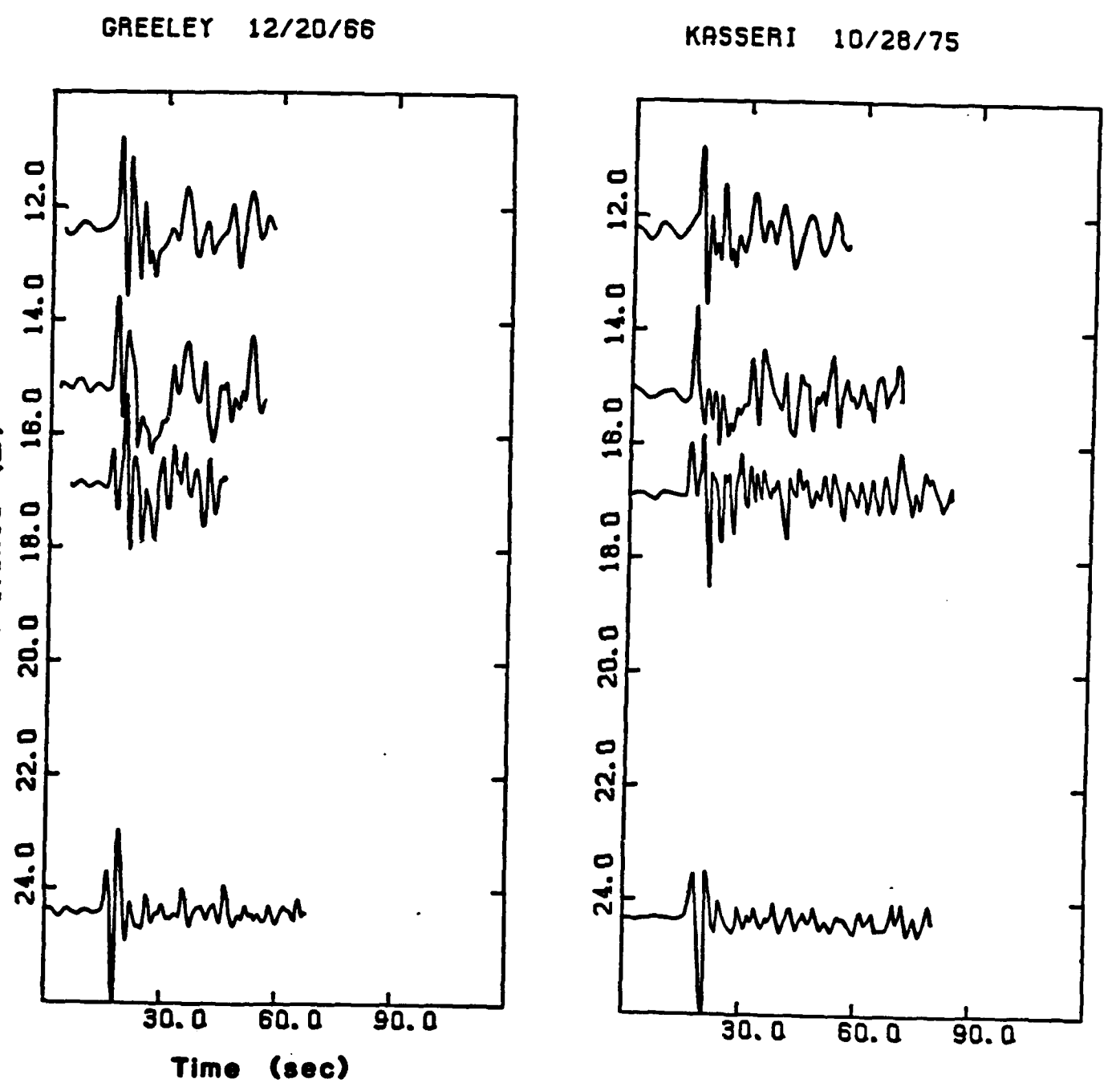
GREELEY 12/20/66
KASSERI 10/28/75
12.0
14.0
16.0
18.0
20.0
22.0
24.0
30.0
60.0
90.0
Time (sec)

Figure 7

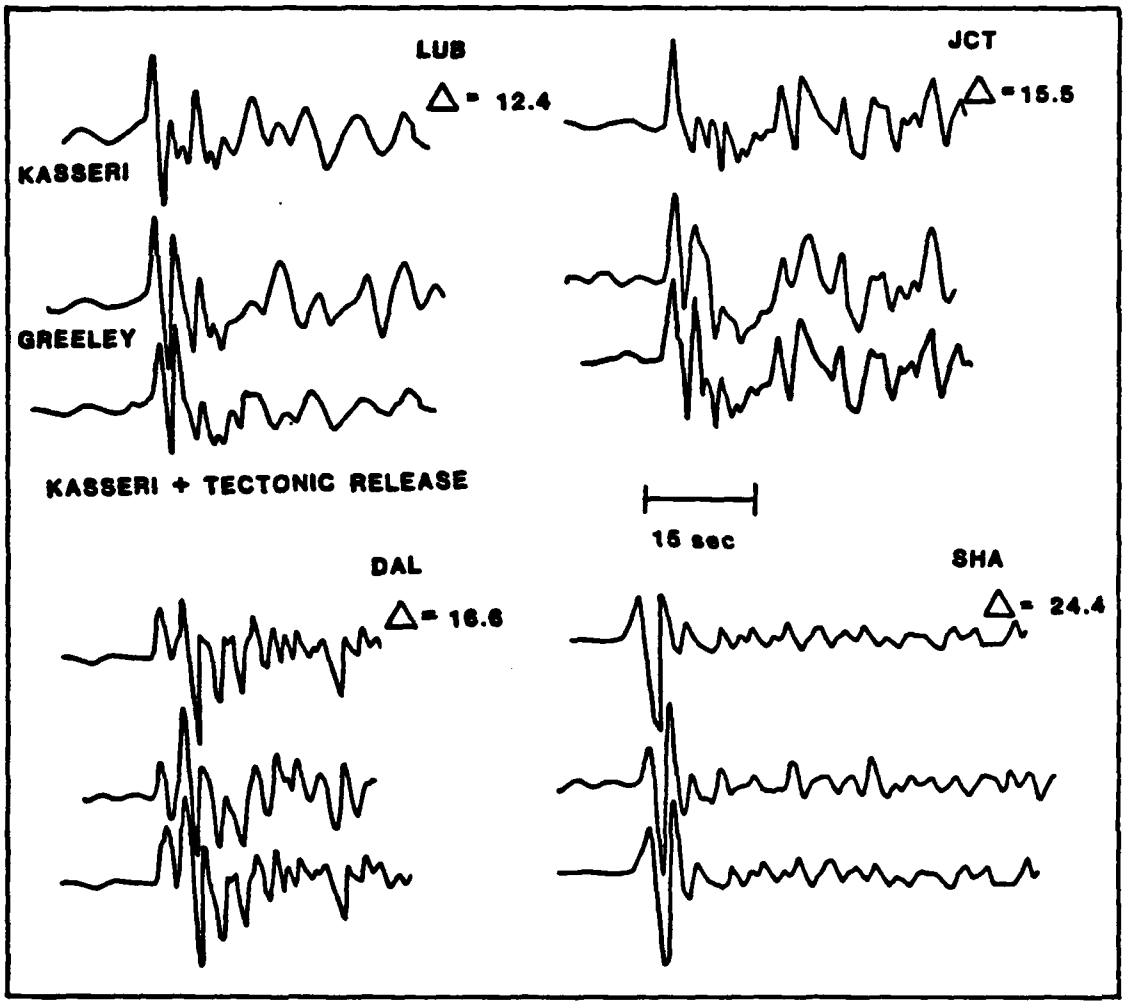
LUB
Δ = 12.4
JCT
Δ = 15.5
KASSERI
GREELEY
KASSERI + TECTONIC RELEASE
15 sec
DAL
Δ = 16.6
SHA
Δ = 24.4

Figure 8

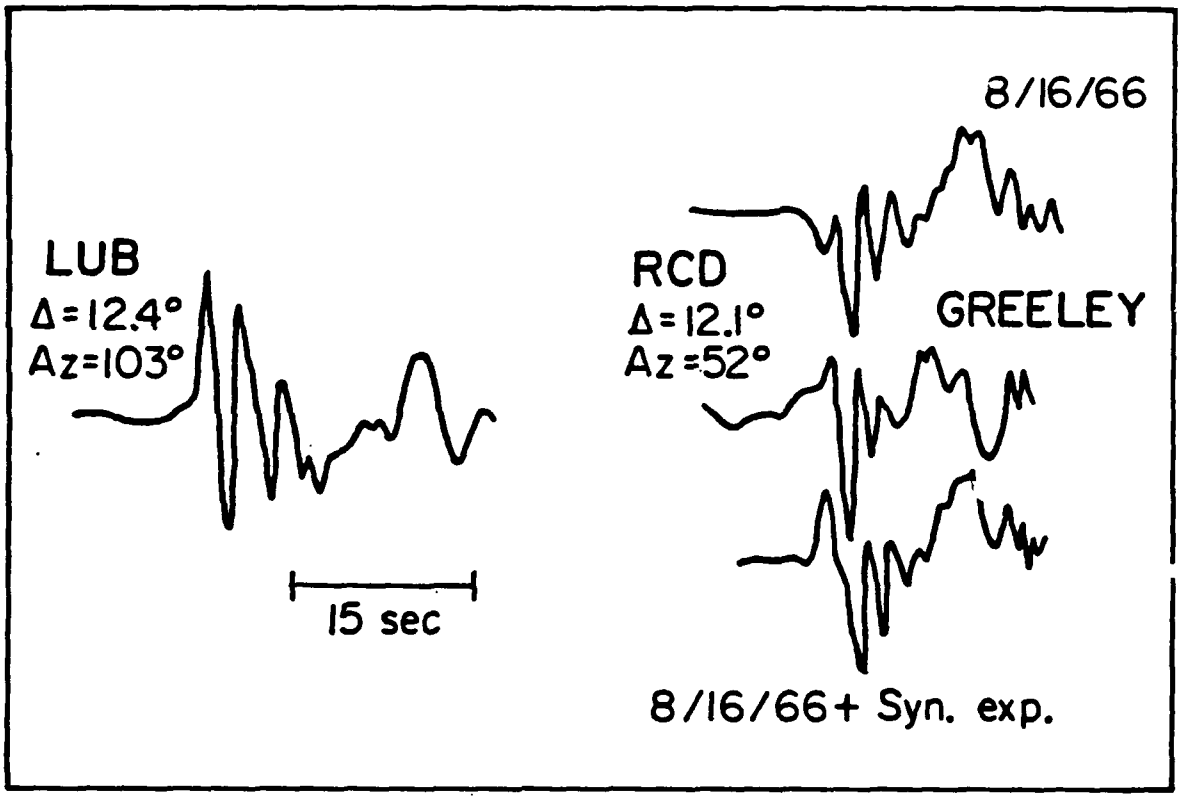
8/16/66
LUB
Δ=12.4°
Az=103°
RCD
Δ=12.1°
Az=52°
GREELEY
15 sec
8/16/66+ Syn. exp.

Figure 9

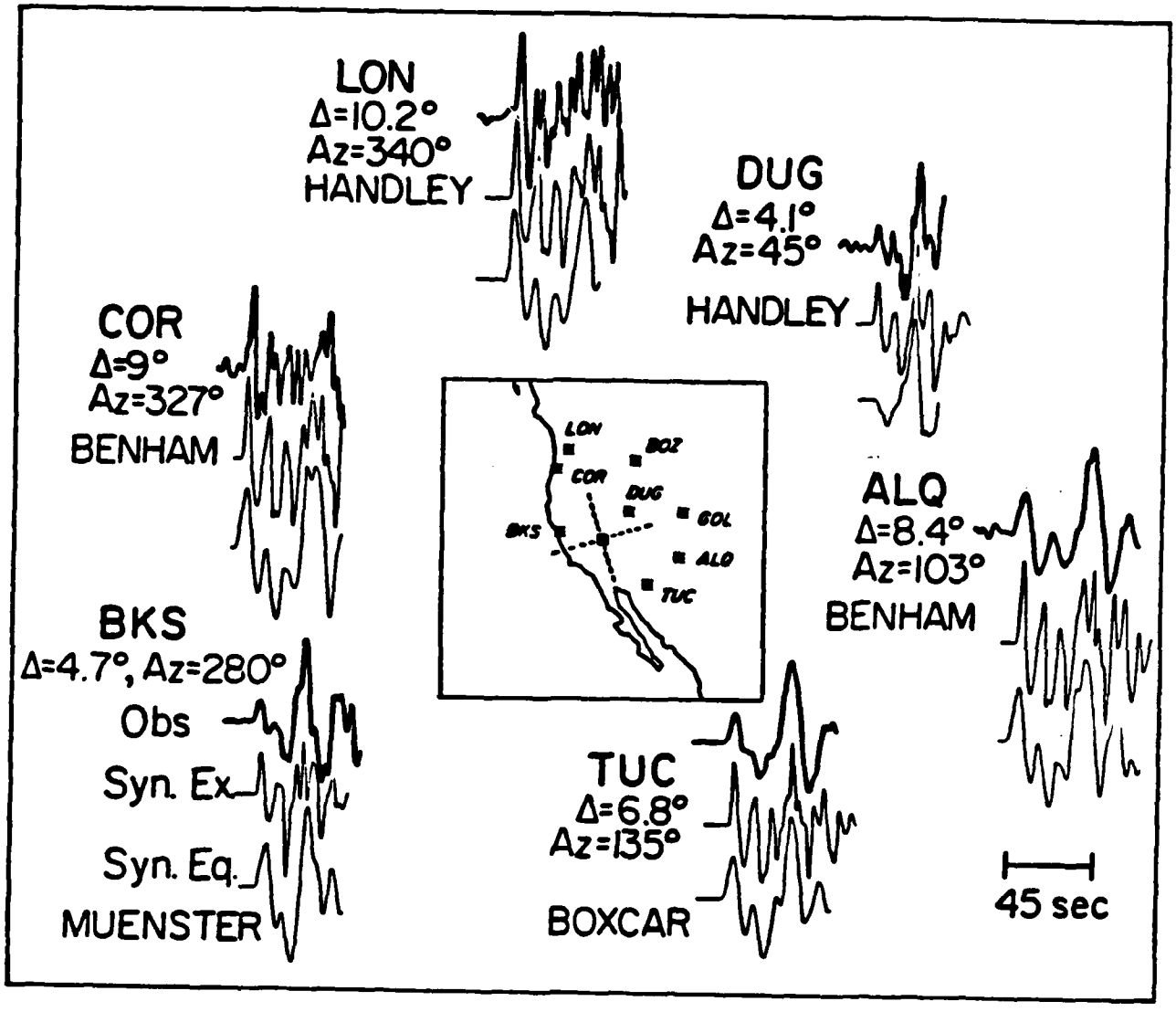
LON
Δ=10.2°
Az=340°
HANDLEY
DUG
Δ=4.1°
Az=45°
HANDLEY
COR
Δ=9°
Az=327°
BENHAM
LON
BOZ
COR
DUG
GOL
BKS
ALQ
TUC
ALQ
Δ=8.4°
Az=103°
BENHAM
BKS
Δ=4.7°, Az=280°
Obs
Syn. Ex
Syn. Eq.
MUENSTER
TUC
Δ=6.8°
Az=135°
BOXCAR
45 sec

Figure 10

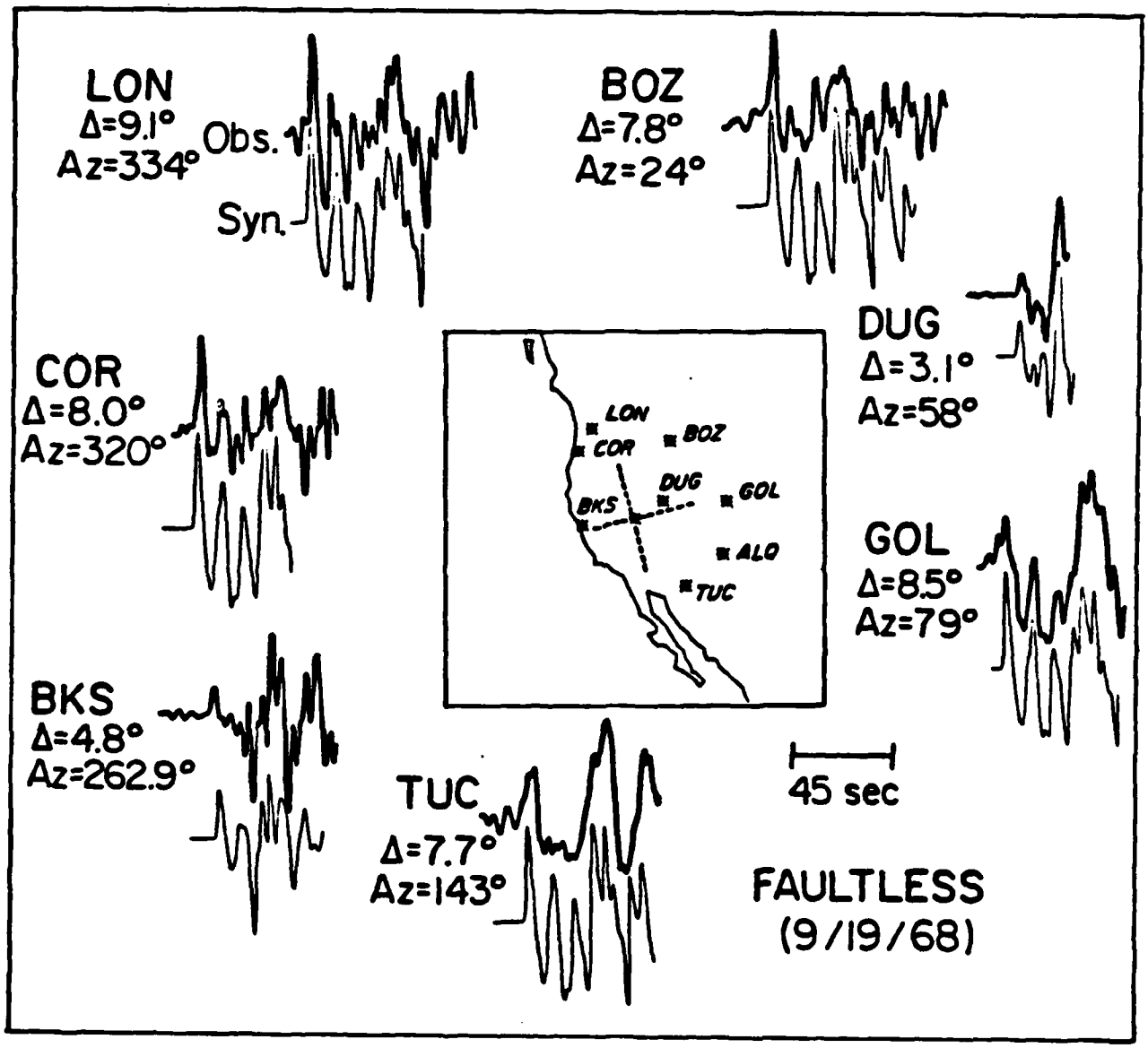
LON
Δ=9.1°
Az=334°
Obs.
Syn.
BOZ
Δ=7.8°
Az=24°
DUG
Δ=3.1°
Az=58°
COR
Δ=8.0°
Az=320°
LON
BOZ
COR
DUG
GOL
BKS
ALO
TUC
GOL
Δ=8.5°
Az=79°
BKS
Δ=4.8°
Az=262.9°
TUC
Δ=7.7°
Az=143°
45 sec
FAULTLESS
(9/19/68)

Figure 11

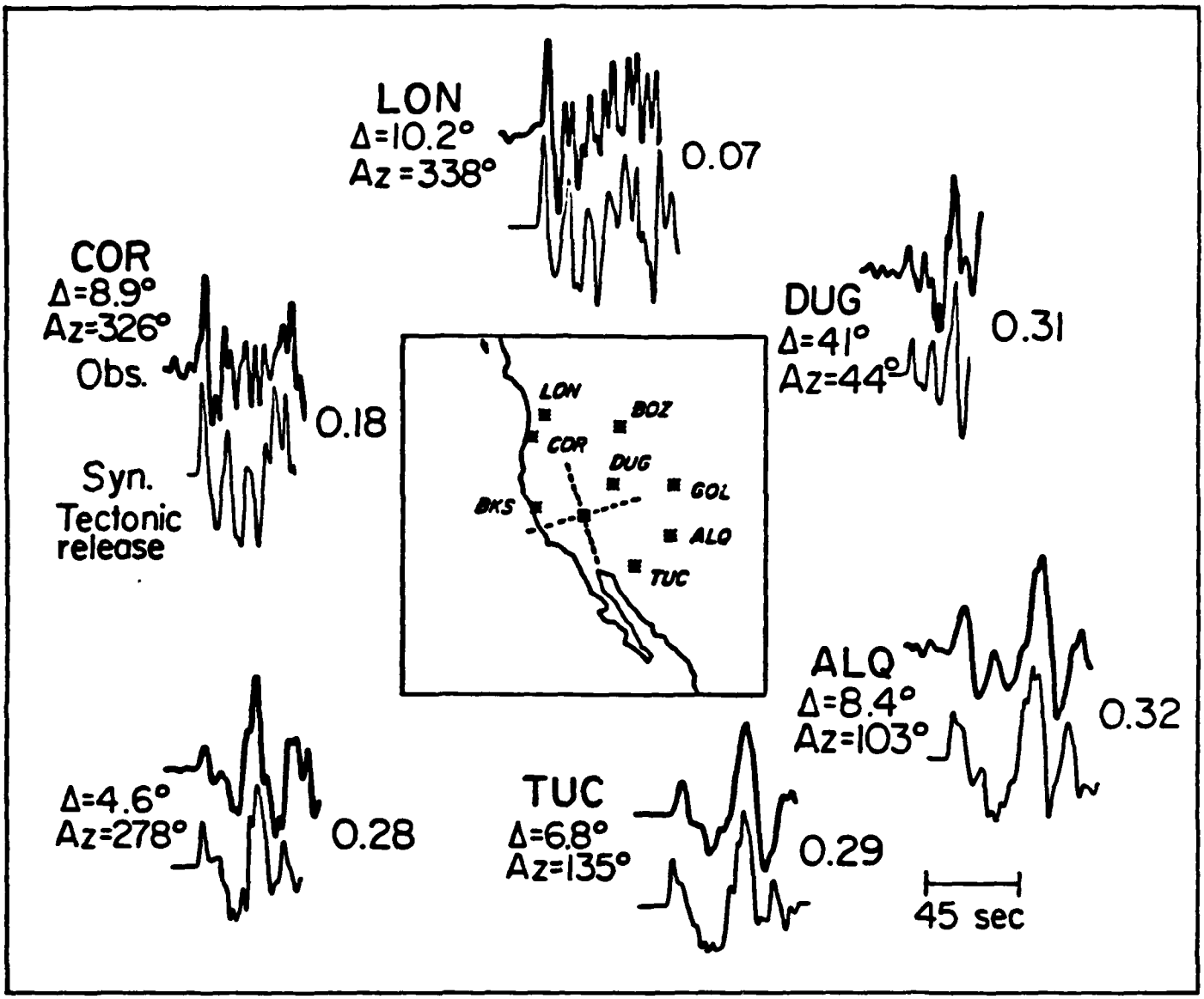
LON
Δ=10.2°
Az=338°
0.07
COR
Δ=8.9°
Az=326°
Obs.
0.18
Syn.
Tectonic
release
DUG
Δ=41°
Az=44°
0.31
LON
BOZ
COR
DUG
GOL
BKS
ALO
TUC
ALQ
Δ=8.4°
Az=103°
0.32
Δ=4.6°
Az=278°
0.28
TUC
Δ=6.8°
Az=135°
0.29
45 sec

Figure 12

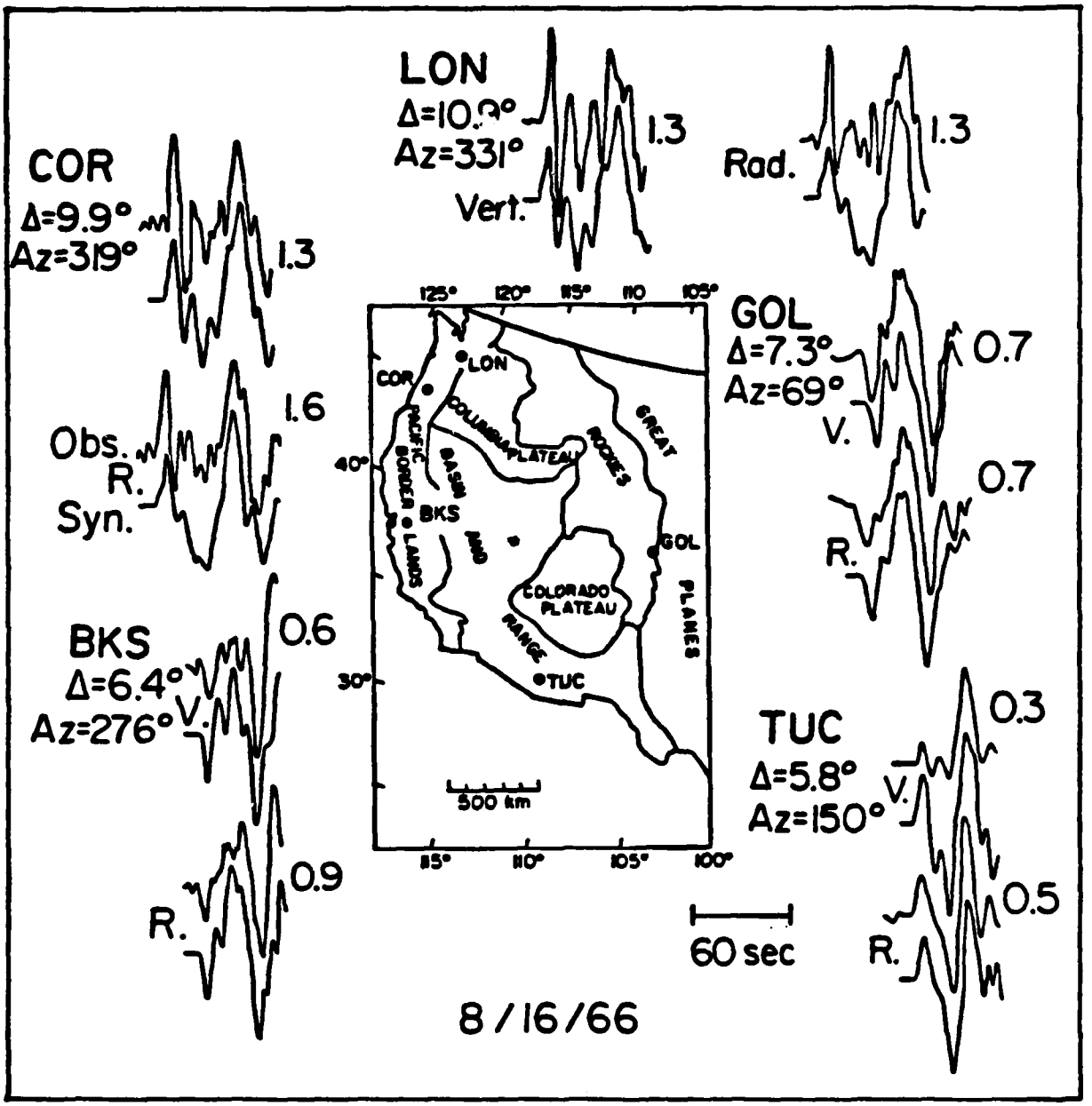
LON
Δ=10.9°
Az=331°
1.3
Vert.
Rad.
1.3
COR
Δ=9.9°
Az=319°
1.3
Obs.
R.
Syn.
1.6
GOL
Δ=7.3°
Az=69°
0.7
V.
0.7
R.
BKS
Δ=6.4°
Az=276°
V.
0.6
R.
0.9
TUC
Δ=5.8°
Az=150°
V.
0.3
R.
0.5
125°
120°
115°
110
105°
40°
30°
COR
LON
BKS
GOL
TUC
PACIFIC BORDER
LANDS
BASIN AND RANGE
COLUMBIA PLATEAU
ROCKIES
GREAT PLAINS
COLORADO PLATEAU
500 km
115°
110°
105°
100°
60 sec
8/16/66

Figure I-1

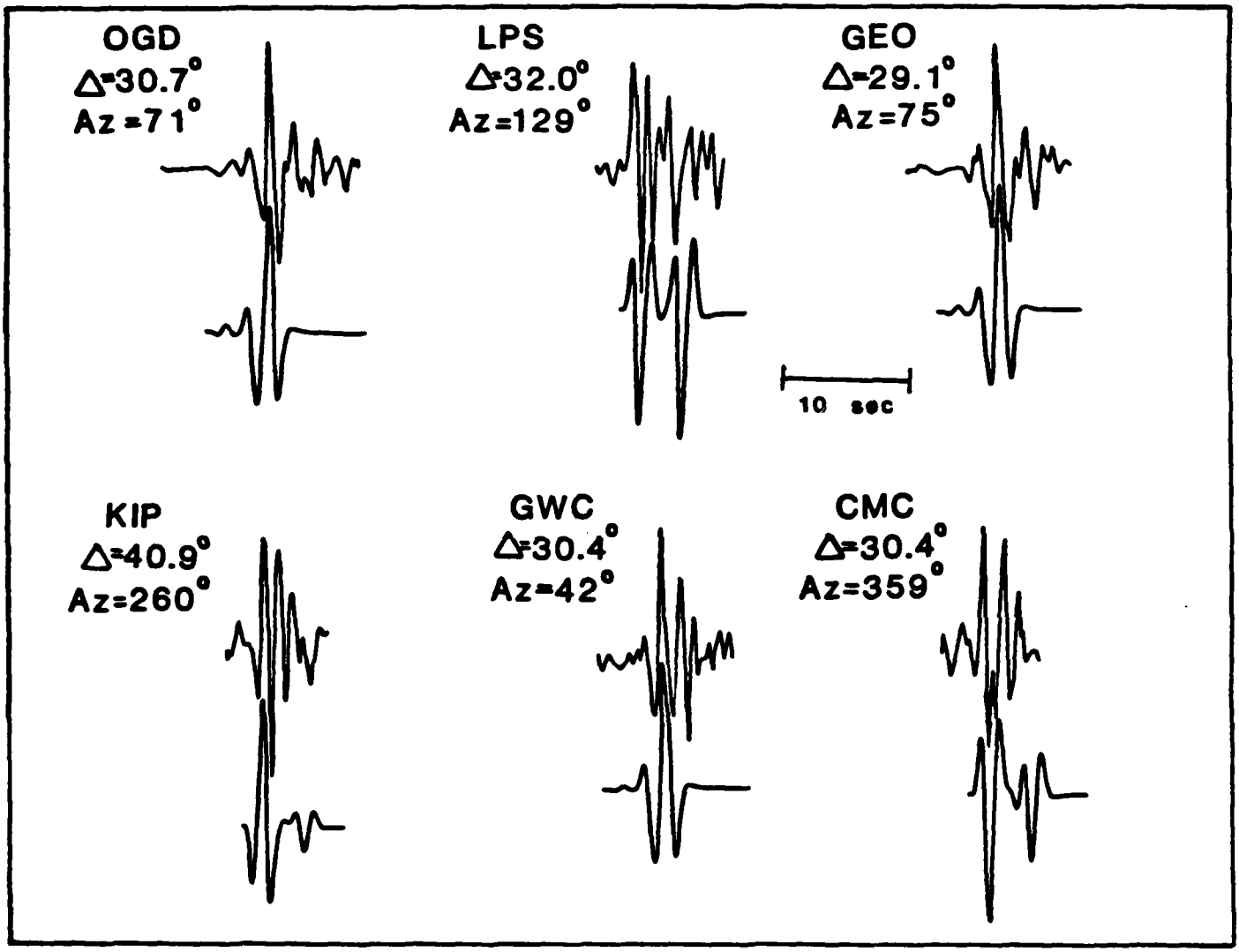
OGD
Δ=30.7°
Az=71°
LPS
Δ=32.0°
Az=129°
GEO
Δ=29.1°
Az=75°
10 sec
KIP
Δ=40.9°
Az=260°
GWC
Δ=30.4°
Az=42°
CMC
Δ=30.4°
Az=359°

Figure I-2